Characterization of the Yeast Rapamycin-sensitive Phosphoproteome

Inauguraldissertation
zur
Erlangung der Würde eines Doktors der Philosophie
vorgelegt der
Philosophisch-Naturwissenschaftlichen Fakultät
der Universität Basel

von

Alessio Cremonesi
Castel San Pietro, TI

Basel, 2012

Genehmigt von der Philosophisch-Naturwissenschaftlichen Fakultät
auf Antrag von

Prof. Dr. Michael N. Hall
Dr. Paul Jenö
PD Dr. Jan Hofsteenge

Basel, den 13.12.2011

Prof. Dr. Martin Spiess
Dekan

Summary

Cell growth is a tightly regulated process, where a cell adapts its growth according to nutrient availability and cellular stress. Tor (Target Of Rapamycin) is an evolutionary conserved protein kinase and central controller of cell growth. It is found in two functionally distinct protein complexes termed TORC1 and TORC2. Rapamycin-sensitive TORC1 mediates temporal control of cell growth whereas rapamycin-insensitive TORC2 mediates spatial control of cell growth. Although many cellular processes regulated by TORC1 have been identified, the molecular mechanisms by which TORC1 signals to these diverse processes are not well understood. For example, only few substrates of either TORC1 or its direct effector SCH9 are known in the yeast *S. cerevisiae*. To identify novel TORC1 targets in a global manner, a quantitative phosphoproteomic strategy was established, which allowed to reproducibly relative quantify more than 2,500 phosphorylation sites in untreated and rapamycin-treated cells. In parallel, a proteomic study was performed to monitor changes in protein abundances induced by rapamycin treatment. In total 55 and 78 proteins were significantly less respectively more phosphorylated upon rapamycin treatment in the phosphoproteomic analysis. Among them there were many proteins already linked to the TORC1 signaling pathway, which functioned as internal control. Many regulated proteins were transcription factors or kinases, which are often present at low copy number in the cell, suggesting an in-depth analysis of the yeast phosphoproteome. Among the hypophosphorylated phosphopeptides the PKA consensus motif was significantly over-represented suggesting a cross-talk between the TORC1 and PKA signaling pathways. This hypothesis was further supported at the molecular level for the protein Maf1, Ksp1 and Ypk3. In addition, to validate and better characterize the phosphoproteomic data, more targeted experiments for some of the regulated phosphoproteins were performed. This revealed the involvement of novel proteins (like Hal5, Isw2, Kkq8, Ldb19, Mtc1, Noc2 and Vtc2) in TORC1 signaling. On these proteins, several rapamycin-regulated phosphorylation sites were mapped and their absolute phosphorylation occupancy was estimated. Interestingly, rapamycin-regulated phosphorylation sites usually exhibited low

to moderate stoichiometries. Subsequent mutagenesis experiment will address the involvement of those specific phosphorylation sites in TORC1 signaling.

Abbreviations

8-Br-cAMP	8- Bromoadenosine- 3', 5'- cyclic monophosphate
CID	collision-induced dissociation
cpm	counts per minute
HA	haemagglutinin
IMAC	immobilized metal affinity chromatography
kDa	Kilodalton
λPPase	λ protein phosphatase
LC-MS/MS	liquid chromatography coupled to mass spectrometry
LTQ	linear trap quadrupole
m/z	mass-to-charge ratio
MS	mass spectrometry
MW	molecular weight
PKA	protein kinase A
PP242	2-(4-amino-1-isopropyl-1H-pyrazolo[3,4-d]pyrimidin-3-yl)-1H-indol-5-ol
RP-HPLC	reverse-phase high-performance liquid chromatography
SDS-PAGE	sodium dodecyl sulfate polyacrylamide gel electrophoresis
SILAC	stable isotope labeling with amino acids in cell culture
(m)Tor	(mammalian) Target of rapamycin
TORC1	Tor complex 1

Table of Contents

1. Introduction

1.1. Posttranslational Modifications Increase Proteome Complexity

The global complement of genes encoded by an organism is known as the genome. Accordingly, in 1994 the term proteome was coined by Marc Wilkins to describe the global set of all proteins encoded by the genome. Both genome size and the number of genes encoded in the genome can vary dramatically from species to species. For example, the human genome contains an estimated 25,000 to 30,000 genes while the genome of the yeast *S. cerevisiae* encodes approximately 6,100 genes. However, the complexity of proteomes usually exceeds many times the complexity of genomes. This is due to transcriptional, translational and posttranslational modifications. Posttranslational modifications can be divided into three broad categories. The first and probably most common is the covalent attachment of chemical groups to amino acid side chains. The second is the hydrolytic cleavage of a precursor polypeptide into two or more mature proteins. The third category is protein splicing [1], in which internal protein segments (inteins) are excised from a precursor protein, followed by ligation of the flanking segments (exteins). The first two types of posttranslational modifications require specific enzymes like kinases, acetylases, methylases, glycosydases or proteases, while protein splicing is an autocatalytic reaction and does not require external enzymes. Interestingly, there are very stable posttranslational modifications because of thermodynamic reasons or of lack of enzymes capable of reversing them. And there are unstable modifications which can be reverted very quickly. Among the last there are reversible modifications such as phosphorylation, acetylation, glycosylation and ubiquitination that allow a protein to oscillate between two different states (e.g. active/inactive). For this reason, a cell usually contains counteracting enzymes for the addition/removal of phosphates (kinases/phosphatases), acetyl groups (acetyltransferares/deacetylases), glycans (glycosyltransferases/glycosidases) and ubiquitin (ubiquitin ligases/isopeptidases).

The pervasiveness of posttranslational modifications is reflected by the high number of enzymes necessary to catalyze these modifications. To date, more than 500 kinases have been estimated to be encoded by the human genome [2]. In the genome of the yeast *S. cerevisie* protein kinases represent the largest gene family with approximately 130 genes [2] and similar proportions have been found in the fly *D. melanogaster* (~240 kinase genes) and the worm *C. elegans* (~450 kinase genes) genomes [2]. However, the number of enzymes catalyzing posttranslational modifications is not the only factor explaining the high complexity of proteomes. A second important parameter is that several different protein substrates can be targeted by the same modifying enzyme. Therefore, if one assumes that the 500 kinases present in the human genome phosphorylate on average five proteins at five different phosphorylation sites, 12,500 different proteomes might be produced in total. This is still an underestimation of the real impact of protein phosphorylation because there are proteins known to be phosphorylated at dozens of sites. For example, more than 15 different phosphorylation sites have been identified in the insulin receptor, which means that at least 32,768 different variants of the receptor could be generated just by differential phosphorylation! Finally, since a protein is often multiply modified with different types of modifications, enormously high numbers of variants of the same protein might exist.

The functional consequences of posttranslational modifications vary from protein to protein, but some common traits can be identified. The introduction of negatively charged groups (e.g. by phosphorylation or sulfation) or the removal of positively charged groups (e.g. by acetylation), for example, dramatically influences the protein microenvironment due to electrostatic interactions. Or the introduction of certain groups, phosphates for instance, can promote protein/protein interactions. Finally, some posttranslational modifications lead to changes of subcellular localization. This is the case for polyubiquitination that targets proteins to the proteasome or lipidation of serines and glycines, which often cause proteins to associate with membranes.

1.2. Protein Phosphorylation

The most frequent and versatile posttranslational modification is protein phosphorylation. It occurs in eukaryotes and less frequently in prokaryotes. The residues phosphorylated in eukaryotic cells are mostly serines, threonines and tyrosines, whose nucleophilic hydroxyl groups attack the electrophilic γ-phosphate of ATP or, less frequently, GTP. In prokaryotes the phosphorylated residues are typically histidines and aspartic acids. In the so called bacterial two-component system [3], signal transduction occurs through the transfer of a phosphate group from ATP to the sensor kinase, a histidine kinase. The activated histidine kinase catalyses the subsequent transfer of the phosphate group to an aspartic acid residue on the response regulator, which stimulates or represses the expression of specific target genes.

It is estimated that a third of all eukaryotic proteins are phosphorylated at some stage in their life cycle and that approximately 2% of all genes in a eukaryotic genome encode protein kinases [2, 4]. This clearly underlines the importance of protein phosphorylation and suggests a tight crosstalk between kinases and their substrates. To fulfill the many complex tasks, a protein kinase must bind to and recognize complex specificity determinants in the substrate besides just binding the phosphorylatable residue. This is reflected by the high variation in the substrate binding site architecture of the different protein kinases.

1.2.1. The Biological Rationale of Protein Phosphorylation

Phosphorylation is a versatile modification that can significantly alter the function of a target protein. It can modulate the catalytic activity of enzymes, it can lead to changes in subcellular localization, affect the half-life of proteins or promote protein/protein interactions. The last case can be illustrated by the epidermal growth factor (EGF) signaling. Binding of EGF to its cognate receptor triggers dimerization of

the receptor to induce trans-phosphorylation at multiple tyrosine residues. This in turn generates specific phosphotyrosine motifs that recruit additional EGF signaling components like the Grb2 adaptor protein through the binding of its SH2 domain to the phosphorylated receptor. In addition to Grb2, phosphatidylinositol 3-kinases (PI3Ks) bind to the phosphorylated EGF receptor via their SH2 domains to locally induce the production of PtdIns(3,4,5)P_3, which is necessary for the recruitment of Pdk1 and Akt to the plasma membrane. Finally, phospholipase Cγ also binds to phosphorylated EGF receptor via its SH2 domain leading to local production of diacylglycerol and Ins(1,4,5)P_3 (IP3). Again, the relevance of such phosphorylation-induced protein/protein interaction is underlined by the number and types of domains devoted to specifically recognize certain phosphorylation motifs [5]. The PTB domain also binds phosphotyrosine motifs, while 14-3-3 proteins and the WW and WD40 domains are necessary to bind specific motifs within phosphoserine residues.

Besides affecting protein/protein interactions, phosphorylation also induces changes in subcellular localization. This is well illustrated by many yeast transcription factors whose nucleo-cytoplasmic distribution is influenced by TORC1-dependent phosphorylation (see below) [6]. For example, phosphorylated Gln3 is kept in the cytosol by binding to its cytoplasmic repressor Ure2, but it rapidly translocates to the nucleus upon dephosphorylation [7]. Protein phosphorylation can also promote ubiquitin-mediated degradation of proteins. This is especially important for cell cycle proteins that must be quickly synthesized and efficiently degraded to ensure that a cell traverses the cell cycle in a regulated and unidirectional way. The yeast proteins Sic1, Far1, Cdc6, Cln1, Cln2 and Swe1 are recognized by an E3 ubiquitin protein ligase called the Skp1-Cdc53-F-box complex (SCF) only after they have been phosphorylated by the Cln-Cdc28 kinase [8]. Phosphorylation primes these proteins for subsequent degradation and ensures that the constitutively active SCF complex only degrades a specific subset of proteins, i.e. those that have been previously phosphorylated by the Cln-Cdc28 kinase.

Another interesting consequence of protein phosphorylation is the binding of positively charged ions to store cations. Phosvitin, an antioxidant protein that accounts

for more than 50% of the total proteins of egg yolk, contains more than 120 phosphoserines, which chelate iron to prevent the oxidation of yolk lipids [9].

1.2.2. Regulation of Protein Phosphorylation

Considering the pervasiveness and physiological relevance of protein phosphorylation it is expected that the biocatalyst responsible for this modification is tightly controlled to prevent aberrant phosphorylation/dephosphorylation. Likewise, it is not surprising that constitutively active protein kinases are responsible for several malignancies (e.g. Bcr-Abl kinase) and are exploited by some viruses to invade a host cell (e.g. v-Src kinase).

Protein kinases are almost always constitutively inactive and they are "switched on" only in response to specific stimuli. They are often subjected to multiple control mechanisms. A notable exception is the constitutively active casein kinase 2 which amazingly enough, phosphorylates more than 300 substrates [10]. There are multiple synergistic modes for keeping protein kinases silent in the basal, un-stimulated state. Some kinases have regulatory and catalytic domains in separate subunits. For example, protein kinase A (PKA) is a tetramer formed by two catalytic (C) and two regulatory (R) subunits. In its inactive state, all four subunits form the inactive R_2C_2 complex while binding of cAMP to the R subunits leads to dissociation of the regulatory subunits to liberate the active C subunits [11]. A similar logic is used by other kinases where regulatory and catalytic subunits or domains are *in cis*. In these kinases activation typically leads to conformational rearrangements to allow access of ATP to the active site. Also, regulatory subunits can act as activators instead of repressors of the kinase activity. This mechanism is used by cyclin-dependent kinases that, as the name implies, are active only when the cyclin subunits are bound to kinase subunits [12].

The aforementioned processes are often insufficient to fully activate a protein kinase. Frequently, protein kinases must be phosphorylated for full activity. This has

been extensively documented for AGC kinases, which are phosphorylated at three well-conserved positions: the activation loop (T-loop), the hydrophobic motif (HM) and the turn motif (TM). The activation loop is a protein segment that connects the N- and C-lobes of the kinase and is in close proximity to the ATP-binding pocket. This loop is connected to the N-lobe through an α-helix known as αC-helix. Phosphorylation of the activation loop by an upstream kinase (Pdk1 in mammals and Pkh1/2 in yeasts) leads to a conformational change in the αC-helix that allows the formation of hydrogen bond interactions crucial for the catalytic activity [13, 14]. Furthermore, phosphorylation of the hydrophobic motif by kinases other than Pdk1 (Pkh1/2), allows it to fold back in a hydrophobic pocket in the N-lobe, which leads to further stabilization of the αC-helix in the active conformation [14, 15]. Finally, turn motif phosphorylation helps stabilizing the rearrangements of the hydrophobic motif and therefore results in an even increased catalytic activity.

In summary, regulation of a protein kinase occurs only under specific circumstances. The many different requirements a protein kinase has to meet before becoming fully activated guarantee multiple-safe mechanisms to prevent aberrant phosphorylation.

1.3. The Eukaryotic Kinome

In analogy to the proteome, the term kinome is referred to the whole complement of kinases encoded by an organism [2]. Sequencing of the major eukaryotic genomes allows to classify the kinome into groups, families and subfamilies. Based on sequence similarities of the catalytic domains, the eukaryotic protein kinases can be divided into 8 groups: AGC, CaMK, CK1, CMGC, RGC, STE, TK and TKL [2]. The human AGC kinase group contains more then 60 different kinases, whereas the yeast genome encodes around 20 AGC kinases. The acronym “AGC” comes from three important and closely related kinase families: the protein kinase A, protein kinase G and protein kinase C.

Interestingly, the activity of all three kinases is allosterically regulated by second messengers [16]. PKC is usually activated by calcium ions and diacylglycerol (DAG) [17], whereas PKA and PKG respond to intracellular cAMP [11] and cGMP [18] levels, respectively. PKB, another important member of the AGC group is regulated by PtdIns(3,4,5)P_3 and PtdIns(3,4)P_2 [19]. The hallmark of the second group, the Ca^{2+}/calmodulin-dependent protein kinase (CaMK) group, is the regulation of the catalytic activity by calcium/calmodulin. The casein kinase (CK1) and the receptor guanylate cyclases (RGC) groups contain only a few but fundamental kinases. The RGC group is an evolutionary recent group since yeast and other lower eukaryotes do not encode RGC kinases. Interestingly both CK1 and RGC groups are enormously expanded in the worm kinome, containing around 80 and 30 different kinases, respectively [2]. The CMGC group owes its name to cyclin-dependent kinases (CDKs), mitogen-activated protein kinases (MAP kinases), glycogen synthase kinases (GSKs) and CDK-like kinases. This rather large group contains several essential kinases, whose aberrant expressions are often associated with pathological conditions [20]. The STE kinase group owes its name to the budding yeast Ste7, Ste11 and Ste20 kinases which are important regulators of the MAPK cascade. The tyrosine kinase (TK) group contains kinases that catalyze phosphate transfer onto tyrosine residues, a function which emerged only late in evolution. As a result, fungi do not encode these enzymes, although tyrosine phosphorylation exists due to the presence of dual specificity kinases. Finally, the tyrosine kinase-like (TKL) group comprises S/T kinases named so because of their close sequence similarity to tyrosine kinases. Like their close relatives, they are not present in fungi but they constitute the largest group in the plant kinome.

1.4. TOR, an Atypical Protein Kinase

In the eukaryotic kinome there are four additional kinase groups which do not share clear sequence similarity with the kinase groups introduced before. They are

therefore named atypical kinases. Among them is the phosphatidylinositolkinase-related protein kinase (PIKK) group. It contains kinases whose catalytic domain resembles the catalytic domain of lipid kinases (PI3K and PI4K) although they do not exhibit lipid kinase activity. The founding members of the PIKK group are Tor1 and Tor2, two protein kinases identified as target of the immunosuppressive drug rapamycin (hence the name Target Of Rapamycin). It is only thanks to rapamycin that these two protein kinases could be originally identified and characterized. Rapamycin, a macrocyclic lactone produced by the bacterium *S. hygroscopicus*, was initially classified as an antifungal agent but due to its immunosuppressive effects its use as an antifungal drug was abandoned. Remarkably, some years later rapamycin attracted much attention due to the discovery of its inhibitory activity on proliferating tumor cells. This made rapamycin very promising for clinical use but it was crucial to identify its cellular target and mode of action before submitting the compound to clinical trials. Since both yeast and mammalian cell growth was inhibited by rapamycin, yeast could be exploited to identify the cellular target of the drug. Therefore, a genetic screen in the yeast *S. cerevisiae* was performed to identify rapamycin resistant mutants [21]. Interestingly, the screen identified three different types of mutants: *fpr1*, *tor1* and *tor2* mutants. After some additional experiments it became finally clear that rapamycin was targeting and inhibiting Tor1 and Tor2 kinase activity upon formation of a complex with the proline isomerase Fpr1.

Biochemical purification of yeast Tor1 and Tor2 revealed that these proteins form two structurally and functionally different multiprotein complexes in the cell, TORC1 and TORC2 [22]. Both complexes are conserved in higher eukaryotes and they perform essential functions. Yeast TORC1 contains either Tor1 or Tor2 and the three proteins Lst8, Kog1 and Tco89 [22-24], whereas TORC2 contains Tor2 together with Lst8, Avo1, Avo2, Avo3 and Bit61 [22-24]. Interestingly, only the function of TORC1 is inhibited by rapamycin, which is probably the consequence of steric hindrance between the TORC2-specific components and the rapamycin/Fpr1 complex. But what is the function of the Tor kinases?

1.4.1. TOR, a Central Controller of Cell Growth

In the late 90s it became clear that TOR (Tor1 and Tor2) is involved in the control of cell growth [25]. This was a surprise as it was initially thought that cell growth was a passive process, in which a cell simply increases biomass in response to the availability of nutrients. Nowadays it is commonly accepted that both TORC1 and TORC2 are activated by nutrients and promote the accumulation of biomass via stimulation of anabolic processes and repression of catabolic processes. The anabolic processes favored by TORC1 are ribosome biogenesis, translation initiation, and nutrient import, whereas autophagy and stress response are among the catabolic processes inhibited by TORC1.

Arguably, ribosome biogenesis is the main anabolic process promoted by TORC1. In terms of energy consumption, ribosome biogenesis is a very "expensive process", since actively growing yeast cells produce on average 2,000 ribosomes per minute [26], requiring the coordinate synthesis and assembly of 78 different ribosomal proteins (RPs) and four rRNA molecules. This in turn necessitates the coordinate action of both RNA Pol I and RNA Pol III as well as additional factors, so-called ribosome biogenesis (RiBi) factors, to process, assemble and export to the cytosol the ribosomal subunits. RP and RiBi gene expression is dependent on RNA Pol II transcription. Therefore it is very reasonable that this process is tightly regulated in response to nutrient cues and, for instance, inhibited under unfavorable growth conditions. The regulation of ribosome biogenesis mainly occurs at the transcriptional level via the action of different transcription factors. Rrn3 is a RNA Pol I transcription factor and interestingly it was found to be degraded upon rapamycin treatment [27], therefore reducing RNA Pol I-mediated synthesis of rRNAs. TORC1 also controls the expression of RP genes via regulation of Fhl1 activity [28-30]. When TORC1 is active, the transcription factor Fhl1 binds to Ifh1 and stimulates RP gene transcription, while under unfavorable growth conditions Fhl1 associates with the corepressor Crf1, which blocks RP gene expression [28] (Figure 1.1). The activity of Crf1 is in turn controlled by TORC1 via the PKA/Yak1 signaling pathway [28]. Besides Fhl1, TORC1 regulates RP and RiBi gene expression via the transcription factor Sfp1, whose function is regulated at the level of subcellular

localization [31]. Active TORC1 directly phosphorylates Sfp1 and promotes its nuclear translocation, where Sfp1 associates with RP and RiBi gene promoters and stimulates their transcription [32] (Figure 1.1). Interestingly it seems that the Rab escort protein Mrs6 is further needed to allow Sfp1 nuclear translocation [32]. Finally TORC1 also regulates RP and Ribi gene expression via the kinase Sch9, which phosphorylates the transcription factors Dot6, Tod6 and Stb3 [33] (Figure 1.1). When TORC1 is active, Dot6, Tod6 and Stb3 are phosphorylated and inactive. Upon TORC1 inactivation they become dephosphorylated and bind RP and RiBi gene promoters to repress their transcription [33]. Furthermore, Sch9 and thus TORC1, positively regulates RNA Pol III-dependent tRNA transcription by phosphorylating and inactivating the Maf1 repressor [34, 35].

Besides promoting ribosome biogenesis, TORC1 positively affects translation initiation. Upon nutrient starvation, the phosphatase Sit4 is no longer repressed by TORC1 and it dephosphorylates and activates the Gcn2 kinase (Figure 1.1). This in turn promotes the phosphorylation of the α-subunit of the translation initiation factor eIF2, which down-regulates general mRNA translation and stimulates the selective translation of the transcription factor Gcn4 [36, 37]. Gcn4 translocation to the nucleus promotes the transcription of a group of genes coding for amino acid synthesis and amino acid permeases (see below). In addition, it seems that TORC1 is also involved in the regulation of Eap1 [38], an eIF4E-interacting protein resembling the mammalian 4E-BPs (Figure 1.1). All these processes also impinge indirectly on ribosome biogenesis, because processing of the 35S rRNA precursor into 25S, 18S, and 5.8S rRNAs requires ribosomal proteins [39]. As a consequence, reduced ribosome biogenesis is caused by both, decreased general translation and decreased rRNA processing.

In accordance with the involvement of TORC1 in promoting cell growth, it is not surprising that this complex also controls cellular nutrient uptake. This is accomplished by the coordinate expression of more than 250 different membrane transporters and permeases [40]. The involvement of TORC1 in the regulation of permease gene expression has been initially demonstrated by transcriptomic experiments [41, 42] and further characterized by more targeted experiments, which revealed that active TORC1

promotes, via inhibition of Sit4, the cytoplasmic retention of the GATA transcription factors Gln3, Gat1 and Dal81 [6, 43-45] (Figure 1.1). As soon as TORC1 senses nutrient starvation, the GATA transcription factors translocate to the nucleus where they stimulate expression of the so-called nitrogen catabolite repression (NCR) genes (e.g. low-affinity permeases, enzymes involved in allantoin and urea metabolism, etc.). Moreover, active TORC1 also regulates the stability of amino acid permeases at the plasma membrane. When TORC1 is inhibited, the phosphatase Sit4 dephosphorylates and activates the Npr1 kinase which in turn stabilizes the general amino acid permease Gap1 at the plasma membrane [46, 47] (Figure 1.1). Vice versa, many high-affinity permeases like the tryptophane-specific permease Tat2 are degraded by ubiquitin-mediated endocytosis. Furthermore, TORC1 inactivation leads to the selective translation of Gcn4 mRNA, a transcription factor involved in the expression of amino acid biosynthesis and permease genes [36].

TORC1, via the transcription factors Rtg1 and Rtg3, also regulates the cellular balance of glutamate and glutamine, two fundamental metabolites necessary for the synthesis of amino acids. Under favorable growth conditions, Rtg1 and Rtg2 are sequestered in the cytosol upon binding to Mks1 and the 14-3-3 proteins Bmh1/2 (Figure 1.1) [48-50]. When TORC1 is inactive, the protein Rtg2 binds to the Rtg1/Rtg3/Mks1 complex to liberate Rtg1/3 which subsequently enter the nucleus, where they promote the expression of the so-called retrograde response pathway (RTG) genes. These genes are particularly important when yeast cells grow in the presence of glucose and nitrogen compounds requiring α-ketoglutarate for assimilation.

As already mentioned, TORC1 not only promotes anabolic processes but also prevents catabolic processes. Among the latter is autophagy that guarantees the recycling of nutrients from degradation of non-essential cellular components. This is vital for the cell to endure and survive periods of nutrient limitation and TORC1 is an important modulator of this process. Under favorable growth conditions TORC1 promotes Atg13 phosphorylation, which leads to its dissociation from the Atg1 kinase and to suppression of autophagy (Figure 1.1) [51]. On the contrary, TORC1 inactivation leads to

dephosphorylation of Atg13 and its subsequent binding to Atg1, an essential requirement for the induction of autophagy [52].

TORC1 also negatively regulates stress response by nutrient limitation. The stress response is mainly regulated at the transcriptional level via expression of proteins required to survive periods of stress [53]. This is accomplished by the transcription factors Msn2 and Msn4, which are usually retained in the cytoplasm when TORC1 is active [6]. They quickly translocate to the nucleus in response to nutrient starvation, via a Sch9-dependent activation of the Rim15 kinase [54, 55] (Figure 1.1).

In conclusion, there is ever-increasing evidence of the positive effects of TORC1 on cell growth, which directly or indirectly controls the activity of kinases and phosphatases and the nucleo-cytoplasmic distribution of transcription factors. However, considering the central role of the TORC1 pathway in regulating cell growth, it is likely that TORC1 signaling is connected to other major signaling pathways. It integrates many cellular inputs into a large network for the control of cellular homeostasis (see below).

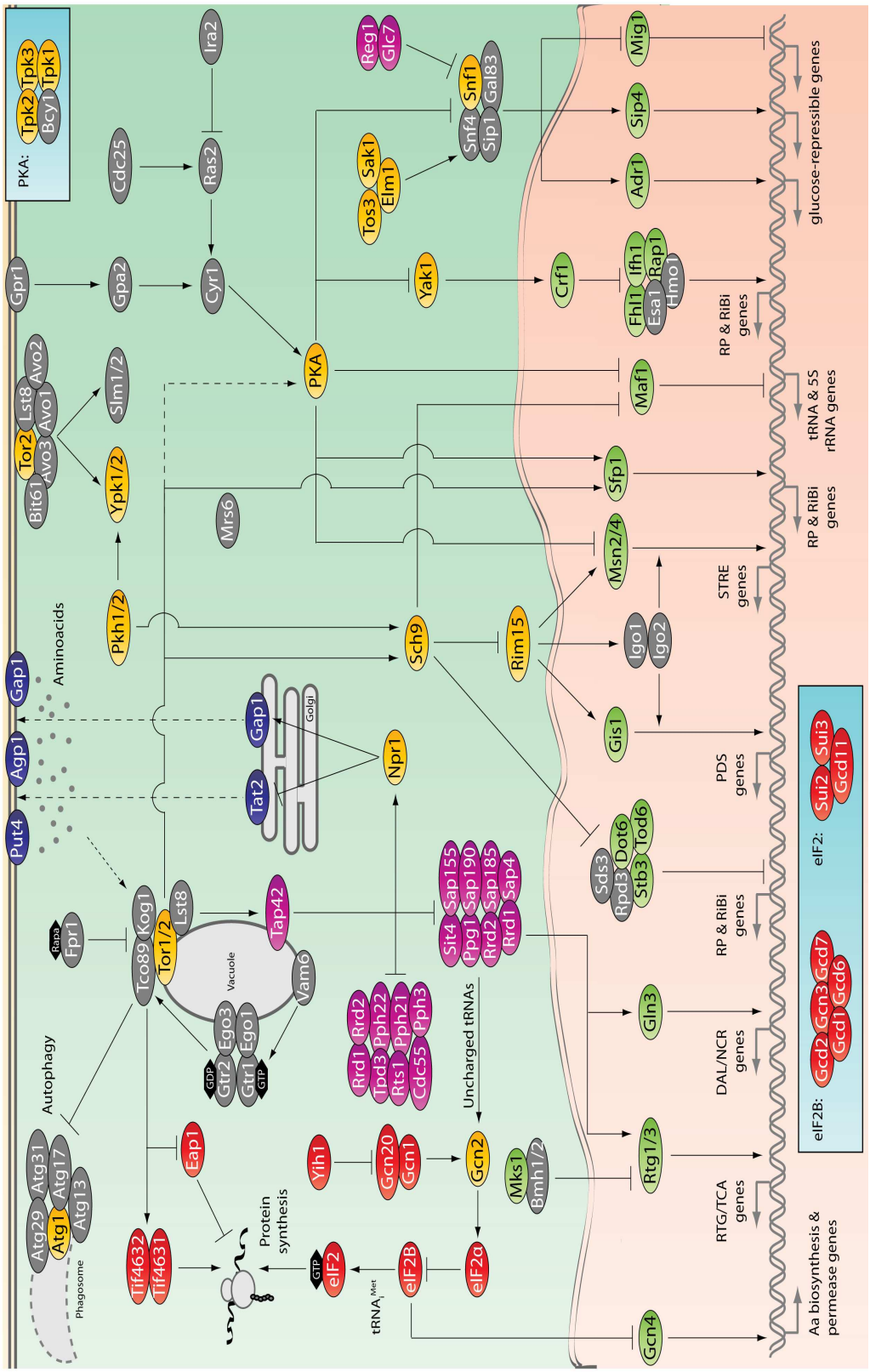

Figure 1.1: The TORC1 signaling pathway in *S. cerevisiae*. Kinases are in yellow, phosphatases and phosphatase-regulatory proteins in purple, proteins regulating transcription in green, proteins regulating translation in red and permeases in dark blue. The inserts represent the single subunits of the protein complexes eIF2B, eIF2 and PKA.

1.4.2. TOR, a Signaling Pathway by its Own?

Evidence supporting the view that the TORC1 is connected to other signaling pathways stems from genetic studies showing a connection between TORC1 and PKA signaling. For example, the Sch9 kinase, one of the few direct substrates of TORC1, has been originally characterized as a multi-copy suppressor of the PKA mutants *cdc25-1*, *cyr1Δ*, *ras1Δras2Δ* and *tpk1Δtpk2Δtpk3Δ* [56]. In accordance with these findings, other genetic studies showed that cells with a hyperactive PKA pathway (e.g. *ira1Δira2Δ*, *bcy1Δ* or $RAS2^{V19}$) are more resistant to rapamycin. Also, the repression of RP genes induced by rapamycin in such cells is less prominent than in wild type cells [57]. Conversely, cells with impaired PKA signaling (e.g. *tpk1Δ*, *tpk1Δtpk2Δ*, *tpk1Δtpk3Δ*) are more susceptible to rapamycin and have impaired RP gene expression [57]. In addition, deletion of *MSN2* and *MSN4* in combination or alone [58] and deletion of *RIM15* [59] rescues the growth defect of yeast mutants with reduced PKA signaling [58]. Similarly, the localization of the transcription factors Msn2 and Msn4 is affected by both TORC1 and PKA signaling [6, 58, 60] (Figure 1.1). Indeed, both rapamycin treatment and impaired PKA activity lead to their nuclear translocation with subsequent expression of stress-inducible (STRE) genes. Furthermore, the interplay between TORC1 and PKA becomes more explicit considering that rapamycin treatment causes a rapid accumulation of the PKA catalytic subunit Tpk1 in the nucleus [61].

Additional support for the idea of a connection between TORC1 and PKA signaling comes from the nucleo-cytoplasmic distribution of Sfp1 and Crf1 (Figure 1.1). As mentioned above, Sfp1 is mainly nuclear under favorable growth conditions but quickly translocates to the cytosol when TORC1 is inhibited. Interestingly, in *bcy1Δ* cells, Sfp1 remains in the nucleus even after rapamycin treatment [31]. Nevertheless, Sfp1 can still partially localize to the nucleus in cells with down-regulated PKA signaling and its localization is still sensitive to rapamycin, which means that TORC1 and PKA act on Sfp1 in a different way [31]. Similarly, the corepressor Crf1 is mainly nuclear when rapamycin is added to yeast cells but this is no more the case in both bcy1*Δ* and $RAS2^{V19}$ cells [28]. Finally, there is evidence showing that Maf1, Atg13 and Rim15 are all

common targets of TORC1 and PKA (Figure 1.1). Inhibition of either TORC1 or PKA leads to Maf1 dephosphorylation and its nuclear translocation and both TORC1 and PKA independently modulate Atg13 phosphorylation [62]. Rim15 is also targeted by both TORC1 and PKA. TORC1 promotes the cytosolic retention of Rim15 and PKA inactivates Rim15 by direct phosphorylation [59, 63].

1.4.3. Direct *Versus* Indirect TORC1 Targets

In spite of the many biological processes controlled by TORC1, the identification of direct TORC1 substrates has lacked behind. Today, only three direct targets of TORC1 have been identified in yeast, while around ten substrates have been found in mammalian cells. The three direct TORC1 targets in yeast are Tap42, Sch9 and Sfp1 (Figure 1.1) [32, 64-67]. Tap42 is a regulator of PP2A and PP2A-like phosphatases and is responsible for controlling the phosphorylation state of Npr1 [47], Rtg1 and Rtg3 [68], Gln3 [69], Gat1 [44], Msn2 and Msn4 [60], and Gcn2 [36]. Sch9 is an AGC kinase that directly phosphorylates Rim15 [63], Maf1 [34] and the repertoire of Sch9 targets has recently been extended to Stb3, Dot6 and Tod6 [33]. Sfp1 is a transcription factor involved in the regulation of RP and RiBi genes [32]. Sch9 and Tap42 are by far the best characterized targets of TORC1 and genetic evidence suggests that they represent the major signaling branches downstream of TORC1. Indeed, cells co-expressing the *tap42-11* and $SCH9^{DE}$ alleles are hyperresistant to rapamycin [34].

The exact mechanism through which TORC1 phosphorylates and regulates the activity of Tap42 is not well understood. The model that fits the observations best suggests that TORC1 phosphorylates Tap42 to enhance its interaction with the catalytic subunits of PP2A (i.e. Pph21 and Pph22) and PP2A-like (i.e. Sit4) phosphatases, which results in inhibition of the phosphatase activity [64]. This model nevertheless, has its caveats. Firstly, yeast cells contain ten times more PP2A phosphatases than Tap42, which means that Tap42 cannot be a stoichiometric inhibitor of the PP2A phosphatases.

Secondly, Tap42 dephosphorylation following rapamycin treatment has a much slower kinetic (50% reduction after 30 minutes) than phosphatase inactivation (< 10 minutes). A possible answer to these conflicting findings is that Tap42 is a positive rather then a negative regulator of PP2A and PP2A-like phosphatases [70]. In this model rapamycin treatment induces a release of phosphorylated Tap42 from TORC1, which is then free to bind and activate the phosphatases. The signal response is eventually terminated by slow dephosphorylation of Tap42. This model is supported by the fact that Tap42 associates at the membrane with TORC1 and quickly (< 10 minutes) dissociates from the membrane upon rapamycin treatment [70]. Furthermore, it has been shown that once in the cytosol, dephosphorylation of Tap42 and Tap42-PP2A disassembly occurs with comparable kinetics (about 30 minutes) [70].

Regulation of phosphatases by TORC1 has been further complicated by the discovery of Tip41 [71]. Tip41 is a negative regulator of TORC1 signaling. Deletion of *TIP41* confers rapamycin resistance, suppresses the growth defect of a *TAP42* mutant (*tap42-11*), prevents dissociation of Tap42 from Sit4, causes Npr1 hyperphosphorylation and promotes Gln3 retention in the cytoplasm [71]. However, since deletion of *TIP41* has no effect on cell growth it is unlikely that it is a central regulator of TORC1 signaling. In addition, active TORC1 results in phosphorylation of Tip41 and reduced binding of Tip41 to Tap42, suggesting that Tip41 must first be dephosphorylated to interact with Tap42. However, it has never been demonstrated that (i) Tip41 dephosphorylation occurs with the same kinetics as activation of the phosphatases and (ii) that Tip41 becomes directly phosphorylated by TORC1.

The regulation of the second TORC1 substrate, Sch9, is much better understood [66]. There is evidence showing that TORC1 phosphorylates Sch9 *in vivo* and *in vitro* on at least six different positions (S711, T723, S726, T737, S758 and S765) clustered in the C-terminus of the protein [66]. These data show that the sequence determinants leading to substrate phosphorylation by TORC1 are less stringent than those used by other kinases. TORC1 seems to have a preference for serines and threonines surrounded by bulky hydrophobic residues at the -4, +1 and +2 position. Similar to Tap42, Sch9 is an important regulator of cell growth and ribosome biogenesis [66].

1.5. The Search for Protein Kinase Substrates

Even though a number of direct TOR targets have been identified, it is conceivable that the TOR proteins must have many more substrates to fulfill the multitude of tasks associated with the control of cellular growth and homeostasis. The search for kinase substrates has proven to be difficult. Many methods exist such as genome-wide screening of kinase substrates spotted on proteome arrays using recombinant protein kinases [72] or the KESTREL (kinase substrate tracking and elucidation) method [73]. In a KESTREL assay a cell lysate is fractionated, typically via anion exchange chromatography, to reduce sample complexity and the resulting fractions are incubated in presence radioactive ATP with the exogenously added kinase. The major problem associated with the KESTREL assay is that a cell lysate contains endogenous kinases which are able to phosphorylate several substrates upon incubation with radioactive ATP, which is causing a high background. An interesting alternative to the KESTREL is the “chemical genetic” approach developed by the Kevan Shokat’s laboratory [74]. Briefly the kinase of interest is mutated by substituting a conserved bulky residue in the ATP-binding pocket with a smaller residue that allows the mutant kinase to use a bulky radioactive ATP analogue for phosphate transfer. In this way only the target(s) of the mutant kinase are phosphorylated thereby reducing background phosphorylations. This technique has been further improved by using ATP analogues that lead to tiophosphorylation instead of phosphorylation of the target substrates. In this way the tiophosphorylated proteins are digested and the resulting thiophosphorylated peptides can be enriched using iodoacetyl-agarose beads for LC-MS/MS analysis [75].

In spite of all these technological improvements, it remains a cumbersome task to screen and identify the physiological substrates of protein kinases. Recent developments in mass spectrometry have shifted the focus towards the sampling of phosphoproteomes from cells treated with specific protein kinase inhibitors to identify differentially phosphorylated kinase effectors. Several elaborate workflows exist for the quantitative analysis of phosphoproteomes from untreated and inhibitor-treated cells. They are often relying on phosphoprotein or phosphopeptide enrichment strategies coupled with high-

resolution mass spectrometry. These large-scale phosphoproteomic workflows have caused a true data explosion over the past decades in regards to the analysis of phosphorylation events in cells. Nevertheless, before becoming a robust and reliable methodology, a number of obstacles needed to be solved.

Analysis of protein phosphorylation by mass spectrometry remains a challenge for at least three reasons. First of all the stoichiometry of protein phosphorylation is usually low. Consequently, only a fraction of the total protein population in a cell carries the modification. To make things worse, certain proteins, especially transcription factors and signaling proteins, are only present in low copy numbers. Moreover, proteins are usually heterogeneously phosphorylated, which means that at any moment in a cell multiple isoforms of the same phosphoprotein coexist. As a result, phosphorylation analysis of complex samples usually leads to the identification of only major phosphorylation sites from highly expressed proteins. To circumvent this problem, several strategies have been developed over the last two decades. In the following two sections these strategies will be reviewed. The first section centers on advances achieved in phosphoprotein and phosphopeptide enrichment aimed at tracing low stoichiometry phosphorylation sites. The second section reviews mass spectrometric advances in analyzing phosphopeptides.

1.5.1. The Search for the Needle in the Haystack

Over the years many techniques have been developed to trace low stoichiometry phosphorylation sites in complex digests of proteins. These are either aimed at enriching phosphoproteins or phosphopeptides. Although the goal of both approaches is the same, there are substantial differences between the enrichment of phosphoproteins and phosphopeptides. First of all, the enrichment of phosphopeptides generates less complex mixtures than the digests of enriched phosphoproteins. At first sight phosphopeptide enrichment is preferred over phosphoprotein enrichment. On the other hand, it implies that the identification of the corresponding proteins after phosphopeptide enrichment

critically hinges on the identification of just the phosphopeptides and therefore requires very stringent search criteria. Phosphoprotein enrichment has also some intrinsic drawbacks. In the first place, the amount of phosphate groups per protein is much lower than the amount of phosphate groups per peptide, which makes the enrichment of phosphopeptides more selective. Moreover, in contrast to phosphopeptides, working with phosphoproteins is complicated by their instability at high and low pH, high temperatures and their susceptibility to organic solvents. As a result, nowadays more alternatives exist for phosphopeptide enrichment in comparison to phosphoprotein-based enrichment strategies.

Enrichment of phosphoproteins is usually performed with phospho-specific antibodies. The use of antibodies is usually restricted to the analysis of tyrosine phosphorylation because anti-phosphoserine and anti-phosphothreonine antibodies are generally of low specificity, probably due to lower immunogenicity of the phosphoserine and phosphothreonine epitopes compared to the bulky phosphotyrosine antigen. This problem can be circumvented using antibodies that recognize phosphorylated serines or threonines surrounded by specific residues, like antibodies to phospho-SQ or phospho-TQ [76]. Another alternative is the use of protein domains that reversibly bind phosphorylated residues, like WW, FHA, SH2 and PTB domains. A third experimental strategy enriches phosphoproteins by β-elimination of the phosphate group to generate dehydroalanine or dehydroaminobutyric acid which in turn reacts with biotin-labeled ethanedithiol [77]. The main advantage of this approach is the ease with which biotinylated phosphopeptides can be isolated via avidin affinity purification. The major drawback is the production of protein degradation products due to the strong alkaline conditions used for β-elimination as well as the occurrence of unwanted side reactions that further complicate MS/MS spectra identification (e.g. reaction of cysteines with biotin, oxidation of methionines and tryptophanes).

As already mentioned above, a wider panel of methods is at hands to enrich phosphopeptides. Analogous to phosphoproteins, phosphopeptides can be enriched via chemical derivatization and much effort has been spent to supply the researcher with a variety of methods [78, 79]. However, as with phosphoproteins, these techniques suffer

from unwanted side reactions. The most widely used and robust approach to enrich phosphopeptides is based on the affinity of phosphate groups for positively charged metal ions (typically iron or gallium). Such ions can easily be immobilized on chelators covalently coupled to a solid matrix. This approach, which was used in the present study, is called Immobilized Metal Affinity Chromatography (IMAC) [80]. All IMAC resins suffer from unspecific binding of peptides rich in aspartic and glutamic acid residues. To avoid this problem, the acidic side chains in peptides are sometimes esterified with methanolic HCl to convert them to uncharged methyl esters [81]. This reaction is, like all chemical reactions, prone to side reactions like deamidation of asparagines and glutamines. Moreover, the low pH used to methylesterify the peptides and the requirement to remove water from the sample can lead to a very low peptide recovery. A second very widespread technique to enrich phosphopeptides makes use of metal oxides like titanium dioxide or zirconium oxide and is called metal oxide affinity chromatography (MOAC). Similar to IMAC, unspecific binding of acidic residues to TiO_2 and ZrO_2 occurs, but can be prevented by methylesterification or by using additives during peptide binding [82]. Importantly, both IMAC and MOAC produce complementary results and are therefore often used in parallel [83]. Alternatively, they can be used sequentially, where IMAC is usually performed as the first step of enrichment and the flow-though is further enriched via MOAC [84]. Both enrichment techniques, IMAC and MOAC, have been used in conjunction with orthogonal fractionation techniques like strong cation exchange (SCX) chromatography or hydrophilic interaction chromatography (HILIC). Both techniques already pre-concentrate phosphopeptides and are very useful to improve the selectivity of IMAC and MOAC. Workflows with various combinations like SCX followed by IMAC [85], SCX followed by TiO_2 [86] or HILIC followed by IMAC [87] have been described that yield comprehensive phosphoproteomes from cell cultures and organs. Unfortunately a study that systematically compares these different approaches does not exist nowadays and it is therefore difficult to objectively conclude which approach yields the best results.

1.5.2. Phosphopeptide Analysis by Mass Spectrometry

Phosphopeptide analysis by mass spectrometry is not straightforward for several reasons. The two main challenges are the sequence identification of a phosphopeptide and the precise localization of the phosphorylation site within the peptide sequence. In fact phosphopeptides do not fragment as well as their unphosphorylated counterparts when they are subjected to collision-induced dissociation (CID).

During CID peptide ions are accelerated in the vacuum followed by a collision with inert gas molecules (usually helium or molecular nitrogen), which transforms the kinetic energy into vibrational energy necessary to break the chemical bonds. Such a fragmentation usually takes place at amide bonds and produces b- and y-ions [88], although the exact fragmentation pattern can vary significantly according to the peptide sequence, the number of arginines and lysines per peptide and the charge state [89]. Fragmentation at amide bonds can be explained by the so called „mobile proton" model [90]. This model states that during excitation, protons that were previously sequestered by arginines and lysines become mobile and protonates sites that were energetically less favored like amide oxigens and nitrogens. These protonation events weaken these bonds to induce dissociation and generation of b- and y-ions. In reality, certain amino acids affect the proton localization and favor cleavage at specific sites [89]. This means that fragmentation spectra are never a product of random cleavages of the amide bonds. The „mobile proton" model also explains the atypical fragmentation observed for many phosphopeptides, which is characterized by dominant peaks corresponding to the neutral loss of phosphoric acid (H_3PO_4) from the precursor ions and reduced backbone fragmentation (Figure 1.2A). The reason of this observation lies in the energetically favored reaction leading to phosphate loss compared with backbone fragmentation at the amide bond promoted by the "mobile proton".

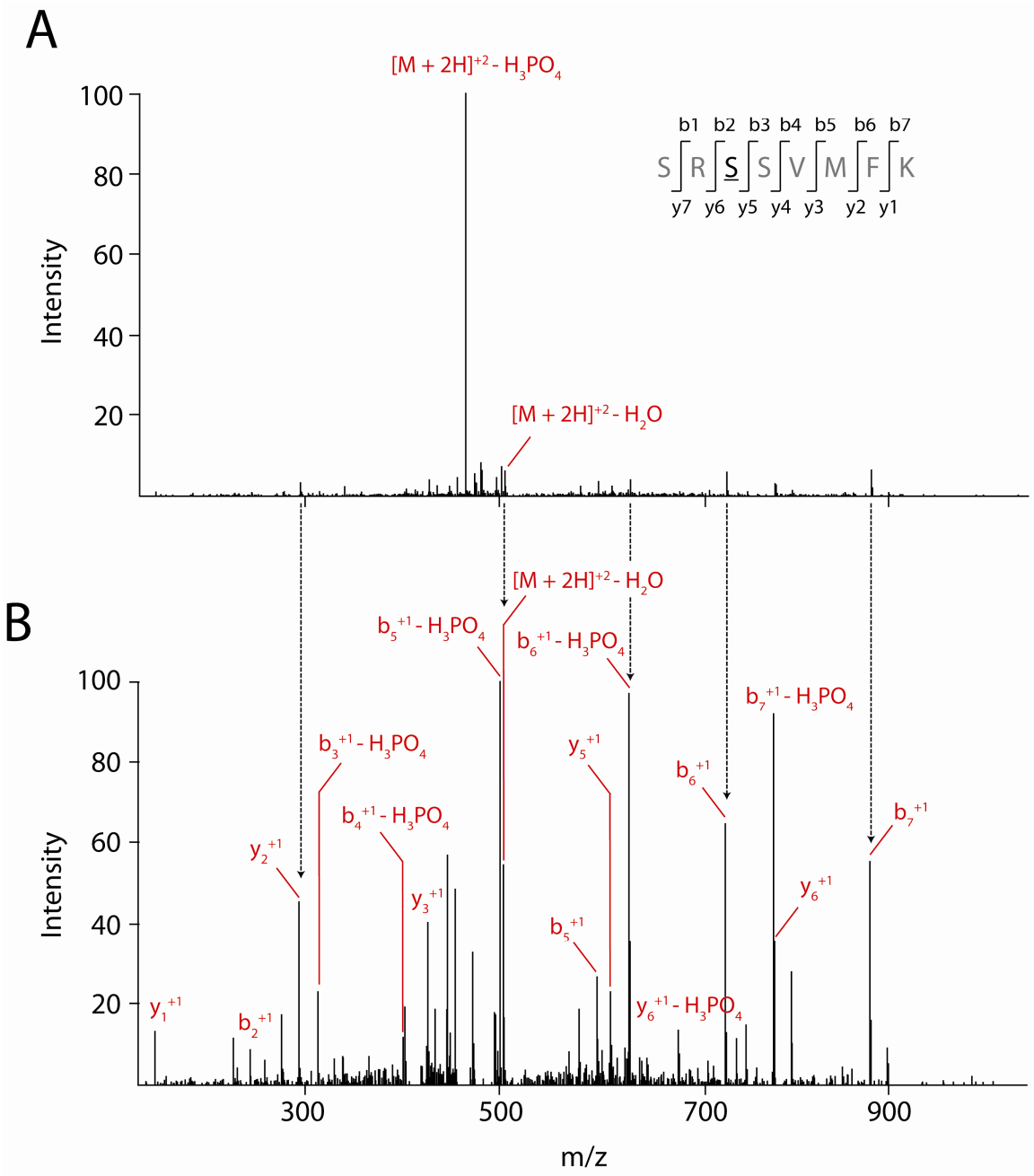

Figure 1.2: CID MS/MS spectra of the yeast phosphopeptide SRSSVMFK (derived from Bcy1). MS/MS spectrum acquired with standard activation parameters (35% normalized collision energy for 30ms) (A) without MSA and (B) with MSA.

Interestingly, during fragmentation of different phosphopeptides there is considerable variation in terms of neutral loss and peptide backbone fragmentation that depends on the chemical composition of the phosphopeptide, its charge state and the collision energy used to activate the precursor ion. For example, neutral loss ions are almost entirely absent in phosphotyrosine-containing peptides because the aromatic ring sterically hinders the chemical bond rearrangements required for the neutral loss product. In addition, the φ-O bond in phosphotytosine does not readily break because it is stabilized by the resonance of the benzene ring. Another important parameter affecting neutral loss is the charge state of the precursor ion. Usually the intensity with which neutral loss occurs decreases with increasing charge because more "mobile protons" are available for backbone fragmentation at higher charge states (Figure 1.3). Moreover, since neutral loss formation is favored over backbone fragmentation because it requires less energy, it is conceivable that mild excitation methods favor the formation of neutral loss over high energy activation methods. This is indeed the case when phosphopeptides are fragmented at lower collision energy and longer activation times in an ion trap (Figure 1.2A).

In conclusion, phosphopeptide fragmentation differs from the fragmentation of non-phosphorylated peptides. This is a consequence of the neutral loss of H_3PO_4 from the side chains of serines and threonines, which competes with backbone fragmentation. Nevertheless, there are many factors influencing the extent to which neutral loss occurs. The chemical composition of the ion (phosphotyrosine-containing peptides do not show a neutral loss), the charge state and the collision energy all determine the fragmentation behavior of phosphopeptides. But which are the consequences of neutral loss on phosphopeptide identification?

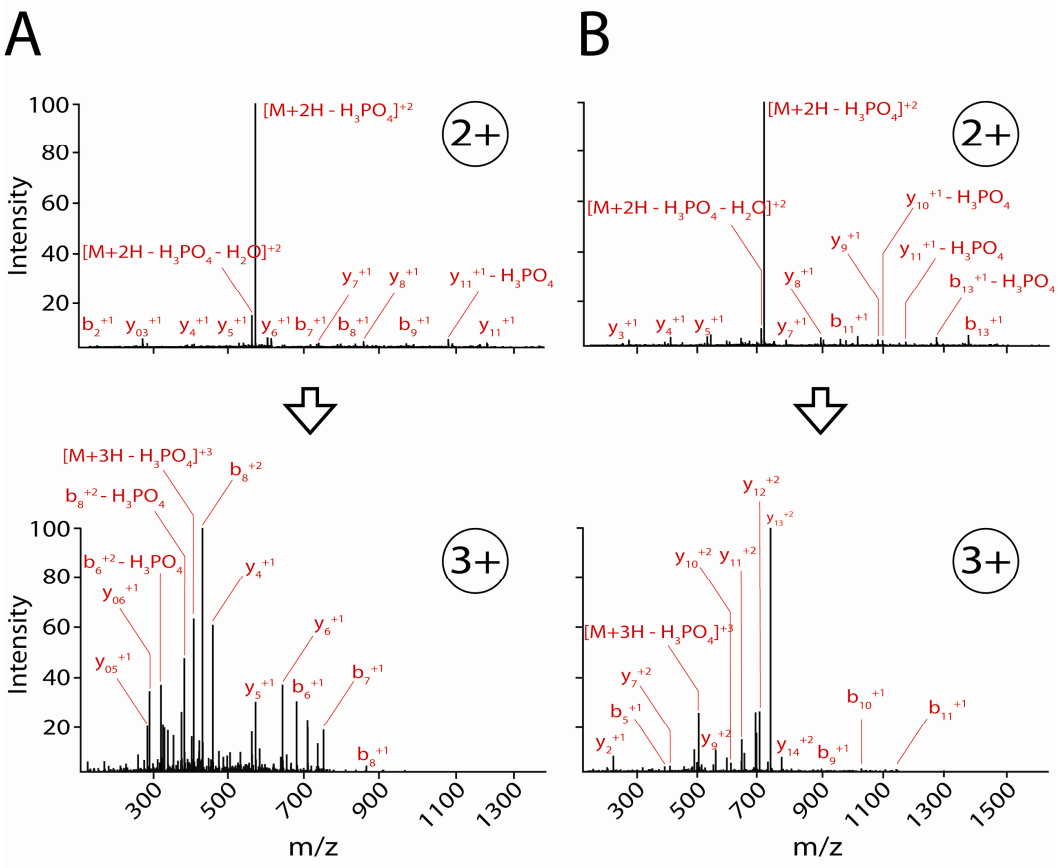

Figure 1.3: Neutral loss intensity decreases with increasing peptide charge state. MS/MS spectra of (A) the tryptic Srf1 phosphopeptide KSGSLEALQNAK and of (B) the tryptic Rnr2 phosphopeptide AAADALSDLEIKDSK.

The major problem is that neutral loss predominates and thereby reduces backbone fragmentation. The few available fragment ions hamper peptide sequence identification and consequently unambiguous phospho-site localization. Indeed, the localization of the site of phosphorylation requires the presence of specific diagnostic backbone fragments in a MS/MS spectrum. This is shown in Figure 1.4, where the presence of a given set of ions (in red) allows to pinpoint the phosphorylation site to a specific residue while excluding a different localization. To circumvent the problem of neutral loss, alternative fragmentation methods have been developed for

phosphopeptides. The most common is the use of MS^3 fragmentation [91, 92], multistage activation (MSA) [93], electron capture dissociation (ECD) [94] and electron transfer dissociation (ETD) [95]. MS^3 fragmentation and MSA are very similar in the sense that both methods require two steps of ion activation. In the case of MS^3 fragmentation the precursor ion that underwent neutral loss is isolated and subsequently fragmented. Since neutral loss of H_3PO_4 can no longer occur, backbone fragmentation is favored. MS^3 has the disadvantage of increasing the duty cycle and that sometimes contradictory sequences are assigned to the same MS^2/MS^3 spectrum pair. To circumvent this problem MSA was developed, where the ion that underwent neutral loss is activated while the fragment ions from the precursor are still present in the trap. This results in a composite spectrum that is the product of the MS^2 and MS^3 spectra (Figure 1.2B). Since in MSA the fragment ions derived from the precursor ion are trapped together with those generated by the neutral loss ion, MSA spectra have increased signal intensities and a greater number of structurally diagnostic ions compared to MS^3 fragmentation. Interestingly, in a study where normal MS^2 fragmentation was compared with MS^3 and MSA fragmentation it was found that all three produce redundant data, therefore reducing the benefits of doing MS^3 and MSA [96]. This is probably a consequence of the increased duty cycle of MS^3 and MSA over MS^2. In addition, even in a MS^2 spectrum containing a dominant ion derived from neutral loss, weak backbone fragmentation is still present (Figure 1.2A), allowing reliable sequence identification and reducing the benefits of performing MSA or MS^3 fragmentations. This phenomenon will probably improve even more over time with the development of new ion traps with increased ion trapping capacities.

Finally, there are two more fragmentation methods said to reduce neutral loss while preserving backbone fragmentation: ECD and ETD. The main common feature between the two methods is the use of electrons to dissociate peptide ions. As a consequence ECD and ETD MS/MS spectra differ significantly from CID MS/MS spectra with respect to the type of ions formed. Especially, ECD and ETD spectra contain c- and z-ions instead of the usual b- and y-ions observed in CID. A particular advantage of ECD/ETD over CID is that much less neutral loss of phosphate occurs so that spectra rich in diagnostic backbone ions are generated. This is extremely helpful when a phosphorylation site needs to be localized and it seems that ECD and ETD are designed

to completely replace CID for phosphopeptide analysis. However, it has been shown that ECD/ETD and CID produce complementary results. In a large-scale study comparing ECD with CID [97] the results were more in favor of CID concerning the total number of phosphopeptide identifications. This puzzling observation can be explained by the use of trypsin for protein digestion, which tends to produce doubly charged peptide ions. Since the cross-section of an ion that can capture an electron is proportional to the square of its charge [98], the doubly charged peptides produced by trypsin cleavage tend to fragment suboptimally during ECD/ETD. Another explanation concerning the poor performance of ECD/ETD over CID is the fact that the major search engines (e.g. Sequest, Mascot) have been initially designed for CID MS/MS spectra obtained in ion traps or time-of-flight mass spectrometers. Finally, 50 times more ions are required for ECD than CID, which increases the duty cycle and reduces the benefit of ECD for the analysis of complex phosphopeptide samples [97]. Nevertheless, even though ECD performed less efficiently than CID, its potential for unambiguous phospho-site localization is well appreciated in the proteomic community [97]. It should be also considered that ECD is typically performed on a Fourier transform ion cyclotron resonance (FTICR) mass spectrometer which records spectra with much higher mass accuracy than ion trap mass spectrometers.

The fact that CID and ECD/ETD produces complementary results, prompted researchers to use both fragmentation technologies in a decision-tree-based MS approach [99]. In this way the benefit of ETD for the fragmentation of large peptides with high charges is combined with the optimal performance of CID for the fragmentation of small peptides with low charges. Another way to circumvent the reduced performance of ECD/ETD for the fragmentation of ions with low charges is the use of alternative proteases, for instance endoproteinase Glu-C and Lys-C [100, 101]. However, the final outcome of phosphopeptide identifications by the use of alternative proteases in conjunction with ETD was very modest [101]. As a result, the use of CID coupled with MSA seems to be so far still the best choice for the analysis of phosphopeptide samples, which also explains its wide-spread use for large-scale phosphorylation studies. On the other hand, ECD and ETD are being improved continuously and it is foreseeable that they will be used more and more as an alternative to CID in future phosphoproteomic studies.

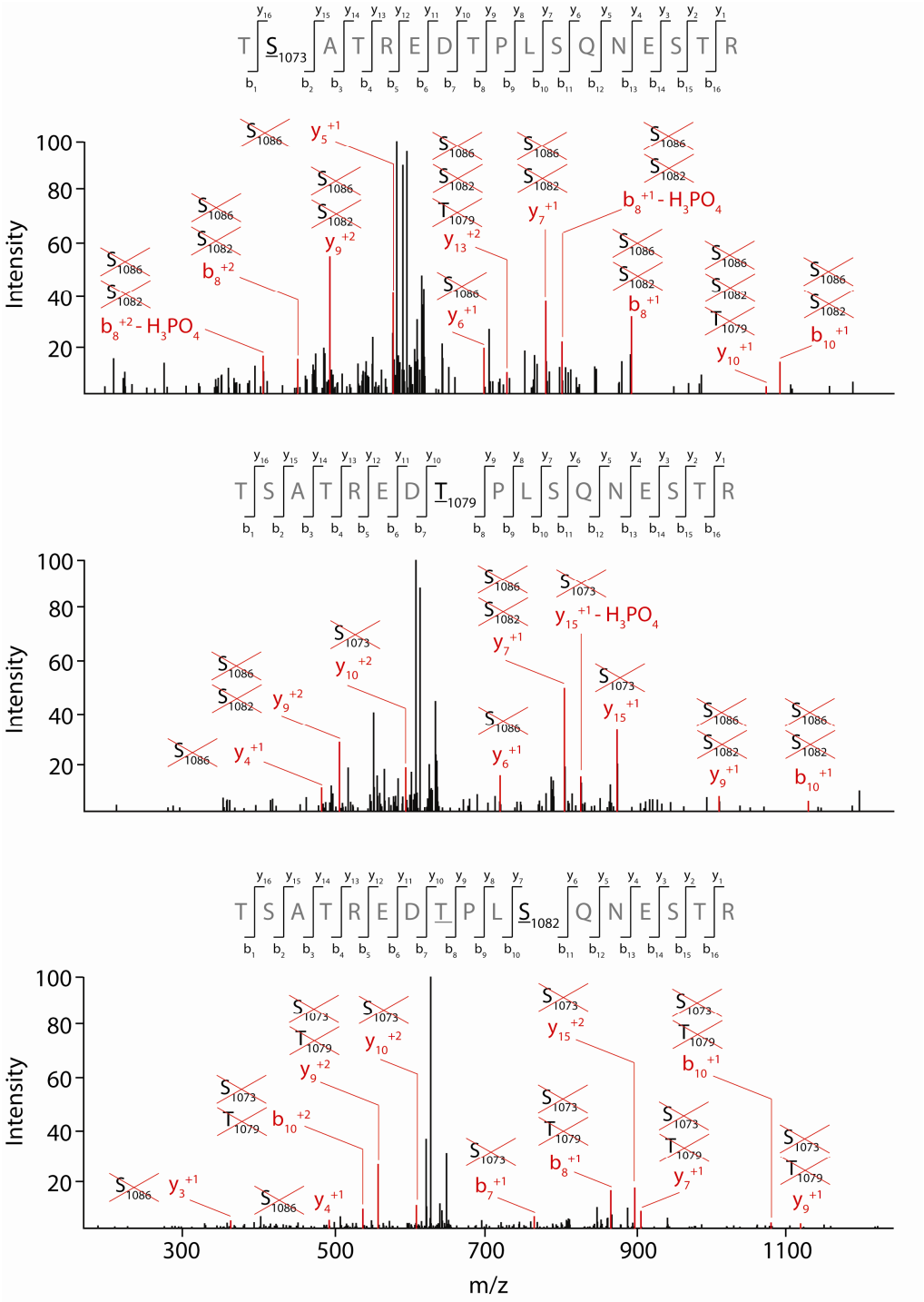

Figure 1.4: MS/MS spectra of three phospho-isoforms of the same peptide (TSATREDTPLSQNESTR derived from Isw2). Detection of specific diagnostic ions (in red) allows to localize in a reliable way the residues carrying the phosphate.

2. Materials and Methods

2.1. Yeast Strains, Media, and Genetic Manipulations

The *S. cerevisiae* strains used in this work are listed in Table 2.1. All constructed strains are isogenic to TB50. Yeast manipulations, including cell cultures, sporulation, tetrad dissections, and genetic techniques, were carried out essentially as described [102]. Cells were grown either in rich YPD medium (1% yeast extract, 1% peptone, 2% glucose, and 2% agar for solid media) or minimal synthetic medium (6.7 g yeast nitrogen base per liter, 2% glucose, relevant amino acids for plasmid maintenance, and 2% agar for solid media). If not stated otherwise, the synthetic medium used for plasmid maintenance contained all amino acids except uracil. Yeast nitrogen base, yeast extract, peptone and agar were purchased from BD Biosciences while amino acids were from Sigma.

Name	**Genotype**	**Ref.**
TB50a	*MATa leu2 ura3 rme1 trp1 his3Δ GAL+ HMLa*	Lab strain
TB50a/@	*MATa/@ leu2/leu2 ura3/ura3 rme1/rme1 trp1/trp1 his3Δ/ his3Δ GAL+/GAL+ HMLa/HMLa*	Lab strain
TB105-1c	*MATa leu2 ura3 rme1 trp1 his3Δ GAL+ HMLa gln3::kanMX4 gat1::HIS3MX6*	Lab strain
AN9-2a	*MATa leu2 ura3 rme1 trp1 his3Δ GAL+ HMLa tor1::kanMX4*	Lab strain
YPJ2	*MATa leu2 ura3 rme1 trp1 his3Δ + HMLa arg4::His3MX6 lys1 ::KanMX4*	This study
YAC1	*MATa leu2 ura3 rme1 trp1 his3Δ GAL+ HMLa hal5::KanMX4*	This study
YAC2	*MATa leu2 ura3 rme1 trp1 his3Δ GAL+ HMLa isw2::KanMX4*	This study
YAC3	*MATa leu2 ura3 rme1 trp1 his3Δ GAL+ HMLa kkq8::KanMX4*	This study
YAC4	*MATa leu2 ura3 rme1 trp1 his3Δ GAL+ HMLa ldb19::KanMX4*	This study
YAC5	*MATa leu2 ura3 rme1 trp1 his3Δ GAL+ HMLa mtc1::KanMX4*	This study
YAC6	*MATa leu2 ura3 rme1 trp1 his3Δ GAL+ HMLa nap1::KanMX4*	This study

YAC7	*MATa leu2 ura3 rme1 trp1 his3Δ GAL+ HMLa reg1::KanMX4*	This study
YAC8	*MATa leu2 ura3 rme1 trp1 his3Δ GAL+ HMLa ubx7::KanMX4*	This study
YAC9	*MATa leu2 ura3 rme1 trp1 his3Δ GAL+ HMLa vtc2::KanMX4*	This study
YAC10	*MATa leu2 ura3 rme1 trp1 his3Δ GAL+ HMLa vtc3::KanMX4*	This study
YAC11	*MATa/@ leu2/leu2 ura3/ura3 rme1/rme1 trp1/trp1 his3Δ/ his3Δ GAL+/GAL+ HMLa/HMLa noc2::KanMX4*	This study
YAC12	*MATa/@ leu2/leu2 ura3/ura3 rme1/rme1 trp1/trp1 his3Δ/ his3Δ GAL+/GAL+ HMLa/HMLa sec7::KanMX4*	This study
YAC13	*MATa leu2 ura3 rme1 trp1 his3Δ GAL+ HMLa HAL5-3HA::KanMX4*	This study
YAC14	*MATa leu2 ura3 rme1 trp1 his3Δ GAL+ HMLa ISW2-3HA::KanMX4*	This study
YAC15	*MATa leu2 ura3 rme1 trp1 his3Δ GAL+ HMLa KKQ8-3HA::KanMX4*	This study
YAC16	*MATa leu2 ura3 rme1 trp1 his3Δ GAL+ HMLa LDB19-3HA::KanMX4*	This study
YAC17	*MATa leu2 ura3 rme1 trp1 his3Δ GAL+ HMLa MTC1-3HA::KanMX4*	This study
YAC18	*MATa leu2 ura3 rme1 trp1 his3Δ GAL+ HMLa NAP1-3HA::KanMX4*	This study
YAC19	*MATa leu2 ura3 rme1 trp1 his3Δ GAL+ HMLa REG1-3HA::KanMX4*	This study
YAC20	*MATa leu2 ura3 rme1 trp1 his3Δ GAL+ HMLa RTS3-3MYC::KanMX4*	This study
YAC21	*MATa leu2 ura3 rme1 trp1 his3Δ GAL+ HMLa UBX7-3HA::KanMX4*	This study
YAC22	*MATa leu2 ura3 rme1 trp1 his3Δ GAL+ HMLa VTC2-3HA::KanMX4*	This study
YAC23	*MATa leu2 ura3 rme1 trp1 his3Δ GAL+ HMLa VTC3-3HA::KanMX4*	This study
YAC24	*MATa leu2 ura3 rme1 trp1 his3Δ GAL+ HMLa NOC2-3HA::KanMX4*	This study
YAC25	*MATa leu2 ura3 rme1 trp1 his3Δ GAL+ HMLa SEC7-3HA::KanMX4*	This study

Table 2.1: Yeast strains used in this study

Yeast strains carrying a plasmid were precultured in selective synthetic medium lacking the corresponding amino acids for plasmid maintenance. They were then diluted into YPD medium and grown for 5 hours to an OD_{600} of 0.8. Metabolic labeling of yeast proteins was done by growing cells in synthetic medium supplemented with either $^{12}C_6$-arginine and $^{12}C_6$-lysine ("light" culture) or $^{13}C_6$-arginine and $^{13}C_6$-$^{15}N_2$-lysine ("heavy" culture) (Cambridge Isotope Laboratories, Andover, MA), each at 30 mg/l. Treatment with rapamycin (LC Laboratories, Woburn, MA) was at 200 ng/ml final concentration

(added from a 1 mg/ml stock solution in 90% ethanol/10% Tween20) for 20 min. Transformation of yeast cells was performed with the LiAc/SS-DNA/PEG method [103]. All deletions and genomically tagged strains were constructed by PCR targeting [104]. The resulting transformants were checked for proper integration by colony PCR.

2.2. Molecular Biology Techniques

The plasmids used in this work are listed in Table 2.2. All plasmids were constructed by cloning into the pHAC plasmids pHAC33 and pHAC195. DNA inserts were generated by PCR amplification of the target gene with two primers each containing a restriction site. The resulting PCR products were gel purified with the NucleoSpin Extract II Kit (Macherey-Nagel, Oensingen, Switzerland) according to the manufacturer's protocol. Both insert and plasmid were digested with the appropriate restriction endonucleases. The digested plasmid was separated on a 2% agarose gel. DNA ligation was done with the T4 DNA ligase kit (Promega AG, Dübendorf, Switzerland) according to the manufacturer's recommendations. The ligation mixture was transformed into Top10 *E. coli* cells (Invitrogen, Lucerne, Switzerland) according to standard procedures. Transformants were selected on LB plates containing ampicillin and the plasmids were isolated with the GenElute Miniprep Kit (Sigma) according to the manufacturer's instructions. The plasmids were stored in 50 µl water at -20°C. Point mutations were constructed using a modified version of the QuikChange Site-Directed Mutagenesis System [105]. The PCR reaction was digested over-night with the restriction enzyme DpnI (New England Biolabs, Allschwil, Switzerland) and the PCR product was subsequently precipitated with 5M potassium acetate and washed with ethanol. After drying the PCR product in a Speedvac, it was resuspended in 10 µl dH_2O. 5 µl of the PCR product were transformed into Top10 *E. coli* cells according to standard procedures. Transformants were selected on LB plates containing ampicillin and plasmids were isolated with the GenElute Miniprep Kit.

Name	Description	Ref.
pHAC33	*CEN, URA3, MCS-3x HA-CYC1 terminator, Amp*	Lab plasmid
pHAC195	*2μ, URA3, MCS-3x HA-CYC1 terminator, Amp*	Lab plasmid
pAC1	*pHAC195::HAL5-3HA (2μ, URA3)*	This study
pAC2	*pHAC195::ISW2-3HA (2μ, URA3)*	This study
pAC3	*pHAC195::KKQ8-3HA (2μ, URA3)*	This study
pAC4	*pHAC195::LDB19-3HA (2μ, URA3)*	This study
pAC5	*pHAC195::MTC1-3HA (2μ, URA3)*	This study
pAC6	*pHAC195::NAP1-3HA (2μ, URA3)*	This study
pAC7	*pHAC195::NOC2-3HA (2μ, URA3)*	This study
pAC8	*pHAC195::REG1-3HA (2μ, URA3)*	This study
pAC9	*pHAC195::VTC2-3HA (2μ, URA3)*	This study
pAC10	*pHAC195::VTC3-3HA (2μ, URA3)*	This study
pAC11	*pHAC33::ISW2-3HA (2μ, URA3)*	This study
pAC12	*pHAC33::ISW2^{T1079A}-3HA*	This study
pAC13	*pHAC33::ISW2^{T1079E}-3HA*	This study
pAC14	*pHAC33::ISW2^{T1079D}-3HA*	This study

Table 2.2: Plasmids used in this study

2.3. Phosphoproteome Analysis

2.3.1. Protein Extraction, Protein Fractionation and In-gel Digestion

200 mL YPJ2 were grown at 30°C in SD medium supplemented with either light or heavy arginine and lysine to an OD_{600} of 0.8. To the "heavy" culture 40 µL 1 mg/ml rapamycin were added and the culture was incubated at 30°C for 20 min. Both cultures were then centrifuged at 4,500 g and 4°C for 10 min. Cell pellets were washed once with 50 ml cold H_2O and resuspended in 2 mL cold lysis buffer (100 mM Tris-HCl, pH 7.5,

2.5% SDS, 10% glycerol, 1x Roche protease inhibitor cocktail (Roche Diagnostics, Basel, Switzerland), 1x phosphatase inhibitor cocktail 1 (Sigma) and 1 mM PMSF (AppliChem, Baden-Dättwil, Switzerland)). The cell suspensions from either light or heavy cultures were distributed into 2 mL screw cap tubes and glass beads were added until the liquid reached the top of the tube. The cells were broken in a bead beater (FastPrep Homogenizer FP120, Thermo Savant) with six 30 sec bursts at maximum speed. Between each burst the lysates were cooled on ice for 2 min. The lysates were centrifuged at 12,000 rpm and 4°C for 10 min and the supernatants were transferred into new tubes and the individual protein concentrations were measured with the bicinchonic acid assay (Sigma). 2.5mg of each protein extract were mixed to obtain a 1:1 light:heavy protein mixture. After adding SDS-PAGE sample buffer the protein mixture was incubated at 98°C for 5 min.

A total of 5 mg proteins (2.5 mg protein from the light and heavy cultures) were separated on a preparative 10% SDS slab gel (15 x 13 x 0.15cm). The proteins were electrophoresed at 10 mA constant current over-night. After electrophoresis, the gel was washed three times for 5 min with H_2O, stained with SimplyBlue SafeStain (Invitrogen, Lucerne, Switzerland) for 1 hr and distained with H_2O water. The gel was then cut horizontally into 16 slices, which were further diced into 1 mm^3 cubes. The gel pieces were distained over-night in 1 mL 50% acetonitrile/50 mM NH_4HCO_3, dehydrated for 10 min with 500 µL 100% acetonitrile and dried in a speed-vac. The proteins were in-gel reduced at 55°C for 60 min by adding to each dried gel plug 1 mL 10 mM DTT (in 50 mM NH_4HCO_3). The remaining solution was discarded from the gel pieces and alkylation was performed in the dark for 30 min by adding 1 mL 50 mM iodoacetamide (in 50mM NH_4HCO_3). To remove unreacted iodoacetamide, the gel pieces were washed three times with 1 mL 50% acetonitrile/50 mM NH_4HCO_3. After the last wash they were dehydrated with 500 µL 100% acetonitrile, dried in a speed-vac and then rehydrated on ice for 1 h in 1 mL 50 mM NH_4HCO_3, pH 8.0 containing 15 ng/µL trypsin (Sigma). Digestion was performed over-night at 37°C. Supernatants were collected into fresh tubes and tryptic peptides were extracted three times with 50% acetonitrile/5% formic acid, followed by a final extraction with 100% acetonitrile. The liquid volume was reduced in a speed-vac to approximately 10 µl to which 290 µl 1% acetic acid were added. A small

drop was spotted onto pH paper and if necessary the pH was adjusted to 2.0-2.5 with 100% acetic acid.

2.3.2. Phosphoproteome Analysis: Peptide Desalting and Phosphopeptide Enrichment

Before enriching phosphopeptides by Immobilized Metal Ion Affinity Chromatography (IMAC) the digests were desalted on disposable C18 MacroSpin columns (500 µl packed resin, The Nest Group, Southborough, MA) according to the manufacturer's instructions. The peptides were eluted from the cartridge with 600 µl 60% acetonitrile/1% acetic acid. The eluates were dried down to 10 µl final volume in a speed-vac and 90 µl IMAC-buffer (30% acetonitrile/250 mM acetic acid) were added. 1 µl of each digest was diluted 200-fold with 2% acetonitrile/0.1% acetic acid and 10 µl were analysed by LC/MS/MS for expression analysis.

For phosphopeptide selection, 40 µl IMAC slurry (PHOS-Select, Sigma) were washed five times with 1 mL IMAC-buffer to remove glycerol from the beads and then loaded into a constricted GELoader tip [106]. The desalted digests were applied to the GELoader IMAC columns and the flow-throughs were collected and re-applied five times. The columns were washed three times with 150 µl IMAC-buffer and the bound phosphopeptides were eluted with three 70 µl desorption steps of 50 mM KH_2PO_4 (pH adjusted to 10.0 with ammonium hydroxide) into 1.5 ml tubes containing 30 µl 10% formic acid. The IMAC eluates were desalted on disposable C18 MicroSpin columns (100 µl packed resin, The Nest Group, Southborough, MA) according to the manufacturer's instructions. After elution with 200 µl 60% acetonitrile/1% acetic acid, the volume was reduced in a speed-vac to about 10 µl and the phosphopeptides were diluted with 40 µl 2% acetonitrile/0.1% formic acid for LC-MS/MS analysis.

2.3.2. Phosphoproteome Analysis: LC-MS/MS Analysis

LC-MS/MS analysis was performed on an LTQ-Orbitrap hybrid instrument (Thermo Scientific, San José, CA). The IMAC eluate was separated by capillary liquid chromatography using a trapping 300SB C-18 column (0.3 x 50 mm) (Agilent Technologies, Basel, Switzerland) and a separating column (0.1 mm x 10 cm) that had been packed with Magic 300Å C18 reverse-phase material (5 µm particle size, Michrom Bioresources, Auburn, CA). A linear 80-min gradient from 2 to 50% solvent B (80% acetonitrile/0.1% acetic acid and) in solvent A (2% acetonitrile/0.1% acetic acid) was delivered with a Rheos 2200 pump (Flux Instruments, Basel, Switzerland) at a flow rate of 100 µl/min. A pre-column split was used to reduce the flow to approximately 100 nl/min. 10 µl of peptide digest were injected with an autosampler thermostatted to 4°C (CTC Analytics, Agilent Technologies, Basel, Switzerland). The eluting peptides were ionized at 1.7 kV.

The LTQ-Orbitrap was operated in a data-dependent mode. A survey scan between m/z 375-1600 was acquired in profile mode in the Orbitrap at 60,000 resolution, followed by 10 MS/MS scans in centroid mode in the LTQ of the 10 most abundant ions. Singly charged ions were omitted from fragmentation and previously selected ions were dynamically excluded for 25 sec. The normalized collision energy was set to 35% and for phosphopeptide analysis multistage activation was enabled. Automatic gain control (AGC) was set to 500,000 and 10,000 for Orbitrap and LTQ, respectively. Scan-to-scan calibration was allowed by setting the lock mass to m/z 445.120025 (Olsen JV, 2005, Mol Cell Proteomics).

2.3.3 Phosphoproteome Analysis: Databank Search and Quantitation of SILAC-Ratios

The raw data from the mass spectrometer were processed with MaxQuant (1.0.12.31) [107] and searched with the Mascot search engine (version 2.2.04, Matrix

Science, London, UK) [108] against a databank containing 31,426 protein sequences. The databank contained forward and reverse (Swiss-Prot) *S. cerevisiae* sequences as well as common protein contaminants. Precursor ion and fragment ion mass tolerances were set to 7 ppm and 0.6 Da, respectively. Maximally two missed cleavages with three labeled amino acids were allowed. Methionine oxidation and phosphorylation of serine, threonine and tyrosine were set as variable modifications, while carbamidomethylation of cysteine residues was set to fixed modification. To increase the confidence in protein identification only peptides with a Mascot score above 20 were accepted. In addition, the posterior error probability (PEP) for each MS/MS spectrum was set to below 0.1 [109].

To further simplify the MaxQuant output data, oxidized methionines were replaced with unmodified methionines and gene products of the Ty retrotransposons and the *S. cerevisiae* virus L-A were removed from the output list. When peptides or phosphopeptides matched several proteins, all proteins were joined together in a unique protein hit, except if one of the proteins contained additional peptides that were not shared by the other proteins. In this case, only those proteins were reported that had the highest number of matching peptides. Phosphopeptides with the same phosphorylation site(s) but different sequences due to incomplete cleavage were grouped together to calculate a unique SILAC ratio. In addition, an average protein SILAC ratio was calculated by combining all SILAC ratios for the non-phosphorylated peptides belonging to the same protein.

2.4. Radioactive Labeling of Yeast Proteins

Yeast extracts were prepared as described above. Purified yeast GST-Npr1 kinase was provided by Simon Hauri (Simon K. Hauri, Molecular and Functional Characterization of the Yeast Npr1 Kinase, Master Thesis, 2007-2009). 30 µl of yeast proteins (~10 mg/ml) were incubated in 20 µl 5x kinase buffer (500 mM Tris-HCl pH 8.0, 2.5% Tween-20, 5 mM DTT, 50 mM $MgCl_2$, 50% glycerol), 2 µl [γ-^{32}P]-ATP (150 kBq/assay) (Hartmann Analytic, Braunschweig, Germany), 2 µl 1 mM ATP, 40 µl of GST-Npr1 (~2 µg) and 6

µl H_2O. The reaction mixture was incubated at 37°C for 30 min in a thermoshaker. The kinase reaction was stopped by adding 20 µl 6x SDS-PAGE sample buffer and boiling at 95°C for 5 min. The kinase assay was separated by SDS-PAGE. The gel was washed three times for 5 min with H_2O and stained with SimplyBlue SafeStain (Invitrogen, Lucerne, Switzerland) for 1 hr, followed by destaining with H_2O. The gel was autoradiographed, and radioactively labeled proteins were in-gel digested essentially as described above and desalted on disposable C18 MacroSpin columns.

2.5. Western Blotting, Phosphatase Treatment and *In vitro* Kinase Assays

200 ml cells were grown in either YPD or SD medium to an OD_{600} of 0.8. If necessary, at this stage yeasts were treated with rapamycin or vehicle for 20 min. After that, cells were harvested by centrifugation at 4,500 rpm and 4°C for 10 min, washed with cold water and centrifuged again. Cell pellets were resuspended in 1 ml lysis buffer (PBS containing 0.5% Tween 20 and 10% glycerol) containing 1x Roche protease inhibitor cocktail, 1 mM PMSF and phosphatase inhibitors (10 mM NaF, 10 mM NaN_3, 10 mM p-nitrophenylphosphate, 10 mM sodium pyrophosphate and 10 mM β-glycerophosphate) and transferred to a 2 ml screw cap tube. Glass beads were added till the liquid reached the top of the tube and the cells were lysed in a bead beater with six 30 sec bursts. In between the bursts, the cells were cooled on ice for 2 min. Cell debris were pelleted at 12,000 rpm and 4°C for 5 min. The protein concentration of the supernatant was determined by the Bradford assay and the same amount of protein for each sample (between 5-15 mg) was transferred to a 1.5 ml tube. The final volume in the tube was adjusted to 800 µl. HA or MYC-tagged proteins were immunoprecipitated over-night on an end-over-end rotator with 25 µL of proteinA-Sepharose beads (50% suspension in PBS, pH 7.3/0.01% thiomerosal) covalently crosslinked to anti-HA antibody (Santa Cruz Biotechnology, 12CA5) or anti-MYC antibody (American Type Culture Collection,

CRL-1729). After over-night incubation at 4oC, the Sepharose beads were washed five times with 1 ml washing buffer (PBS, pH 7.3 containing 10% glycerol and 0.5% Tween-20) at 500 g for 1 min at 4°C. After the last wash step, the wash buffer was completely removed with a Hamilton syringe. For SDS-PAGE, the tagged proteins were eluted from the beads with 25 µl 2x SDS-PAGE sample buffer by boiling at 95°C for 5 min and electrophoresed on mini-gels (Bio-Rad, Reinach, Switzerland). The proteins were transferred onto nitrocellulose. For western blotting, anti-HA (mouse monoclonal, Cell Signaling) and anti-MYC (mouse monoclonal, American Type Culture Collection, CRL-1729) antibodies were used.

For λ phosphatase treatment, the pull-downs were washed five times with 1 ml washing buffer as described above, followed by two washes with 0.8 ml phosphatase buffer (50 mM Tris-Cl pH 7.5, 0.1 mM EDTA, 5 mM DTT, 0.01% BRIJ35, 2 mM $MnCl_2$). After the last wash step, the phosphatase buffer was completely removed from the beads with a Hamilton syringe and the beads were resuspended in either 20 µL phosphatase buffer or in 20 µL phosphatase buffer supplemented with 25 U λ protein phosphatase (Sigma). The tubes were incubated on a thermoshaker for 30min at 30°C. To stop the reaction 4 µL 6x SDS-PAGE sample buffer were added to each sample and the tubes were boiled at 95°C for 5 min. SDS-PAGE, protein transfer and western blotting were done essentially as described above.

2.6. *In vitro* Kinase Assay

For *in vitro* kinase assays, pull-downs from 800 ml yeast cultures were prepared. After over-night immunoprecipitation of the tagged proteins, the beads were washed five times with 1 ml washing buffer (PBS, pH 7.3 containing 10% glycerol and 0.5% Tween-20), followed by two washes with 0.8 ml kinase buffer (50 mM HEPES, pH 7.5, 10 mM $MnCl_2$, 1 mM EGTA, 0.01% Tween-20 and freshly added 2.5 mM DTT). After that, the beads were resuspended in 5 µl 4x kinase buffer, 11.3 µl H_2O, 0.7 µl 190 µM PP242 (or 0.7 µl DMSO), 0.2 µl 100 µM ATP, 0.4 µl [γ-^{32}P]-ATP (150 kBq/assay), 2.4 µl

recombinant mTOR (Invitrogen, Lucerne, Switzerland). For the kinase assays, the mTOR stock solution was diluted ten fold into 20 mM HEPES, pH 7.5, 0.02% Tween-20, 2 mM DTT, 0.1 mg/ml BSA so that 100 ng mTOR was used per assay. The kinase assays were incubated on a thermoshaker at 30°C for 30 min and stopped with 4 µl 6x SDS-PAGE sample buffer and boiling at 98°C for 5 min. The tubes were then briefly spun and 24 µl of the supernatant was loaded on minigels (Bio-Rad, Reinach, Switzerland). The gels were washed three times for 5 min with H_2O and stained with SimplyBlue SafeStain for 1 hr. The gel was then destained with H_2O, wrapped in Saran foil and exposed on a Phosphor Screen for 18 hours (GE Healthcare). The Phosphor Screen was developed on a Typhoon FLA 9000 (GE Healthcare).

2.7. LC-MS/MS Analysis of Protein Immunoprecipitates

For LC-MS/MS analysis immunoprecipitates from 800 ml yeast cultures were prepared. The tagged proteins were immunoprecipitated over-night with 25 µl antiHA-Sepharose beads essentially as described above. The beads were subsequently washed 10 times with 1 ml washing buffer (PBS, pH 7.3 containing 10% glycerol and 0.5% Tween-20) and, after the last wash, the residual liquid was removed with a Hamilton syringe. Bound proteins were eluted by incubating the beads with 50 µl 0.2% SDS on a thermoshaker for 20 min. After a short spin, the supernatant was transferred to a new tube. The proteins were precipitated by adding 12.5 µl 100% TCA and incubation on ice for 2 hours. The proteins were pelleted at 12,000 rpm and 4°C for 20 min. The precipitate was washed with 1 ml 20% TCA and 1 ml acetone (-20°C). The protein precipitate was dried in a speed-vac for 10 min and dissolved in 10 µl of the appropriate resuspension buffer (Table 2.3). The proteins were reduced at 37°C with 10 mM TCEP for 30 min and alkylated in the dark with 50 mM iodoacetamide for 60 min. Before digestion, the urea concentration was reduced to 0.8 M with the appropriate dilution buffer (Table 2.3). The proteins were digested over-night with 0.25 µg of the appropriate protease. Protein digestion was performed at 37°C, except for the Glu-C digestion that was carried out at

25°C. The next day, the digests were acidified by adding 5.3 µl 100% formic acid (final concentration of 5%) and they were desalted on C18 Stage Tips (Thermo Scientific, Reinach, Switzerland) according to manufacturer's instructions. Peptides were eluted with 30 µl 80% acetonitrile/5% formic acid. The digests were dried in a speed-vac and dissolved in 30 µl 0.1% TFA for LC-MS/MS analysis.

Liquid chromatography was performed using a ProteoCol trap C18 column (0.15 x 10 mm, 3 µm particle size, 300Å) (SGE Analytical Science, Victoria, Australia) and a separating column (0.1 x 100 mm) that had been packed with Magic 300Å C18 reverse-phase material (5 µm particle size, Swiss Bioanalytics, Birsfelden, Switzerland). The columns were connected on line to an Orbitrap FT hybrid instrument (Thermo Finnigan, San Jose, CA). The solvents used for peptide separation were 0.1% acetic acid (solvent A) and 80% acetonitrile/0.1% acetic acid and in water (solvent B). Peptides were injected via a 2 µl loop onto the trap column with the capillary pump of an Agilent 1200 system (Agilent Technologies, Basel, Switzerland) set to 5 µl/min. After 15 min, the trap column was switched into the flow path of the separating column. A linear gradient from 2 to 35% solvent B in 60 min was delivered with an Agilent 1200 nano pump at a flow rate of 500 nl/min. After 60 min the percentage of solvent B was increased to 60% in ten minutes and further increased to 80% within 2 min. The eluting peptides were ionized at 1.7 kV. The mass spectrometer was operated as previously described for the phosphoproteome analysis. Briefly, full scans were acquired between m/z 375-1600 in profile mode in the Orbitrap at 60,000 FWHM nominal resolution, followed by the fragmentation of the 10 most intense ions in the LTQ. Singly-charged ions were not fragmentated and dynamically exclusion was set at 25 sec.

Mass spectral data were searched with Mascot (version 2.2.04) against a databank containing 31,426 protein sequences from forward and reverse (Swiss-Prot) *S. cerevisiae* sequences as well as common protein contaminants. The search parameters were as described above except that arginines and lysines were kept unmodified. The data were filtered using an expectation value below 0.05 and a Mascot score higher than 20. The searches were exported in Excel sheets and oxidized methionines were replaced with normal methionines.

Enzyme	Resuspension buffer	Dilution buffer
Trypsin, Endoproteinase Lys-C	500mM Tris-HCl, pH8.6, 8M urea	50mM Tris-HCl, pH 7.4, 5mM $CaCl_2$
Endoproteinase Asp-N	250mM sodium phosphate, pH 8.0, 8M urea	50mM sodium phosphate, pH 8.0
Endoproteinase Glu-C	250mM ammonium carbonate, pH 8.0, 8M urea	25mM ammonium carbonate, pH 8.0

Table 2.3.: List of the appropriate resuspension and dilution buffers for each protease.

2.8. Phosphomapping of HA-Nap1

2.8.1. *In vitro* Phosphorylation of HA-Nap1

HA-Nap1 immunoprecipitates were obtained from 4 l yeast cultures as described above. The immunoprecipitates were washed five times with 1 ml washing buffer (PBS containing 0.5% Tween 20 and 10% glycerol). For Nap1 dephosphorylation, the immunoprecipitates were further washed twice with 0.8 ml 1x phosphatase buffer (50 mM Tris-Cl pH 7.5, 0.1 mM EDTA, 5 mM DTT, 0.01% BRIJ35, 2 mM $MnCl_2$). The dephosphorylation reaction was as previously described. After dephosphorylation, the beads were washed five times with washing buffer (PBS containing 0.5% Tween 20 and 10% glycerol), followed by two washes with 0.8 ml 1x kinase buffer (50 mM HEPES, pH 7.5, 10 mM $MnCl_2$, 1 mM EGTA, 0.01% Tween-20 and freshly added 2.5 mM DTT). The *in vitro* kinase reaction was performed as described above. If necessary half of the immunoprecipitates were treated with DMSO (control) and the second half with PP242. After *in vitro* phosphorylation of Nap1 with [γ-^{32}P]-ATP, the beads were washed extensively until no radioactivity was detected in the wash. At this stage Nap1 was eluted

from the beads by adding 50 µl 0.2% SDS and incubation on a thermoshaker for 20 min. Proteins were precipitated with TCA, digestion and peptide desalting were as described above, except that the peptides were desalted on disposable C18 MicroSpin columns. Radioactively labeled peptides were isolated by C18 reverse-phase chromatography.

2.8.2. Reverse-Phase Chromatography

Reverse-phase chromatography was done on a Zorbax SB-C18 reverse-phase HPLC column (0.5 x 150 mm, 5.0 µm particle size, Agilent Technologies, Basel, Switzerland) connected to an Agilent 1260 Infinity Capillary LC System (Agilent Technologies, Basel, Switzerland) at a flow rate of 10 µl/min. The column was equilibrated with 98% solvent A (0.1% TFA) and the digest was injected via a micro-autosampler. After 10 min, the peptides were eluted with a linear 60 min gradient from 2% to 80% solvent B (80% acetonitrile, 0.09% TFA). The effluent was monitored at 220 nm and 280 nm and fractions were collected every 2 min with a microtiter plate fraction collector. Each fraction was dried in a speed-vac and resuspended in 30 µl 0.1% TFA. 5 µl were used for liquid scintillation counting and the remaining part was used for LC-MS/MS as described.

2.10 Quantitative Real-time PCR Analysis

Cells were grown in SD medium to an OD_{600} of 0.8. Cultures were treated with drug vehicle or rapamycin (200 ng/ml) for 30 minutes before total RNA was isolated using the RNeasy Mini Kit (Quiagen, Magden, Switzerland) according to the manufacturer's instructions. Additionally, to remove genomic DNA DNase I (Quiagen, Magden, Switzerland) treatment was performed directly in the RNeasy column. RNA purity and quantity were assessed spectrophotometrically. cDNA was generated from 3

µg of RNA using SuperScript II reverse transcriptase (Invitrogen, Lucerne, Switzerland) and random nonamers (Sigma) according to the manufacturer's instructions. Each cDNA sample was diluted ten fold with nuclease-free water (Ambion, Rotkreuz, Switzerland). The cDNA was then analyzed by qPCR in a StepOnePlus real-time PCR machine (Applied Biosystems, Zug, Switzerland) using the SYBR Green method. Gene-specific primers (Table 2.4) were designed with the Beacon Designer software. The reaction was set up by mixing 2 µl cDNA template with 7.5 µl 2x Power SYBR Green PCR Master Mix (Applied Biosystems, Zug, Switzerland), 5 µl nuclease-free water and 0.3 µl of each forward and reverse primer (200 nM each). All reactions were run in duplicate. The qPCR conditions were 95°C for 10 minutes, followed by 40 cycles with denaturation at 95°C for 15 seconds and annealing/elongation at 60°C for 1 minute. Expression for each target gene was normalized to actin and the reference sample (TB50a untreated) was normalized to 1.

Name	Sequence
INO1_fwd	TTAATGGTTCACCGCAGAATAC
INO1_rev	GCCAGAACAGACTTCAACTTG
SIP4_fwd	GCTCCTCTAACGCAATCACTG
SIP4_rev	AGGGAAGTCAATTTTCGCACAG
ACT1_fwd	ATGGATTCTGAGGTTGCTG
ACT1_rev	CCTTGGTGTCTTGGTCTAC

Table 2.4: Primers used for qPCR analysis

2.9. Glycogen Staining

Staining of intracellular glycogen was performed with iodine vapor as previously described [25].

3. Results

3.1. Establishing a Workflow for the Qualitative Analysis of the Rapamycin-Sensitive Yeast Phosphoproteome

Although it is known that TORC1 regulates many cellular processes, the molecular mechanisms by which TORC1 signals to diverse processes are not well understood. To date, only Tap42 [65], Sch9 [66] and Sfp1 [32] have been identified as direct TORC1 substrates. For a global understanding of the phosphorylation sites regulated by TORC1 and for the identification of novel TORC1 targets, phosphoproteomes obtained from untreated or rapamycin-treated yeast cells were compared. In particular, those phosphorylation events that are decreased following rapamycin treatment can in principal, be regarded as direct substrates of TORC1.

In a first comparison of the phosphoproteomes, proteins from untreated or rapamycin-treated yeast cells were digested with trypsin in solution, and phosphopeptides were enriched via IMAC. The resulting phosphopeptides were analysed by LC-MS/MS and the proteins were identified by databank searching. Surprisingly, except for phosphopeptides of highly expressed proteins, the total number of identified phosphopeptides was disappointingly low (results not shown). This is attributable to the high complexity and the extremely large dynamic range of the peptides present in the digest that leads to the fragmentation of only the most abundant phosphopeptides in the mass spectrometer. Therefore, it was obvious that the yeast extract needed to be fractionated in some way to reduce sample complexity and to increase proteome coverage. To date several separation techniques to fractionate entire proteomes have been used independently or in combination, such as strong cation exchange chromatography (SCX [91]), hydrophilic interaction liquid chromatography (HILIC [87]), and SDS-PAGE [110]. SCX and HILIC fractionations are done at the peptide level and involve separations according to peptide charge and hydrophilicity, respectively. Therefore they are very useful to further concentrate the negatively-charged and hydrophilic

phosphopeptides. On the other side, SDS-PAGE fractionation is a convenient method because it allows to directly lyse the cells in SDS buffer. Due to the strong denaturing effect of SDS, inadvertent dephosphorylation of proteins by phosphatases can be effectively suppressed. For this reason and for the inherent simplicity of gel electrophoresis, the proteomes from control and rapamycin-treated yeast cells were separated by SDS-PAGE. Two preparative SDS-gels were run in parallel, one for the separation of an extract from untreated and the other for the separation of an extract from rapamycin-treated cells. The two gels were sliced individually into horizontal bands and the gels slices were digested with trypsin. Before phosphopeptide enrichment, tryptic peptides were desalted on C18 reverse-phase columns. Several column formats were tested to make sure that the maximal binding capacity of the packing material was not exceeded. The use of MacroSpin columns containing 200 µl bed volume of C18 material was optimal for the desalting of the tryptic peptides generated from a single gel slice (~400 µg), since no peptide losses were observed in the column flow-through (data not shown).

After desalting, the phosphopeptides were enriched via immobilized metal ion affinity chromatography (IMAC [80]). At this stage two types of enrichment procedures were tested. In one case, Fe(III)IMAC resin was added directly to one half of the peptide pool and phosphopeptide enrichment was done by incubating the solution on a shaker for one hour ("In-solution IMAC" [110]). The other half of the peptide pool was loaded onto a micro-column packed into a constricted GeLoader tip ("IMAC column" [106]). The phosphopeptide enrichment on the micro-column was far better than in-solution enrichment, since the number of identified phosphopeptides was two times higher (Figure 3.1A). The effect of the peptide to resin ratio on the selectivity of the IMAC enrichment was also evaluated. Tryptic digests from individual gel slices were spiked with radioactively labeled yeast phosphopeptides and the distribution of the radioactivity in the flow-through and the eluate of the IMAC micro-column was measured. The radioactive phosphopeptides were obtained after digesting a mixture of yeast proteins previously phosphorylated by the Npr1 kinase. Such a heterogeneous mixture of radiolabelled phosphopeptides was favored over a mixture of a few standard phosphopeptides because it more closely resembles the complex mixture obtained from

yeast cells. The radiolabeled phosphopeptide pool contained about 60,000 cpm in total from which 2,000 cpm were used for each tracer experiment. The highest recovery of radiolabelled phosphopeptides in the eluate was observed when a ratio between 0.1 to 1 mg peptide per 30 µl packed IMAC resin was used (Figure 3.1B). Notably, a constant amount of radioactivity was always present in the flow-through, even at very low peptide to IMAC ratios. This is perhaps due to extremely basic phosphopeptides that are unable to bind to the Fe^{3+} of the IMAC resin. However, no significant radioactivity was detected in the washing steps once the phosphopeptides had bound to IMAC, which indicates that most of the phosphopeptide losses occur during the binding step. In addition, at all peptide to IMAC resin ratios a discrete amount of radioactivity corresponding to 20% of the total loaded radioactivity was lost in the flow-through and the eluate. These phosphopeptides most likely bind irreversibly to IMAC.

The IMAC eluates from the gel slices were analyzed individually by LC-MS/MS on an LTQ-Orbitrap hybrid mass spectrometer. To fragment as many different peptides as possible, after each survey scan, ten precursor ions were subjected to fragmentation in the LTQ part of the instrument (Top10 strategy [111]). Also, to reduce peptide co-elution, a shallow LC-gradient of less than 0.3 % solvent B change per minute was applied. Moreover, phosphopeptides are known to undergo intense neutral-loss of H_3PO_4 upon collision induced dissociation. As a consequence, a predominant signal corresponding to the dephosphorylated peptide and reduced backbone fragmentation is observed [111]. To obtain richer fragmentation spectra that yield unambiguous identifications during databank searching, multistage activation [111] was performed on the selected precursor ions. Figure 3.2A summarizes the overall procedure to qualitatively analyze the phosphoproteomes from both control and rapamycin-treated cells.

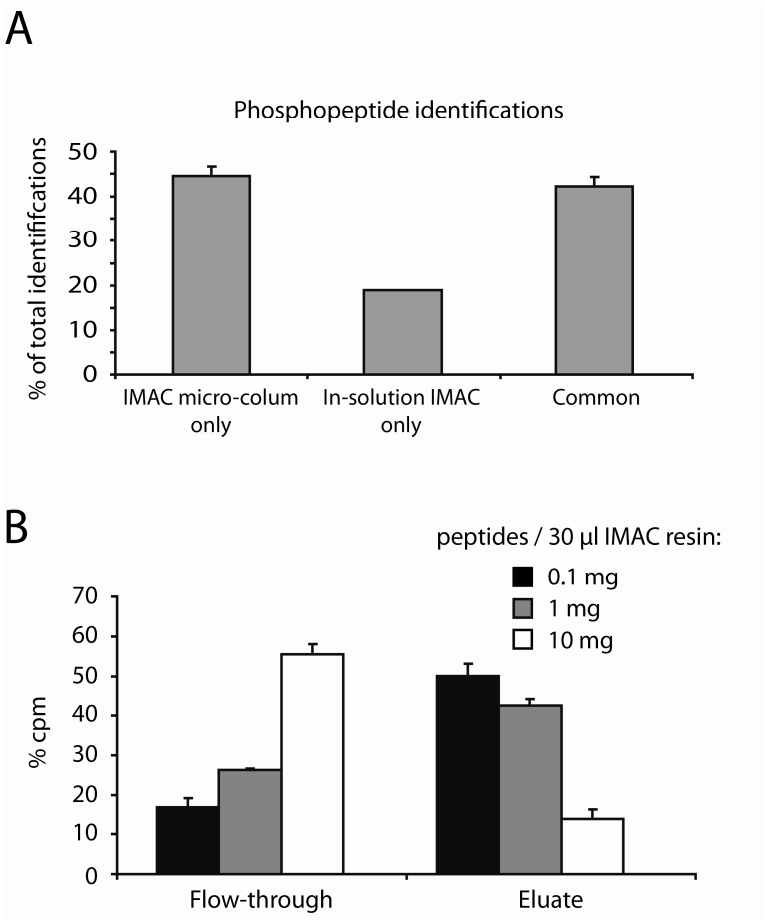

Figure 3.1: (A) Comparison between on-column and in-solution phosphopeptide enrichment. (B) Influence of the peptide to resin ratio on the selectivity of the IMAC enrichment. The phosphopeptide distribution between flow-through and eluate was monitored by measuring the radioactivity of ^{32}P-labeled phosphopeptides.

In total 850 unique phosphoproteins (1,683 unique phosphopeptides) from vehicle-treated cells versus 803 phosphoproteins (1,661 unique phosphopeptides) from rapamycin treated cells were identified (Figure 3.2B and Appendix I-II). The ratio of pSer:pThr:pTyr was 61:8:1 and 65:10:1 for untreated and rapamycin treated cells, respectively (Figure 3.2B). This compares well to previously reported pSer:pThr:pTyr ratios in mammalian cells (79:17:4) [112]. The tyrosine phosphorylation detected in this study probably is caused by dual-specificity kinases in yeast [113]. Interestingly, a relationship was observed between incompletely cleaved peptides and phosphorylated

peptides identified in the phosphoproteome. In the untreated and rapamycin-treated samples there were 35% and 33% incompletely cleaved phosphopeptides, respectively, while these values were much lower for the non phosphorylated peptides (15% and 12%, respectively). This is very likely due to inhibition of the protease cleavage site by the neighboring phosphorylated residue (Figure 3.2C). Indeed, most of the incompletely cleaved phosphopeptides had phosphorylation sites in close proximity to arginine and lysine residues when compared to fully cleaved phosphopeptides. The average peptide length in the untreated and rapamycin-treated phosphoproteomes was 14 and 13 amino acids, respectively. These values do not differ significantly from previously published phosphoproteomes, where SCX instead of SDS-PAGE was used for fractionation [92]. This is surprising as one would assume that in-gel digestion tends to release small peptides from the gel matrix, while large peptides do not diffuse out of the polyacrylamide matrix. However, the fact that in both studies a comparable average peptide length was observed could be attributable to the reverse-phase desalting step that tends to bind very long peptides irreversibly.

In the phosphoproteomes from both untreated and rapamycin-treated cells, the majority of the phosphopeptides (80%) carried one phosphate, while 17% were doubly phosphorylated peptides (Figure 3.2B). This distribution agrees well with the findings of Bodenmiller *et al.* (84% singly and 15% doubly phosphorylated peptides) [83]. This distribution is specific to IMAC selection, since it was reported that other enrichment procedures like titanium dioxide (TiO_2) enrich almost only singly phosphorylated peptides [83]. Another interesting observation is that the highest number of phosphopeptides was detected in the high mass range of the gel and it decreased steadily towards the low mass range. In both phosphoproteomes 85% of all phosphopeptides were contained in gel slices above 40 kDa. A possible explanation is the exceedingly high concentration of ribosomal proteins in the lower part of the gel. The high concentration of peptides derived from ribosomal proteins can effectively compete and eventually displace phosphopeptides from low-abundance phosphoproteins present in these bands.

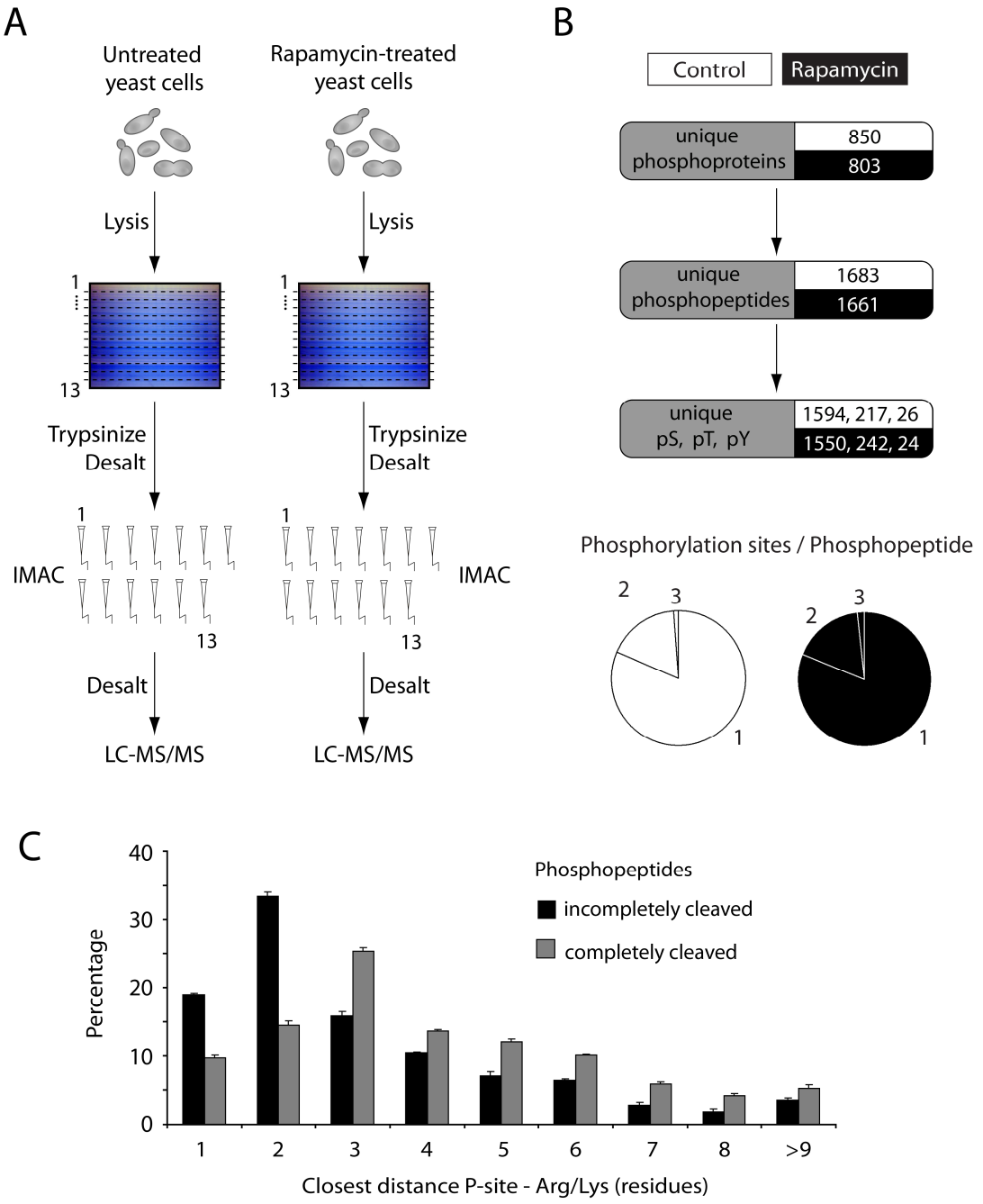

Figure 3.2: (A) Schematic overview for the qualitative TORC1 phosphoproteome of *S. cerevisiae*. (B) Summary of the results from a single phosphoproteomic experiment. The numbers in the white and black boxes represent phosphoproteins/phosphopeptides/phosphorylation sites from untreated or rapamycin treated cells, respectively. The pie charts (white: untreated; black: rapamycin-treated) illustrate the number of phosphorylation sites per phosphopeptide (C) Amino acids between phosphorylation and cleavage sites. 1 means that the phosphorylation site is adjacent to the cleavage site.

Interestingly, the qualitative phosphoproteome contained several known components of the TORC1 signaling pathway (Figure 3.3 and Appendix I-II). For example, several transcription factors involved in RP and RiBi gene expression like Fhl1, Ifh1, Tod6, Dot6 and Stb3 could be identified [28-30, 33]. Several phosphatase subunits (Cdc55, Rts1, Tpd3, Sap155, Sap190) and the kinase Sch9 were also present [64-66]. Moreover, a number of transcription factors indirectly controlled by TORC1 could also be identified in the present phosphoproteomic analysis: Gat1, Gis1, Maf1, Mks1, Msn2/4 and Rtg1/3. Many phosphorylation sites of the rapamycin-activated protein kinase Npr1, which plays a crucial role in the trafficking of Gap1 to the plasma membrane [46, 47] were detected. The permease Gap1 itself along with other nutrient permeases (Agp1, Bap2, Can1, Dal4, Dip5, Fui1, Gnp1, Put4 and Tat2) was found phosphorylated in the phosphoproteome. Also heavily phosphorylated was the protein Atg13, a key regulator of autophagy [51]. Several phosphorylation sites mapping to various proteins functioning in translation initiation were also identified, for instance Gcn2, eIF2α, Eap1 and several subunits of the eIF2B and eIF2 complexes. Finally, phosphorylation sites on Tco89 and Bit61, two subunits of TORC1 and TORC2, were also found in the phosphoproteomic analysis [22-24]. Interestingly, components of other signaling pathways known to interact with the TORC1 pathway were also well represented in the phosphoproteome. For example, several phospho-sites from the PKA subunits Bcy1 and Tpk3 and from the upstream PKA regulators Gpr1, Gpa2, Ira2 and Cyr1 could be mapped. Likewise, the phosphoproteome contained phosphopeptides from the Snf1 kinase, its effectors Adr1, Sip4 and Mig1 as well as its upstream regulators Reg1, Sak1 and Elm1. Considering all these findings, the phosphoproteomic workflow established in the present work allows the tracking of rapamycin-sensitive phosphorylation events associated with many components of the TORC1 signaling pathway.

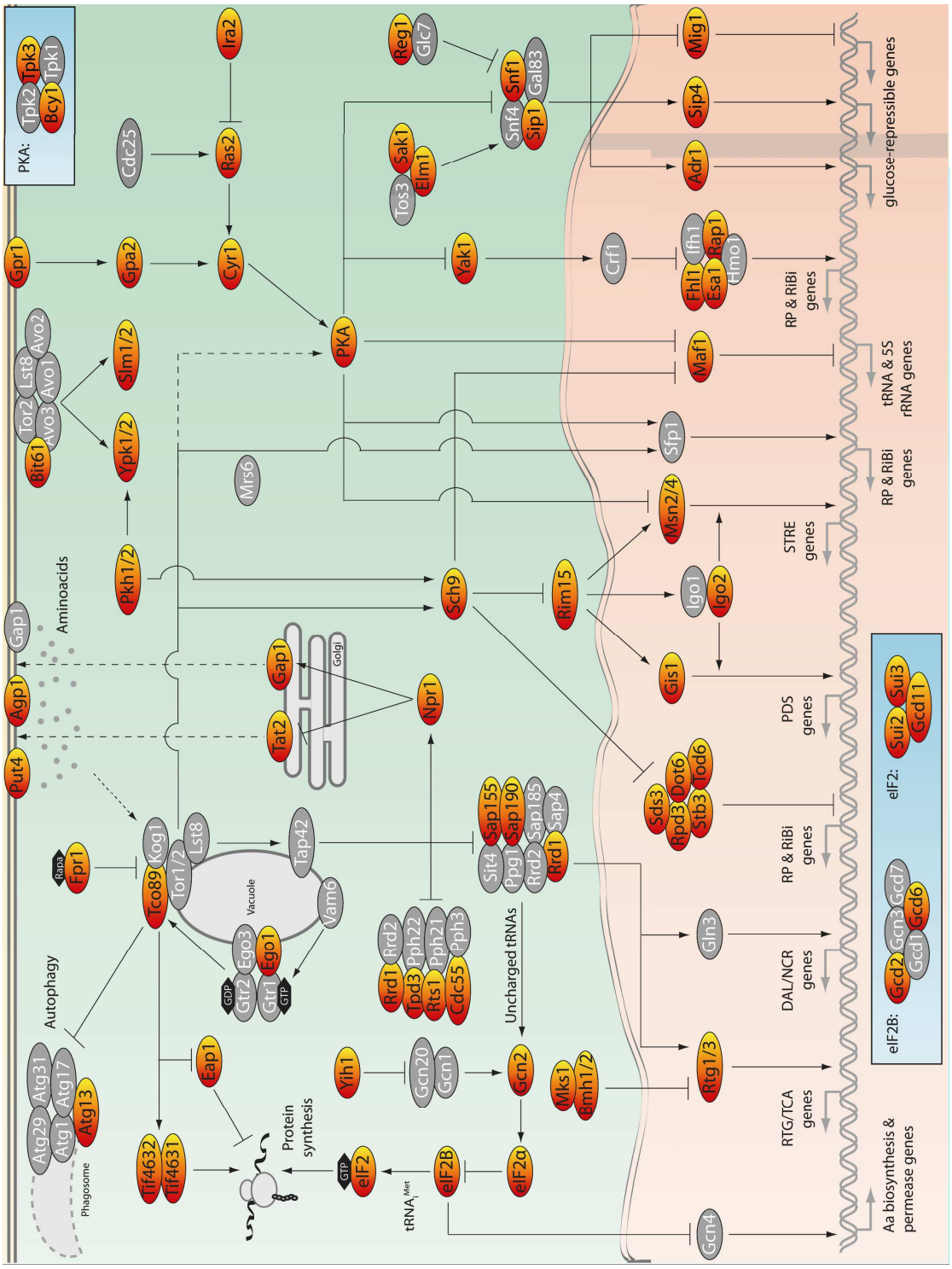

Figure 3.3: Schematic overview of the TORC1 signaling network. Proteins in orange are found phosphorylated in the qualitative phosphoproteome. The inserts illustrate the single protein components of PKA and the eIF2 and eIF2B complexes.

3.2. The Quantitative Rapamycin-Sensitive Phosphoproteome *of S. cerevisiae*

In the first section a qualitative phosphoproteomic strategy was presented, which enables the detection of several physiologically relevant phosphorylation sites known to be regulated by TORC1. Interestingly, for some of these proteins a qualitative difference in phosphorylation following rapamycin treatment could already be seen. For example, T273 phosphorylation on Sch9 and S232/S233 phosphorylation of the Sch9 substrate Rps6 were detected only in untreated cells (Appendix I-II), which agrees well with the fact that TORC1 directly phosphorylates and activates Sch9 (the activating phospho-sites are S711, T723, S726, T737, S758 and S765 [66]), which in turn phosphorylates Rps6 at S232 and S233 [66]. Likewise, many phosphorylation sites on Atg13 (S355, T379, S382, S461, S644 and S646) and Gat1 (S291 and S399) were present only in untreated cells (Appendix I-II) [51]. However, for other TORC1-regulated proteins the effect of rapamycin treatment was not evident. For example, the same phosphorylation sites between control and rapamycin-treated cells were found in Maf1, Msn2/4, Npr1 and Rim15 (Appendix I-II). This, however, does not exclude regulation on these sites. Previous studies revealed down-regulation of a number of phosphorylation sites on Npr1 following rapamycin treatment [114]. Therefore, it is important to be able to *quantitate* in relative terms the effect of rapamycin on the site occupancy of all observable phosphorylation sites.

In a first attempt to quantitate relative changes of phosphorylation, the tryptic peptides obtained from each gel slice were chemically derivatized with the isobaric iTRAQ reagent [115]. Even though quantitative derivatization of all peptides was achieved with the iTRAQ reagent (Appendix III), the total number of peptides and phosphopeptides was much lower than in the unlabeled phosphoproteome (164 vs. 1,683 unique phosphopeptides). The low yield of peptides, observed also by other laboratories, is probably a consequence of the higher charge state of iTRAQ-modified peptides in comparison to the unlabeled counterparts. This leads to very complex fragmentation spectra that are difficult to identify by data bank searching [116]. A similar trend,

although much less pronounced, was also observed in the present study, where the percentage of doubly, triply and higher charged ions was 88%, 11%, 1% versus 83%, 15%, 2% for the unlabeled and iTRAQ-labeled phosphopeptides, respectively. Since the iTRAQ approach was unsatisfactory, it was decided to perform relative quantification by stable isotope labeling with amino acids in cell culture (SILAC [117]).

In contrast to iTRAQ, SILAC has the distinct advantage that the protein extracts from control and rapamycin-treated cells are mixed in equal amounts before fractionation, thus reducing experimental variation, time and number of samples to be processed. Similar to the original qualitative phosphoproteomic workflow, phosphopeptides from in-gel digested proteins were enriched by IMAC, and the resulting phosphopeptide pools were sequentially analyzed by LC-MS/MS (Figure 3.4A). To increase the phosphoproteome coverage and, equally important, to obtain statistically sound results, four independent biological replicates were processed. The advantage of performing different experiments to increase phosphoproteome coverage is illustrated in Figure 3.4C. Essentially, only 50% of the total phosphopeptides have been identified and quantified in three or more experiments and 20% of the total hits have been found in just one out of four experiments.

Even though a complete set of phosphopeptides could only be obtained with repeated runs, the reproducibility of the SILAC ratios was very high. The SILAC ratios of each phosphopeptide from each individual experiment were compared to the average ratio of all other combined experiments and in all four cases high correlation values were obtained (Figure 3.4D). In total 2,487 unique phosphopeptides and 2,607 unique phosphorylation sites mapping to 972 phosphoproteins were quantified (Figure 3.4B and Appendix IV). These values agree well with previously published yeast phosphoproteomes: Gruhler *et al.* quantified 729 phosphorylation sites (from 503 *S. cerevisiae* phosphoproteins), while in more recent studies up to 2,887 quantitative phosphorylation sites had been reported [92, 100, 110, 118].

The abundance of the quantified phosphoproteins was compared to the protein abundance of all yeast open reading frames (ORFs), which were estimated in a previous study from genome-wide protein affinity purification experiments [119]. For this, the cumulative percentages of all yeast ORFs and of the proteins quantified in the

phosphoproteome were plotted. The two curves were perfectly superimposable (Figure 3.4E), indicating that the dynamic range of the SILAC-labeled phosphoproteins closely follows the previously determined expression levels in yeast. Equally important, the data suggest that there is no bias in the phosphoproteome towards highly expressed proteins so that low abundant phosphoproteins are equally well quantified than high abundance phosphoproteins. This is important when considering the many effects TORC1 exerts on signaling proteins such as transcription factors, protein kinases and phosphatases, which are typically present in low copy numbers in yeast cells.

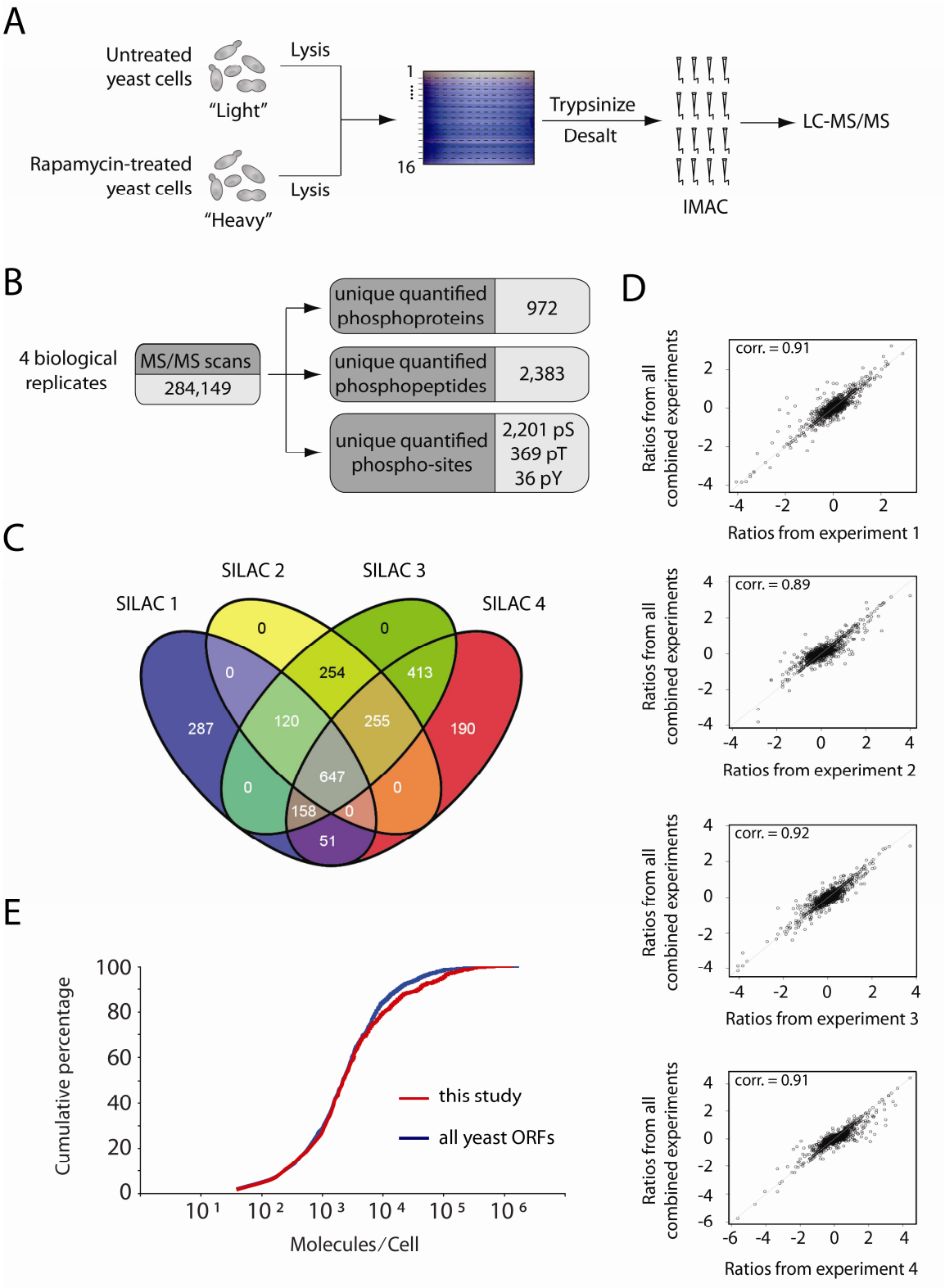
A
Untreated yeast cells
"Light"
Rapamycin-treated yeast cells
"Heavy"
Lysis
Lysis
1
16
Trypsinize
Desalt
IMAC
LC-MS/MS
B
4 biological replicates
MS/MS scans
284,149
unique quantified phosphoproteins
972
unique quantified phosphopeptides
2,383
unique quantified phospho-sites
2,201 pS
369 pT
36 pY
C
SILAC 1
SILAC 2
SILAC 3
SILAC 4
0
0
254
413
287
120
255
190
647
0
0
158
0
51
D
corr. = 0.91
Ratios from all combined experiments
Ratios from experiment 1
corr. = 0.89
Ratios from all combined experiments
Ratios from experiment 2
corr. = 0.92
Ratios from all combined experiments
Ratios from experiment 3
corr. = 0.91
Ratios from all combined experiments
Ratios from experiment 4
E
Cumulative percentage
Molecules/Cell
this study
all yeast ORFs

Figure 3.4: (A) Overview of the experimental approach for the quantitative TORC1-regulated phosphoproteome of *S. cerevisiae*. (B) Summary of the unique phosphoproteins/phosphopeptides that were quantified from four biological replicates. (C) Venn diagram for the overlap of quantitated phosphoproteins from the four biological replicates. (D) Evaluation of the biological reproducibility. The SILAC ratios from each single experiment were compared to the average ratios of all combined experiments. (E) Comparison between the protein abundances of all *S. cerevisiae* open reading frames (blue line) and the phosphoproteins quantified in this study (red line). Protein abundance data were retrieved from a genome-wide protein affinity purification study [119].

To identify those proteins whose changes in phosphorylation were significantly affected by rapamycin, four biological replicates for sound statistical significance were performed. For estimating the experimental variance, a control experiment was devised by mixing a light and a heavy cell culture without rapamycin treatment so that theoretically all SILAC ratios should be equal to 1. Any deviation from a ratio of 1.0 is caused by experimental variation so that a proper threshold for the rapamycin-treated cell cultures can be set. Since the SILAC ratios obtained from MaxQuant range from 0 to 1 for down- and from 1 to infinite for up-regulation, all ratios were log2-transformed to obtain a symmetrical distribution. For the control experiment, an average SILAC ratio of 0.02 with a standard deviation of 0.28 was obtained. Based on these values, the threshold for a significant up- or down-regulation of the four biological replicas following rapamycin treatment was set to twice the standard deviation of the control experiment (± 0.56). However, some phosphopeptides were observed in only one experiment (Figure 3.4C) but had a large change in the extent of phosphorylation. For such potentially interesting phosphorylation sites, the threshold was set to four times the standard deviation of the control experiment (± 1.12). With the above filters 78 proteins had up-, and 55 proteins had down-regulated phosphorylation following rapamycin treatment (Table 3.1 and 3.2).

In the present phosphoproteome many significantly up- or down-regulated phosphoproteins have previously been linked to TORC1 signaling (Table 3.1 and 3.2). Consistent with the first qualitative phosphoproteome and previously published data, a clear decrease in phosphorylation of Atg13 and Sch9 was observed [51, 66]. In contrast to the qualitative phosphoproteome, the effect of rapamycin on the phosphorylation of

other TORC1-regulated proteins, like Maf1, Npr1 and Rim15 became now clearly apparent (Table 3.1 and 3.2) [34, 47, 59].

It should be noted that not all changes observed in the phosphoproteome are caused by specific phosphorylation events. Previous reports have shown that a very short treatment with rapamycin (<20 min) already induces substantial transcriptional changes of specific sets of genes [41, 42]. As a result, a change in the extent of phosphorylation of a given protein could be just as well the consequence of the altered mRNA level. To discriminate between changes in gene expression or phosphorylation induced by rapamycin, the present phosphoproteomic data were compared with previously published microarray data obtained from rapamycin-treated yeast cells [42]. A comparison of the two data sets showed that in 25% of all proteins the regulation was probably a consequence of altered transcriptional levels rather than altered phosphorylations (third column in Table 3.1 and 3.2). However, for 13% of the proteins an inverse correlation between the change in phosphorylation and mRNA levels was observed (third column in Table 3.1 and 3.2). This clearly rules out that these changes in phosphorylation were an indirect effect of a change in gene expression. Obviously altered mRNA levels do not necessarily correspond to changes in protein levels. This is because not only protein synthesis but also protein stability and degradation are important determinants affecting the overall protein abundance. Furthermore, the mRNA needs to be processed and translated before alterations on protein expression become evident. Therefore, a comparison between phosphoproteomic and transcriptomic data does not always allow deciding whether a phosphorylation change is due to a change in protein abundance or not. To see if a change in the extent of phosphorylation is a consequence of altered translation/degradation or phosphorylation, an aliquot of each sample was analyzed by LC-MS/MS before IMAC selection to quantitate the proteins in relative terms. In theory, based on the intensity of the ensemble of peptides belonging to the same protein, it should be possible to see if the expression of this protein is altered or not. Unfortunately, because of the enormous peptide complexity, only 34% of the proteins which were identified in the phosphoproteome could be traced in the LC-MS/MS runs of the digests prior to IMAC enrichment (Appendix V). In spite of the low proteome coverage, it was possible to monitor the relative expression levels of 1,328 yeast proteins (fourth column

in Table 3.1 and 3.2 and Appendix V). Interestingly, only 1.2% of the observed proteins had up- or down-regulated protein expression in response to rapamycin (Table 3.3), which means that the transcriptional effects exerted by rapamycin usually take more than 20 minutes to alter protein expression. Among the regulated proteins, 12 had higher, and 4 lower expression levels following rapamycin treatment (Table 3.3). Consistent with published microarray data [42], among the up-regulated proteins there were several permeases (Agp1, Can1, Dip5, Gap1, and Ptr2) as well as the enzyme Dur1,2 responsible for urea catabolism. Moreover, in accordance with the negative control of TORC1 on glycogen synthesis, the expression of the glycogen synthase enzymes Gsy1/2 was found to be significantly increased after rapamycin treatment.

Hyperphosphorylated proteins (part I)

	Phospho Site (Av. Ratio ± SD)	mRNA	Protein
CAN1	S 38 (2.92 ± 1.19)	↑	↑
CDC33	S 30 (12.90) *		→
CIN5	S 196 (2.29 ± 0.49)		
	T 198 (1.96 ± 0.20)		
CLA4	T 447 (1.74 ± 0.08)		→
DAL81	S 860, S 862 (2.52) *		
DBF2, DBF20	T 544 (2.68) *		
DCS2	S 63 (2.49 ± 0.11)	↑	
	T 64 (2.73 ± 0.38)		
DED1	S 535, S 539 (21.480) *		
	S 535 (5.90 ± 1.69)	↓	
	S 539 (6.93 ± 3.14)		
DIP5	T 10, S 11 (2.36) *		
	S 11 (3.64 ± 0.08)		
	S 11, S 17 (4.21) *		
	T 12 (3.36 ± 1.43)	↑	
	S 13 (3.57 ± 0.96)		
	S 17 (2.36 ± 0.16)		
	S 18 (2.28 ± 0.19)		
	S 22 (2.12 ± 0.46)		
EAF1	T 971 (1.84 ± 0.18)		
ECM3	S 338 (4.76) *	↓	
EFR3	S 735 (1.94 ± 0.43)	↓	
ELP4	S 222 (1.96 ± 0.06)	↓	→
GCS1	S 157 (2.08 ± 0.39)		→
GDH2	S 482 (2.64 ± 1.42)	↑	
GIN4	S 666 (2.14 ± 0.21)		→
GIS1	S 694, S 696 (2.12 ± 0.17)		
	S 425 (2.50 ± 1.02)		
GPH1	T 31 (2.33 ± 0.59)	↑	↑
GYP5	S 834 (1.77 ± 0.00)		
HAL5	S 17 (1.80 ± 0.22)		
	S 17, S 19 (3.95) *		
HBT1	S 303 (2.24) *		
	S 956, S 959, S 962 (1.56 ± 0.03)	↑	
HOM3	S 332, S 344 (6.77) *		→
	T 333, S 344 (4.82) *		
IGO1	S 64 (2.43 ± 0.57)		
ISW2	T 1079 (1.83 ± 0.29)		
ITR1	S 46 (4.70 ± 1.97)		→
	T 12, S 26, S 31 (1.66 ± 0.05)		
KEL1	S 613, S 621 (4.08) *		→
KIN2	S 888 (3.19 ± 0.65)	↓	
KKQ8	S 21 (1.98 ± 0.05)		
	S 75 (2.96) *		
LDB19	T 795 (6.64 ± 0.58)		

	Phospho Site (Av. Ratio ± SD)	mRNA	Protein
LSB3	T 298, S 303 (3.00) *	↑	
	S 300, S 303 (2.35) *		
LYP1	S 87, T 90 (2.30) *		
MDG1	S 287 (9.00) *		
	S 288 (3.37 ± 1.87)	↑	
	S 291 (6.17) *		
MEP2	S 484, S 487, S 490, S 491 (2.23) *		
	S 487, S 490, S 491 (2.43) *	↑	
	S 490, S 491 (2.44 ± 0.66)		
	T 459 (3.21 ± 0.72)		
MLF3	S 74 (2.73) *		
MRE11	S 560 (1.52 ± 0.03)	↑	
MSC3	S 363 (1.99 ± 0.10)		
MTC1	S 75 (4.42 ± 1.48)		→
NCL1	S 424 (2.81 ± 0.27)	↓	→
NEW1	S 1181 (1.94 ± 0.27)	↓	→
NOC2	S 70 (2.62 ± 0.85)	↓	→
NSG2	S 90, S 93 (3.27 ± 1.17)		
	S 90 (2.01 ± 0.35)		→
	S 93 (2.51 ± 0.71)		
	S 49 (1.87 ± 0.14)		
NUS1	S 60 (4.55) *		
ORM1	S 29, S 32 (3.25 ± 0.21)		
	S 29, S 34 (3.50) *		
	S 32, S 34 (2.82 ± 0.60)		
	S 32 (2.04 ± 0.40)		
	S 35, S 36 (3.19) *		
OSH3	T 352 (2.56 ± 0.54)		
	S 209 (2.08 ± 0.33)		
PAN1	S 1003 (1.78 ± 0.23)		→
PAR32	S 246 (3.11 ± 0.88)		
	S 36, S 39 (4.90) *	↑	
	S 39 (2.50 ± 0.89)		
PCL7	S 58 (2.62) *	↑	
PDR12	S 56 (2.93 ± 1.49)		→
PDR16	S 346 (2.25 ± 0.26)		→
PSP2	S 340 (2.03 ± 0.26)		
PTR2	S 39, S 45 (1.71 ± 0.20)		
	S 6, S 9 (1.83 ± 0.05)		
	S 36, S 39, S 45 (1.97 ± 0.11)		
	Y 49, S 54 (3.16 ± 0.19) *	↑	
	Y 49 (3.71) *		
	S 52, S 54 (2.97) *		
	S 52 (3.00 ± 0.05) *		
PUT4	S 47 (4.30) *	↑	
RAS2	T 227 (4.19) *	↑	→

Hyperphosphorylated proteins (part II)			
	Phospho Site (Av. Ratio ± SD)	**mRNA**	**Protein**
RSC2	T 243 (3.29 ± 1.06) S 682 (2.36 ± 0.7)		
RTS3	S 47, S 50 (5.68) * S 47 (3.03) * S 238 (8.84) * S 241 (8.06 ± 3.81)	↑	
RTT107	T 532 (2.45 ± 0.74)		
SCP160	T 50 (1.51 ± 0.03)	↓	→
SEC7	S 772 (7.08 ± 0.28)		→
SMI1	S 200, S 201 (1.79 ± 0.2) S 202, S 203 (2.21) *		
SPN1	T 15 (1.89 ± 0.19)		→
SSD1	S 480 (3.03 ± 0.2) T 482 (2.90 ± 0.39)		→
SSK2	S 39 (2.18 ± 0.01)		
TCB3	S 1340, T 1350 (1.73 ± 0.14)		→
TEA1	T 755 (1.82 ± 0.16)		
TIF4632	T 196 (1.91 ± 0.31)		→
TIF5	T 191 (3.90 ± 1.1)	↓	→
TPS3	S 148 (1.68 ± 0.22)	↑	→
TSL1	S 147 (3.84 ± 1.11) S 73, S 77 (5.24 ± 1.11) *	↑	
TSL1	T 75, S 77 (10.10) * S 77 (1.72 ± 0.32)	↑	
YBR287W	S 228 (5.74 ± 2.58) S 231, S 234 (2.96 ± 0.06) S 231 (7.09) *		
YBT1	S 936 (8.98 ± 1.7) *		→
YGR125W	S 149 (2.40) *		
YGR237C	T 638 (2.55 ± 0.71)	↑	→
YLR152C	S 287 (4.78) * S 273 (1.64 ± 0.05)	↑	
YLR257W	S 7 (6.42) * T 44 (10.680 ± 5.29) S 137 (2.92 ± 1.89)	↑	
YOR051C	S 30, S 33 (2.86) * S 30, T 34 (3.04 ± 0.67) S 33 (2.46) *	↓	
YPR172W	S 99, T 103 (2.45 ± 0.18) T 101 (2.57) * T 103 (3.14) *	↑	
YSC84	S 301, S 311 (1.86 ± 0.09) S 274 (2.71 ± 0.36)		→
ZEO1	S 25 (1.85 ± 0.24)	↑	→

Table 3.1: Rapamycin-induced increase of phosphorylation. For each protein the regulated phosphorylation site(s) and the fold-increase (Av. Ratio ± SD) is given. Significantly increased (↑) or decreased (↓) mRNA levels after rapamycin treatment [42] are indicated. The fourth column shows increased (↑) or unchanged (→) protein expression measured in the proteomic analysis. An asterisk (*) marks phosphopeptides identified only in one experiment.

Hypophosphorylated proteins			
Protein	**Phospho Site (Av. Ratio ± SD)**	**mRNA**	**Protein**
AMD1	T 136 (0.38 ± 0.09) S 138 (0.31 ± 0.09)		→
ATG13	S 554 (0.09) * S 649 (0.29 ± 0.19) S 346, S 348 (0.08 ± 0.01) S 379 (0.28 ± 0.12)		
BNI4	S 43 (0.43) *		
BOI1	S 147 (0.46) *		
BUL1	S 195 (0.47 ± 0.11)		
CCR4	S 281, T 285 (0.63 ± 0.03)		
CLB3	S 33 (0.37) *		
DNF3	S 908 (0.27) *		
DOT6	S 245 (0.33 ± 0.04) S 247 (0.44) *		
EAP1	S 281 (0.51 ± 0.07) S 282 (0.57 ± 0.15)		
ESF1	S 223 (0.65 ± 0.02)	↓	→
FIN1	S 36 (0.51 ± 0.09)	↑	
FRA1	S 56 (0.48 ± 0.16)		
GAT1	S 270 (0.34 ± 0.16)	↑	
GCN2	S 577 (0.18 ± 0.02) S 569, S 572 (0.07 ± 0.02)		
GIN4	S 502 (0.30) *		→
GNP1	S 111 (0.35 ± 0.09) S 113 (0.27 ± 0.05)	↓	
IRA2	S 631 (0.02) *		
KCS1	S 581 (0.37 ± 0.05) S 537 (0.42) *		
KSP1	T 526, S 529 (0.35 ± 0.05) S 827 (0.27 ± 0.01) S 883, S 884 (0.11) * S 884 (0.40) *		
LHP1	S 19 (0.51 ± 0.13)	↓	→
MAF1	S 90 (0.25 ± 0.08) S 209 (0.29) *		
MET2	T 272 (0.31) *		
MKS1	S 518 (0.43 ± 0.18)		
MOB2	S 38 (0.61 ± 0.04)		
NAP1	T 20, T 24, S 27 (0.10) * T 20, T 24 (0.47 ± 0.10) T 20 (0.42) *		→
NAP1	T 24 (0.59 ± 0.00)		→
NPR1	S 255, S 260 (0.30) * S 353, S 356 (0.33 ± 0.16) S 257, S 260 (0.10) *	↑	
ORC2	S 188 (0.54 ± 0.05)	↓	
PCT1	S 16, S 19 (0.31 ± 0.04) S 19 (0.52 ± 0.02)	↑	→
PPH21, PPH22	S 272 (0.37) *		
PTR2	S 594 (0.35) *	↑	↑
RCN2	S 198 (0.41) *		
REG1	S 570 (0.41 ± 0.04)		
RIM15	S 1047 (0.52 ± 0.00)		
RPC82	S 392 (0.47 ± 0.12) S 394 (0.46 ± 0.10)	↓	
RPH1	S 587 (0.33) *		
RPL12A	S 38 (0.57 ± 0.08)	↓	→
SCH9	S 726 (0.22 ± 0.11)	↓	
SER33	S 20 (0.28 ± 0.05) S 22, S 29 (0.08 ± 0.04) S 22 (0.33 ± 0.10)		→
SKY1	S 445 (0.55 ± 0.05)		
SLA2	S 308 (0.55 ± 0.08)		→
SSD1	S 155 (0.37) * S 164 (0.56 ± 0.07)		→
STB3	S 337 (0.43 ± 0.12)		
STM1	S 55 (0.29) *	↓	→
SWI5	T 490, S 492 (0.37) *		
TGL1	T 460 (0.44) *		
UBR1	T 291, S 296 (0.62 ± 0.04)		
UBX7	S 388 (0.53 ± 0.08)		
URK1	S 14, S 17 (0.14) * S 14 (0.12 ± 0.04)	↓	
VTC2	S 196 (0.40) * S 583 (0.24 ± 0.03) S 182, S 187 (0.07) * S 182 (0.37 ± 0.02)		→
VTC3	S 592 (0.54 ± 0.15)		→
YBR028C	T 82 (0.23) *		
YJL016W	S 350 (0.50 ± 0.02)		→
YML119W	S 72 (0.39) *		
ZUO1	S 50 (0.58 ± 0.14)	↓	→

Table 3.2: Rapamycin-induced decreased of phosphorylation. For each protein the regulated phosphorylation site(s) and the fold-decrease (Av. Ratio ± SD) are given. Significantly increased (↑) or decreased (↓) mRNA levels after rapamycin treatment [42] are indicated. The fourth column shows increased (↑) or unchanged (→) protein expression measured in the proteomic analysis. An asterisk (*) marks phosphopeptides identified only in one experiment.

Increased abundance		
	Av. Ratio ± SD	mRNA
AGP1	2.39 *	↑
CAN1	3.47 *	↑
CIS3, HSP150, PIR1, PIR3, YJL160C	2.27 ± 0.43	↑
DIP5	2.86 ± 1.20	↑
DUR1,2	3.14 ± 1.20	↑
GAP1	5.66 ± 1.80	↑
GSY1, GSY2	1.61 ± 0.10	↑
INO1	3.01 *	↑
MSC1	2.15 ± 0.56	↑
OM45	1.73 ± 0.10	↑
PTR2	2.13 ± 0.37	↑
REP1	2.50 ± 0.43	

Decreased abundance		
	Av. Ratio ± SD	mRNA
PHO84	0.55 ± 0.08	↓
UFD2	0.31 *	
YLL054C	0.26 ± 0.26	
YNR021W	0.35 *	

Table 3.3: Rapamycin-induced increase or decrease in protein abundance. For each protein the fold-change in protein quantity (Av. Ratio ± SD) is shown. Increased (↑) or decreased (↓) mRNA levels after rapamycin treatment [42] are indicated. An asterisk (*) marks proteins identified in only one experiment.

To determine if TORC1 controls phosphorylation of specific sequence motifs, the sequences surrounding the rapamycin-regulated phospho-sites were analysed with the Motif-X algorithm (Figure 3.5 [120]). For sites whose extent of phosphorylation did not change, no clear kinase consensus was found except acidic sites (data not shown), which is a consequence of preferential binding of acidic phosphopeptides to the IMAC resin. For the peptides whose extent of phosphorylation was down-regulated upon rapamycin treatment, the top scoring motif was RRxS (the phosphorylated residue is underlined). The same motif was underrepresented in the phosphopeptides whose phosphorylation was up-regulated (Figure 3.5). In addition, the related motif RxxS appeared in both the up- and down-regulated phosphopeptides (Figures 3.5). Finally, the two motifs SP and SxxS were also present, but only in the up-regulated phosphopeptides. The same result was obtained when the rapamycin-sensitive phosphoproteome from Huber *et al.* was

analysed by Motif-X [34]. From this analysis, it appears that the RRxS consensus site is a primary target motif for TORC1-dependent phosphorylation.

Notably, the RRxS/T consensus becomes specifically phosphorylated by protein kinase A (PKA [121, 122]). Out of the 55 proteins whose phosphorylation was decreased upon rapamycin-treatment, 10 had decreased phosphorylation at PKA sites (Fra1, Gcn2, Kcs1, Ksp1, Lhp1, Maf1, Mks1, Ssd1, Vtc2, and Yjl016w). Interestingly, Fra1, Ksp1, Lhp1, Maf1, and Ssd1 have been shown to be PKA targets *in vitro* [72, 121] and Maf1 is phosphorylated and negatively regulated by PKA and TORC1 *in vivo* [34, 35, 123, 124]. Moreover, the localization of the serine/threonine protein kinase Ksp1 is affected by PKA [125], and Gcn2, Kcs1, Ksp1, Lhp1, Mks1, and Ssd1 have been linked to TORC1 and PKA signaling either genetically or biochemically (www.yeastgenome.org). These observations suggest that the PKA and TORC1 pathways are interconnected and that TORC1 may modulate PKA activity. It is important to note that not all PKA target motifs in our phosphoproteome were affected by rapamycin treatment, like the PKA sites in the two well-known PKA targets Msn2 and Nth1.

To confirm these findings, targeted analyses were performed for some PKA substrates, with particular emphasis on the effect of rapamycin treatment on the *in vivo* phosphorylation of the known or suspected PKA substrates Ksp1, Maf1 and Ypk3 (also known as Ybr028c and Kbn8). The regulated phosphorylation sites on these three proteins that were identified in the phosphoproteome are listed in Table 3.4 (the phosphorylation sites in bold conform to the PKA consensus site).

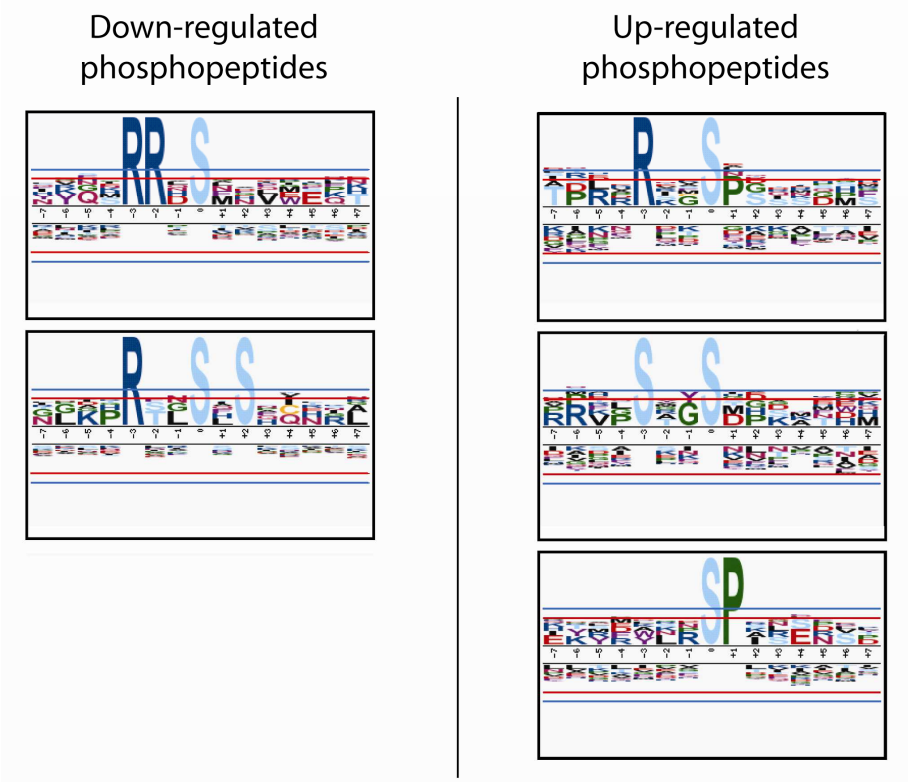

Figure 3.5: Motif analysis of the peptide sequences surrounding the rapamycin down- (left panel) and up-regulated (right panel) phosphorylation sites. For the Motif-X algorithm, the phosphorylation sites were extended by 7 residues on each side. The height of the residues is proportional to their binomial probabilities based on the background database (SGD). The red lines represent a p-value of 0.01 (after multiple hypothesis correction) and the blue lines represent the significance threshold used in the Motif-X analysis. Motifs are ranked from top to bottom.

Protein	Description (SGD)	Regulated phospho-site (Av. Ratio ± SD)	Direction
Ksp1	Ser/Thr protein kinase required for haploid filamentous growth.	T526, S592 (0.35 ± 0.05) **S827 (0.27 ± 0.01)** **S883, S884 (0.11)** **S884 (0.40)**	Decreased
Maf1	Negative regulator of RNA polymerase III in response to nutrients and stress.	**S 90 (0.25 ± 0.08)** **S 209 (0.29)**	Decreased
Ypk3	AGC kinase phosphorylated by PKA.	T 82 (0.23) **S 207 (0.67 ± 0.05)**	Decreased

Table 3.4: Proteins chosen to investigate the *in vivo* effect of rapamycin on the PKA consensus sites. All three proteins were found to be regulated in the phosphoproteome at sites with a perfect PKA consensus motif (phospho-sites in bold). The average fold change in phosphorylation and the corresponding standard deviation (SD) was calculated from all four phosphoproteomic experiments (Appendix IV).

To investigate the effect of rapamycin treatment on the *in vivo* phosphorylation of Maf1, Ksp1 and Ypk3, phosphorylation of these proteins was probed with an antibody specific for the phosphorylated consensus PKA target motif (anti-RRxS/T). As reported previously [123], PKA-dependent Maf1 phosphorylation was reduced after rapamycin treatment (Figure 3.6A), which agrees well with the phosphoproteome data (Table 3.4). Other reports, however, show activation of Maf1 by PKA via the TORC1 effector Sch9. Since Sch9 is a member of the AGC kinase family, it can directly phosphorylate the PKA consensus sites in Maf1 [34, 35]. To demonstrate that TORC1 activates PKA to phosphorylate Maf1, the cell permeable, phosphodiesterase resistant cAMP analogue 8-Bromo-cAMP [126] was used to activate PKA in rapamycin-treated yeast cells, in which TORC1 and Sch9 are inactive (Figure 3.6B). As expected, TORC1 inactivation upon rapamycin treatment resulted in a strong reduction of Maf1 phosphorylation at PKA sites and addition of 8-Br-cAMP to the cells restored Maf1 phosphorylation at the same sites (Figure 3.6B). Likewise, phosphorylation of both Ksp1 and Ypk3 at PKA consensus site(s) decreased upon rapamycin treatment (Figure 3.6A), which again agrees with the phosphoproteomic data (Table 3.4). Moreover, like Maf1, but to a lesser extent, activation of PKA with 8-Br-cAMP counteracted the inhibitory effect of rapamycin on the phosphorylation of Ypk3 at PKA sites (Figure 3.6B). Similar experiments were performed for the PKA substrates Cdc25, Cki1, Msn2, and Yak1. For Cdc25, Yak1, and Cki1 no phosphorylation by LC/MS/MS was detected at their PKA sites and for Msn2, no change in phosphorylation was found at the site residing in the PKA motif. Accordingly, no change in phosphorylation upon rapamycin treatment was detectable using the anti-RRxS/T antibody (Figure 3.6C). Thus, both large scale and targeted analyses suggest that TORC1 activates PKA towards a specific subset of substrates (e.g. Ksp1, Maf1 and Ypk3).

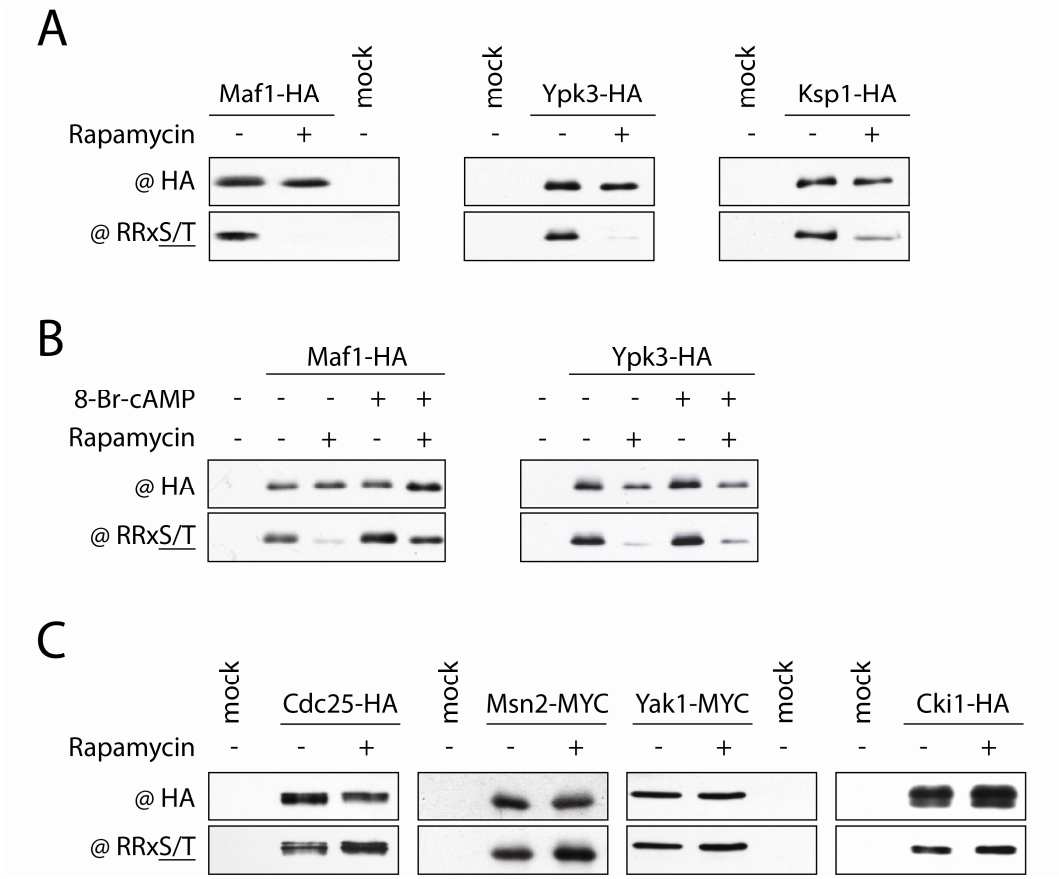

Figure 3.6: Influence of TORC1 inhibition on *in vivo* PKA substrate phosphorylation. (A) Rapamycin negatively affects the phosphorylation state at PKA sites of Maf1, Ypk3 and Ksp1. The blots were probed with an antibody against the HA tag (@ HA) or against the phosphorylated PKA consensus sequence (@ RRxS/T). (B) Constitutive PKA activation with 8-Br-cAMP compensates the rapamycin-induced dephosphorylation at PKA sites of Maf1 and Ypk3. The blots were probed as in (A). (C) Effect of rapamycin treatment on PKA substrates whose consensus sequence phosphorylation was not altered. The blots were probed as in (A).

3.3. Validation of the Phosphoproteomic Data

In 2009 another yeast rapamycin-regulated phosphoproteome was published [34]. A comparison of the two studies revealed surprisingly little overlap. Although the total number of rapamycin-regulated phosphoproteins was very similar in the two studies (133 vs. 129), only 29 phosphoproteins (13 down- and 16 up-regulated) were common (Figure

3.7). Among the phosphoproteins identified exclusively in this study, there are many which have already been shown to be clearly involved in TORC1 signaling (Gcn2, Npr1, Rim15 and Ssd1). Other phosphoproteins represented in this study were shown to have altered sensitivity to rapamycin, caffeine or wortmannin resistance upon gene deletion (Figure 3.7). This clearly shows that depending on the approach and conditions used, complementary phosphoroteomes are obtained. Nevertheless, this also means that a thorough validation of the phosphoproteomic data is required, especially regarding those proteins that were found in just one of the two studies. Moreover, the observation that a protein contains rapamycin-sensitive sites is definitely an important indicator of its involvement in TORC1 signaling, but it needs further validation by additional experiments. Indeed, even a significantly regulated phospho-site may have no functional consequence. This is because the phosphorylation changes measured in the phosphoproteome are relative rather than absolute changes. In addition, the protein coverage in the phosphoproteome is typically low due to the high dynamic range and the complexity of the sample. As a consequence, additional regulated phospho-sites could be missing for each phosphoprotein identified in the phosphoproteome. For these reasons, it was important to further investigate some of the identified rapamycin-sensitive phosphoproteins to check whether they were real TORC1 effectors.

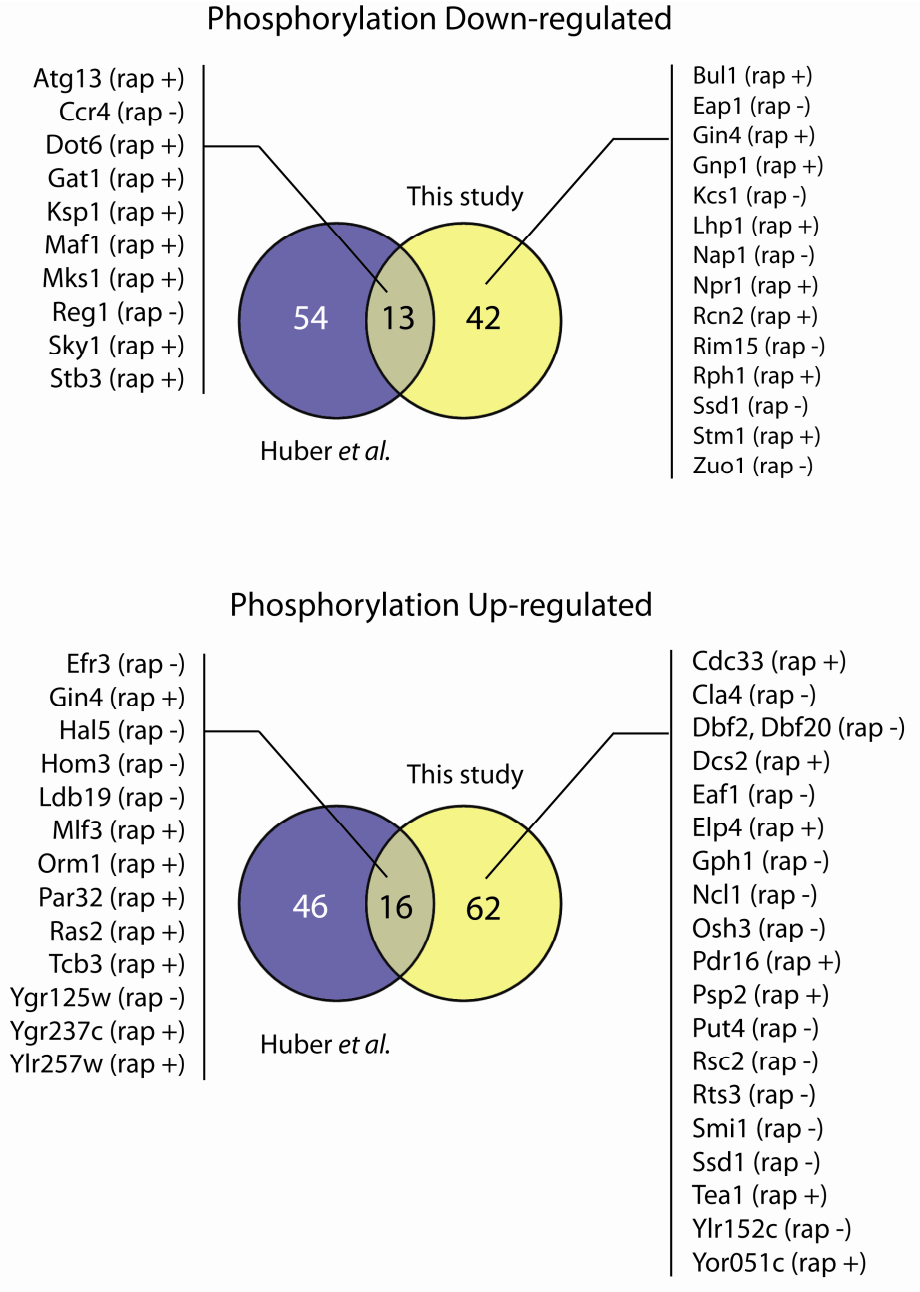

Figure 3.7: Overlap between the present and a previously published rapamycin-sensitive phosphoproteome [34]. The regulated phosphoproteins common to both studies are listed on the left while regulated phosphoproteins unique in the present study are listed on the right of the Venn diagrams. (rap +) and (rap -) indicate increased or decreased resistance to rapamycin in the corresponding null mutants.

Twelve proteins that were found to be significantly affected in phosphorylation by rapamycin were chosen for further investigation. This choice was based on the following criteria: firstly, we focused only on phosphoproteins identified in the present study. Secondly, priority was given to those phosphoproteins that were found to be regulated in at least three out of four independent experiments. Thirdly, proteins whose biological functions could be linked to TORC1 downstream signaling were preferred over less well-characterized proteins.

Twelve proteins were chosen for additional investigation, eight of them (Hal5, Isw2, Kkq8, Ldb19, Mtc1, Noc2, Rts3, and Sec7) were more phosphorylated following rapamycin treatment, and four had decreased phosphorylation upon rapamycin treatment (Nap1, Reg1, Vtc2, and Vtc3) (Table 3.5). Hal5 and Kkq8 are members of a class of serine/threonine kinases involved in regulating various plasma membrane transporters. They are homologous to the Npr1 kinase, which has already been shown to be a target of TORC1 signaling [47]. Noc2 is a plausible target of TORC1 signaling since it is involved in the intranuclear transport of ribosomal precursors [127], an important step in ribosome biogenesis. Ldb19 is implicated in the regulation of stability of plasma membrane permeases [128], which may explain its involvement in nutrient uptake and TORC1 signaling. Nap1 was particularly interesting due to its physical interaction with TORC1 [129] and because its deletion affects the localization of the kinase Gin4 [130], another protein found to be significantly affected by rapamycin (Table 3.1 and Table 3.2). Vtc2 and Vtc3 are subunits of the vacuolar transporter chaperone complex. They are attractive candidates because TORC1 has been shown to localize to the vacuolar membrane [131]. Isw2 is interesting because it represses *INO1* expression [132] and its protein product is also increased upon rapamycin treatment in the proteomic analysis (Table 3.3). The regulatory subunit Reg1 of the Glc7 phosphatase is required for the dephosphorylation and inactivation of the kinase Snf1, which had been shown to become more phosphorylated at T210 upon rapamycin treatment [133, 134]. Rts3 is a putative component of the protein phosphatase type 2A (PP2A) and it is interesting because TORC1 controls the activity of PP2A and PP2A-like phosphatases [64]. Finally, the proteins Mtc1 and Sec7, even though unrelated to TORC1 at a first glance, were included

for validation as they had reproducibly large changes in phosphorylation following rapamycin treatment (Mtc1: 4.24 ± 0.93; Sec7: 7.08 ± 0.28).

Protein	Description (SGD)	Regulated phospho-site (Av. Ratio ± SD)	Direction
Hal5	Putative protein kinase involved in the regulation of Trk1/Trk2 transporters.	S17 (1.77 ± 0.26) S17, S19 (3.95)	Increased
Isw2	ATP-dependent DNA translocase involved in chromatin remodeling.	T1079 (1.83 ± 0.29)	Increased
Kkq8	Putative S/T kinase. Member of the Npr1/Hal5 protein kinase family	S21 (1.98 ± 0.05) S75 (2.96)	Increased
Ldb19	Protein involved in regulating the endocytosis of plasma membrane proteins by recruiting the ubiquitin ligase Rsp5 to its target.	T795 (6.64 ± 0.58)	Increased
Mtc1	Protein of unknown function. Interacts with ribosomes.	S75 (4.42 ± 1.48)	Increased
Nap1	Involved in the transport of H2A and H2B histones to the nucleus. Involved in regulating mictotubule dynamics during mitosis. Controls bud morphogenesis.	T20 (0.42) T20, T24 (0.47 ± 0.10) T20, T24, S27 (0.10) T24 (0.59 ± 0.00)	Decreased
Noc2	Protein that mediates intranuclear transport of ribosomal precursors	S70 (2.62 ± 0.85)	Increased
Reg1	Regulatory subunit of the protein phosphatase Glc7. Negatively regulates glucose-repressible genes.	S570 (0.41 ± 0.04)	Decreased
Rts3	Putative component of the protein phosphatase type 2A complex.	S47 (3.03) S47, S50 (5.68) S238 (8.84) S241 (8.06 ± 3.81)	Increased
Ses7	GEF factor for ARF proteins involved in proliferation of the Golgi. Regulates ER-to-Golgi transport.	S772 (7.08 ± 0.28)	Increased
Vtc2	Subunit of the vacuolar transporter chaperone (VTC) complex involved in membrane trafficking, microautophagy and non-autophagic vacuolar fusion.	S182 (0.37 ± 0.02) S182, S187 (0.07) S196 (0.40) S583 (0.24 ± 0.03)	Decreased
Vtc3	Subunit of the vacuolar transporter chaperone (VTC) complex involved in membrane trafficking, microautophagy and non-autophagic vacuolar fusion.	S592 (0.54 ± 0.15)	Decreased

Table 3.5: Phosphoproteins whose extent of phosphorylation was significantly altered by rapamycin treatment selected for further studies. Protein functions were retrieved from SGD (http://www.yeastgenome.org/).

To check the role of the above proteins in TORC1 signaling, (1) the rapamycin sensitivity and (2) the glycogen accumulation of the corresponding deletion mutants were investigated; (3) their SDS-PAGE mobility was monitored to check if rapamycin treatment was able to induce a shift in migration; and (4) an in-depth LC-MS/MS analysis was performed to confirm the regulated phosphorylation sites identified in the phosphoproteome and to check for the presence of additional rapamycin-sensitive sites.

3.3.1. Rapamycin Sensitivity, Glycogen Accumulation and Electrophoretic Mobility Shift

The rapamycin sensitivity of the null mutants was compared with the one of the wild-type strain TB50**a** (Figure 3.8A). This is an important indicator, because many known TORC1 effectors cause sensitivity or resistance to rapamycin when deleted (e.g. *gln3Δ, kog1Δ, lst8Δ, msn4Δ, npr1Δ, rim15Δ, sch9Δ, sfp1Δ, tco89Δ, tor1Δ*). Similarly, the strains *isw2Δ*, *reg1Δ*, *hal5Δ* and *ldb19Δ* are more sensitive to rapamycin because they mimic the *tor1Δ* phenotype. Interestingly, while *reg1Δ*, *hal5Δ* and *ldb19Δ* have been shown to be less sensitive to rapamycin in strains with a different background, it has never been shown that *ISW2* deletion confers sensitivity to rapamycin. Moreover, in contrast to the published rapamycin sensitivity [135], no change in rapamycin resistance of the *nap1Δ* mutant was observed. The rapamycin sensitivity of *sec7Δ* and *noc2Δ* could not be investigated, because both null mutants were not viable (Figure 3.8B).

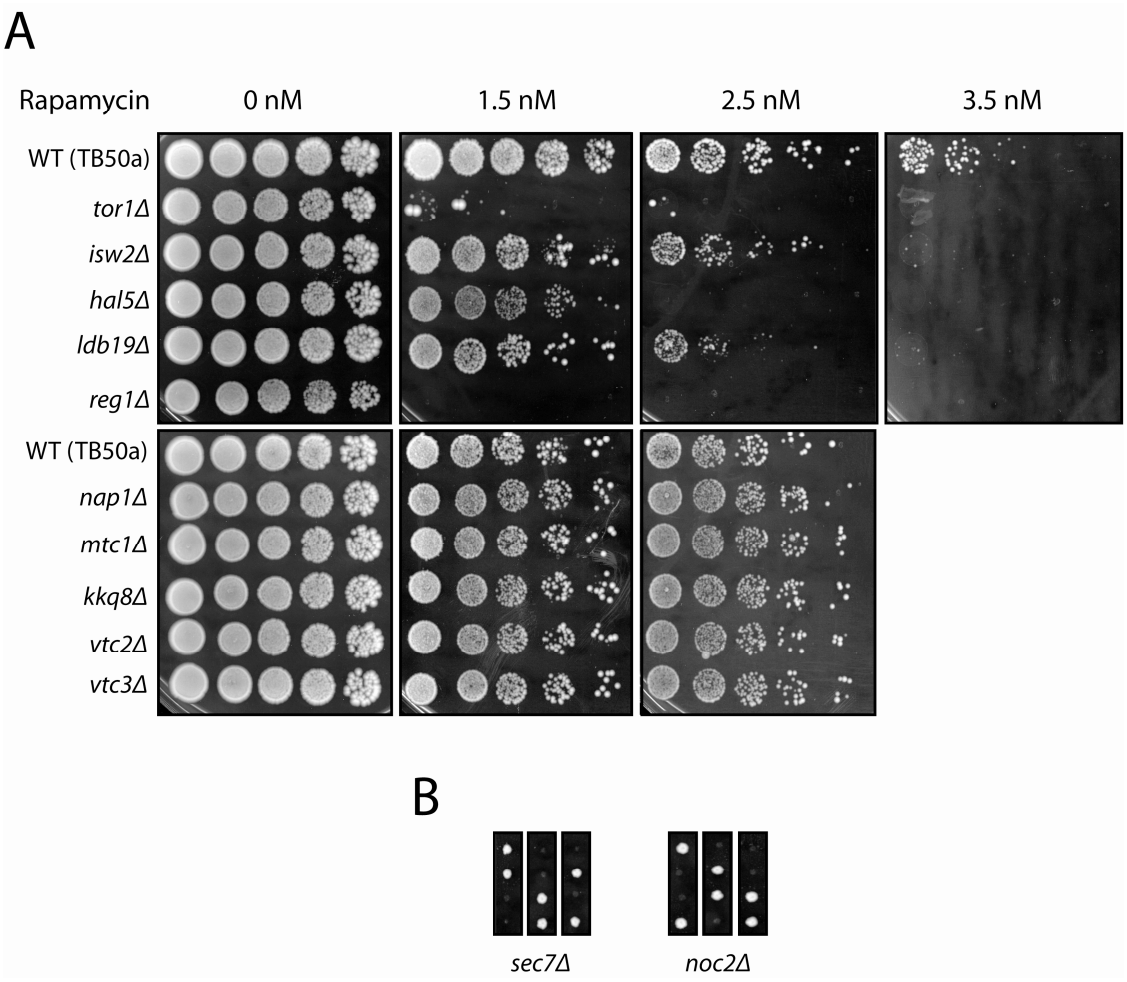

Figure 3.8: (A) Sensitivity of the null mutants against increasing concentrations of rapamycin. The null mutants were compared to the rapamycin sensitivity of the wild-type strain TB50a and the hypersensitive *tor1Δ* mutant. (B) Tetrad dissection of heterozygous *sec7Δ/sec7* and *noc2Δ/ noc2* mutants. The homozygous deletion strains are not viable.

To cope with stress, such as nitrogen starvation, yeast cells typically increase the synthesis of the storage carbohydrates glycogen and trehalose [136]. Because nitrogen starvation causes inactivation of TORC1, *tor1Δ* mutants accumulate more glycogen than wild type cells [25]. Therefore, altered accumulation of glycogen upon deletion of a gene is a good indication whether a protein is involved in TORC1 signaling or not. For example, deletion of *KOG1*, *TCO89*, and *NPR1* leads to increased glycogen accumulation, and individual deletions of *ATG1*, *ATG13*, *ATG17*, and *RIM15* accumulate

less glycogen than wild type cells [137]. However, it is also known that pathways other than TORC1 impinge on glycogen synthesis, such as the PKA and Snf1 pathways. For example, both *bcy1Δ* cells with constitutively active PKA signaling and *snf1Δ* cells have reduced glycogen accumulation [138, 139]. Therefore, altered glycogen accumulation and rapamycin sensitivity are indicators (but by no means certain) that a gene is part of the TORC1 signaling pathway.

Concerning the mutants selected for the phosphoproteome validation, *ldb19Δ*, *hal5Δ*, *reg1Δ* and *isw2Δ* deletions clearly increased glycogen accumulation, which was even more pronounced after rapamycin treatment (Figure 3.9). *reg1Δ* was expected to cause increased glycogen accumulation due to its role in targeting the Glc7 phosphatase to the Snf1 kinase. Dephosphorylation inactivates the kinase activity of Snf1 and *snf1Δ* cells accumulate less glycogen than the wild type [139]. As a result, *REG1* deletion should lead to an increase in phosphorylation and activation of Snf1 and therefore increase glycogen levels.

The observation that deletion of *ISW2*, a chromatin remodeling factor, has increased glycogen accumulation is more difficult to explain. This mutation is probably only indirectly related to glycogen metabolism, because glycogen levels are also affected by cellular stress, which may be caused by perturbation of chromatin structure. Nevertheless, it has also been shown that *ino1Δ* cells accumulate less glycogen and *INO1* transcription is repressed by Isw2. This has been clearly observed in the proteomic analysis as well, where the Ino1 protein level was significantly increased upon rapamycin treatment (Table 3.3). Consequently, *ISW2* deletion should relieve the repression on *INO1* expression and as a result lead to increased glycogen accumulation.

Ldb19 is a protein involved in endocytosis of plasma membrane permeases and, as such, abnormal glycogen accumulation in *ldb19Δ* could be a consequence of decreased nutrient uptake impinging on TORC1. Less clear is the phenotype of *hal5Δ*, a protein involved in the regulation of Trk1/2 potassium transporters. Maybe the abnormal phenotype observed in *ldb19Δ* is a consequence of cellular stress because it is known that *hal5Δ* mutants are more susceptible to various types of stresses (e.g. hyperosmotic, ionic, doxorubicin and cisplatin hypersensitivity).

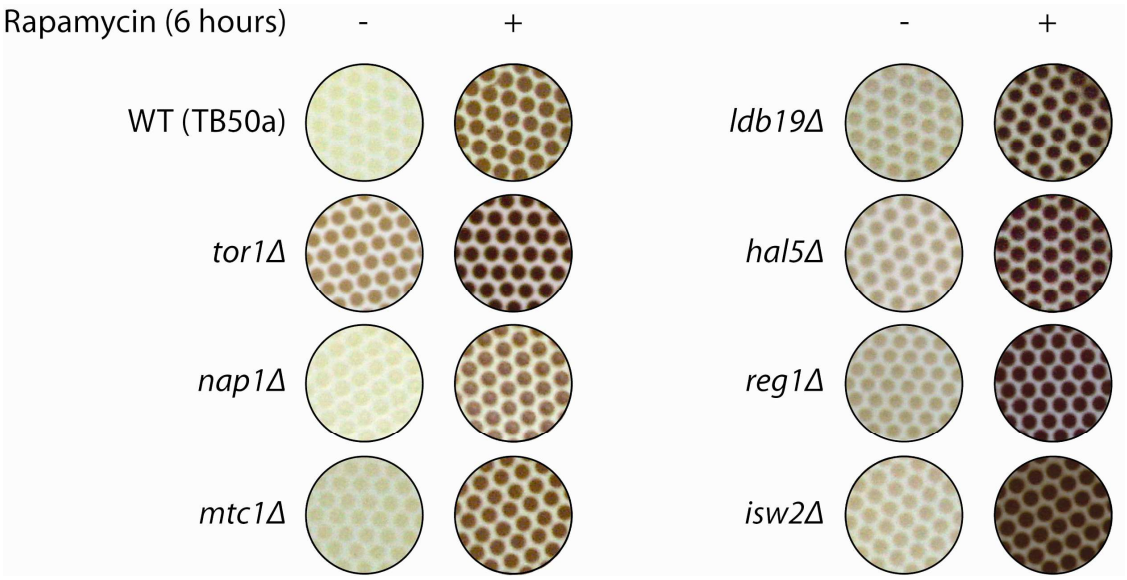

Figure 3.9: Glycogen accumulation of rapamycin- or vehicle-treated yeast cells. Glycogen accumulation of the individual deletion mutants was compared to the wild-type TB50a strain and the *tor1Δ* strain.

Next, the gel migration of the selected candidates was checked since protein phosphorylation often induces a shift in electrophoretic mobility [140]. For the majority of the tested proteins, no shift in electrophoretic migration following rapamycin treatment was seen. This can in part be explained by the high molecular weight of the proteins tested. Also, a migration shift is unlikely to occur if the change of phosphorylation induced by rapamycin is small or if the overall site occupancy is low (see 3.2.2). Nevertheless, rapamycin treatment of Ldb19-HA and Kkq8-HA led to shifts in migration, and interestingly, an increase in protein abundance upon rapamycin treatment (Figure 3.10A). The expression of Rts3-MYC was also up-regulated probably by an increase in the mRNA level (Fig. 3.9A, Table 3.1) [41, 42]. Since for Ldb19 and Kkq8 no change in mRNA abundance was reported [41, 42], the observed increase in protein abundance could be due to increased protein stability perhaps brought about by phosphorylation. The mobility shift of Ldb19-HA and Kkq8-HA was reversed with λ protein phosphatase treatment (Figure 3.10B). Notably, for Ldb19-HA two isoforms approximately 7-8 kDa

apart were detected (Figure 3.10A-B). The mass shift conforms to a modification of Ldb19 by ubiquitin. This protein was reported to be ubiquitinated at K486 by the E3 ubiquitin ligase Rsp5 [128]. Interestingly, it seems that both isoforms are affected by treatment with rapamycin. Similar to Ldb19-HA, the change in the electrophoretic mobility of Kkq8-HA induced by rapamycin could be better appreciated when the protein was treated with λ protein phosphatase (Figure 3.10B). In conclusion for all proteins except Ldb19-HA and Kkq8-HA, no clear change in migration was observed. In the case of Ldb19-HA, Kkq8-HA and Rts3-MYC a change in protein abundance was also apparent. Finally, for Sec7-HA a slight change in migration was observable, but it was evident only for a degradation product of Sec7-HA and not for the intact protein.

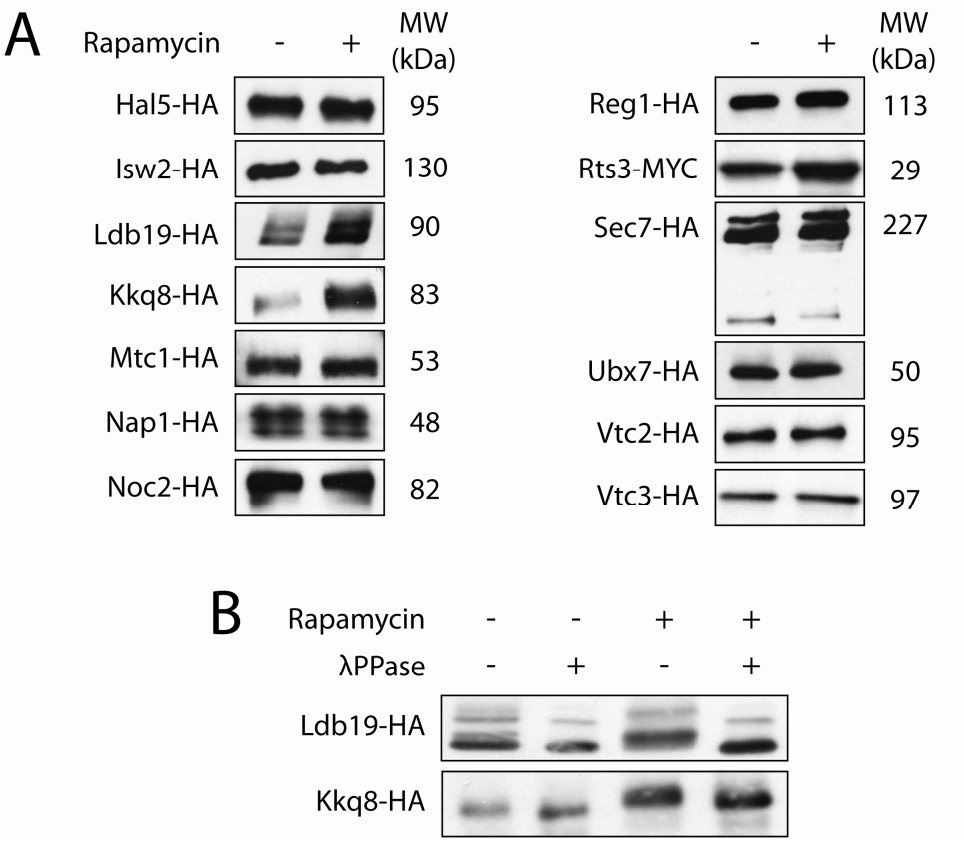

Figure 3.10: (A) Comparison of the electrophoretic migration of HA-/MYC-tagged candidate proteins isolated from untreated (-) or rapamycin-treated (+) cells. (B) In addition to rapamycin treatment, the immunoprecipitates of Ldb19 and Kkq8 were further treated with (+) or without (-) λ protein phosphatase.

3.3.2. In-depth LC-MS/MS Analysis of Selected Regulated Phosphoproteins

Mapping phosphorylation sites on a system-wide scale yields a wealth of information that can be used to better define signaling cascades. Nevertheless, often a discrepancy exists between the data obtained from in-depth LC-MS/MS analysis of isolated proteins and those found in large-scale mapping projects inasmuch as more phosphorylation sites are usually found in isolated systems. Therefore, for each candidate protein, the presence of additional phosphorylation sites was investigated by in-depth LC-MS/MS analysis. This type of analysis also addresses a second question namely the lack of mobility shift of the proteins selected for validation.

The in-depth LC-MS/MS analysis consisted in the isolation of each protein by immunoprecipitation from untreated and rapamycin-treated cells, protein digestion using different proteases to increase protein coverage, and subsequent LC-MS/MS analysis. Typically, the immunoprecipitates were first checked by data-dependent MS/MS to confirm the presence of the phosphorylation sites found in the quantitative phosphoproteome and to search for additional phosphorylation sites. This was then followed by a targeted LC-MS/MS experiment to better localize the phosphorylation site(s) in the peptides. Inclusion lists allow acquiring many more MS/MS spectra per phosphospeptide so that many MS/MS scans can be added for a much safer localization of the site of phosphorylation. Finally, single-reaction monitoring of specific precursor ion/fragment ion transitions was sometimes performed to be able to quantify phosphorylation changes of coeluting phosphopeptide isoforms. Notably, in all these experiments no phosphopeptide enrichment was performed so that an estimate of the site occupancy of a given phosphorylation site could be done.

To quantify the occupancy of a phosphorylation site, the ion intensity of the phosphopeptide was normalized to the sum of the ion intensities of the phosphopeptide and the corresponding non-phosphorylated peptide. Assuming equal efficiency of ionization of the unphosphorylated and its phosphorylated counterpart, this ratio should reflect the absolute occupancy of a given phospho-site, i.e. its phosphorylation stoichiometry. To determine site occupancy, the detection and identification of two ion signals, one for the phosphorylated and the other for the non-phosphorylated peptide, is

required. This is in contrast to SILAC quantitation that compares the signal intensities of only the phosphopeptides from treated and untreated cells. To estimate the fold change in phosphorylation at a given site, the normalized values for each phosphopeptide from control and rapamycin treated samples were then divided by each other. Since the value from the rapamycin treated sample was divided by the value from the untreated sample, a ratio greater than 1 indicates increased phosphorylation in the presence of rapamycin, and vice versa (Figure 3.11).

In-depth analysis of the proteins selected for validation yielded the same phosphorylation sites as identified in the phosphoproteome (Figure 3.11 [phospho-sites in red] and Table 3.6). Not surprisingly, the in-depth LC-MS/MS analysis revealed additional phosphorylation sites that escaped detection in the phosphoproteome (Figure 3.11 [phospho-sites in black] and Table 3.6). This is particularly evident for Kkq8-HA, where nine additional phospho-sites were quantified (Table 3.6). It is remarkable that the majority of the phosphorylation sites responding to rapamycin treatment have low to moderate site occupancy (Figure 3.11). Two different factors might account for this observation. First of all, as already mentioned, the calculation of the phospho-site stoichiometry assumed that the phosphorylated and unphosphorylated peptides ionize equally well. It is, however, not known for all instances if, and how much, the presence of a negatively charged phosphate affects the ionization of peptide. Obviously, in case the phosphorylated peptide ionizes less efficiently than the unphosphorylated cognate, the stoichiometry of phosphorylation can be grossly underestimated. A second reason explains why the rapamycin-regulated sites do not have high site occupancy, which is due to technical issues related to the presence of multiple phosphorylations in the same peptide. This can be well illustrated by the calculation of the stoichiometry of T619 in Ldb19-HA, which was assessed using the ion tracing of the phosphopeptide GHVL$\underline{T}_{619}$PHSTR and the peptide GHVLTPHSTR. However, in the same sample the incompletely cleaved phosphopeptides GHVL$\underline{T}_{619}$PHS$\underline{T}_{623}$RDIR and GHVLTPHS$\underline{T}_{623}$R-DIR could be identified as well. Since the stoichiometry of T619 was calculated comparing only the completely cleaved phosphopeptide/peptide pair, it was probably underestimated because part of the peptides containing this phosphorylation was present as incompletely cleaved phosphopeptide GHVL$\underline{T}_{619}$PHS$\underline{T}_{623}$RDIR.

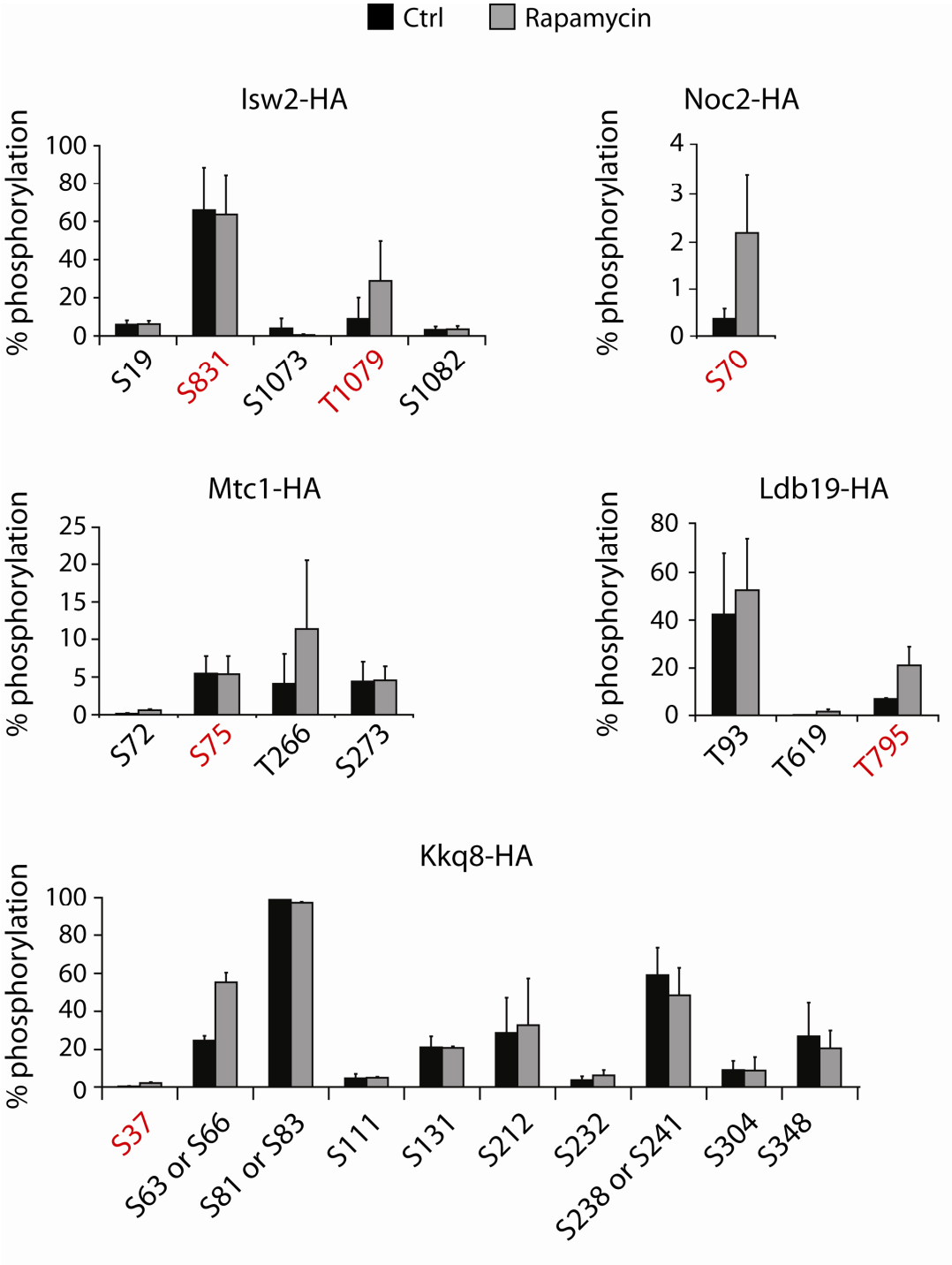

Figure 3.11: Phospho site occupancy as a function of rapamycin treatment of selected HA-tagged proteins. The site occupancy is expressed as the percentage of the LC/MS signal of the phosphorylated peptide versus the sum of the signals of the phosphopeptide and its unphosphorylated counterpart. The sites marked in red were found in the quantitative phosphoproteome.

Protein	Only in the phosphoproteome	Only in the in-depth LC-MS/MS	Common
Isw2-HA		S19, **S1073**, S1082	S831, T1079
Ldb19-HA		T93, **T619**	**T795**
Mtc1-HA	S336, S337, S339, S340, S342, S436	*S75**, **T266**, S273	***S72****
Noc2-HA			**S70**
Kkq8-HA	**S21, S75**	**S63** or **S66**, S81 or S83, S111, S131, S212, S232, S238 or S241, S304, S348	S37

Table 3.6: Comparison of the phosphorylation sites found in the quantitative phosphoproteome and in the in-depth LC-MS/MS analysis. Residues in bold are sensitive to rapamycin treatment. An asterisk indicates conflicting site assignment between the phosphoproteome (italic bold) and the in-depth analysis (italic).

As can be seen from Table 3.6, for Mtc1 and Kkq8 some phospho-sites previously found in the phosphoproteome were missing in the in-depth LC-MS/MS analysis. For Mtc1, six phospho-sites (S336, S337, S339, S340, S342 and S436) have been exclusively identified in phosphoproteomic analysis and are localized in the peptides EADATPDDDR$\underline{S}_{336}\underline{S}_{337}I\underline{S}_{339}\underline{S}_{340}N\underline{S}_{342}$NK and QKESEDEDEDDEIIDP$\underline{S}_{436}$EWVK. Both peptides are exceptionally acidic and are particularly well enriched by IMAC because of the clustered glutamic and aspartic acids. It is therefore possible that these missing phospho-sites were not identified in this approach because the phosphorylated peptides are not abundant enough and can only be detected after phosphopeptide selection. The missing phospho-sites S75 and S21 of Kkq8 could be identified but not quantified in the in-depth LC-MS/MS analysis. This is due to the proximity of these phosphorylation sites to lysines and arginines, which prevent cleavage by trypsin. As a result, incompletely cleaved phosphopeptides are generated, whose sequences differ from the completely cleaved unphosphorylated peptides. As a consequence, the ion tracing between the phosphopeptide and its unphosphorylated counterpart cannot be compared. This is particularly obvious for S75 in Kkq8, which is located one residue down-stream of the

trypsin cleavage site. However it was rather puzzling that S21 blocks the trypsin cleavage site located three residues down-stream of the protease cleavage site (R18). Indeed, as shown in Figure 3.2C, the phosphorylation site can hinder the cleavage by the protease when it is less than three residues apart from the cleavage site, which was not the case for S21 in Kkq8. However, a careful inspection of the LC-MS/MS raw data revealed that the serine immediately following the trypsin cleavage site (S19) was also phosphorylated (Figure 3.12), which is located exactly after R18.

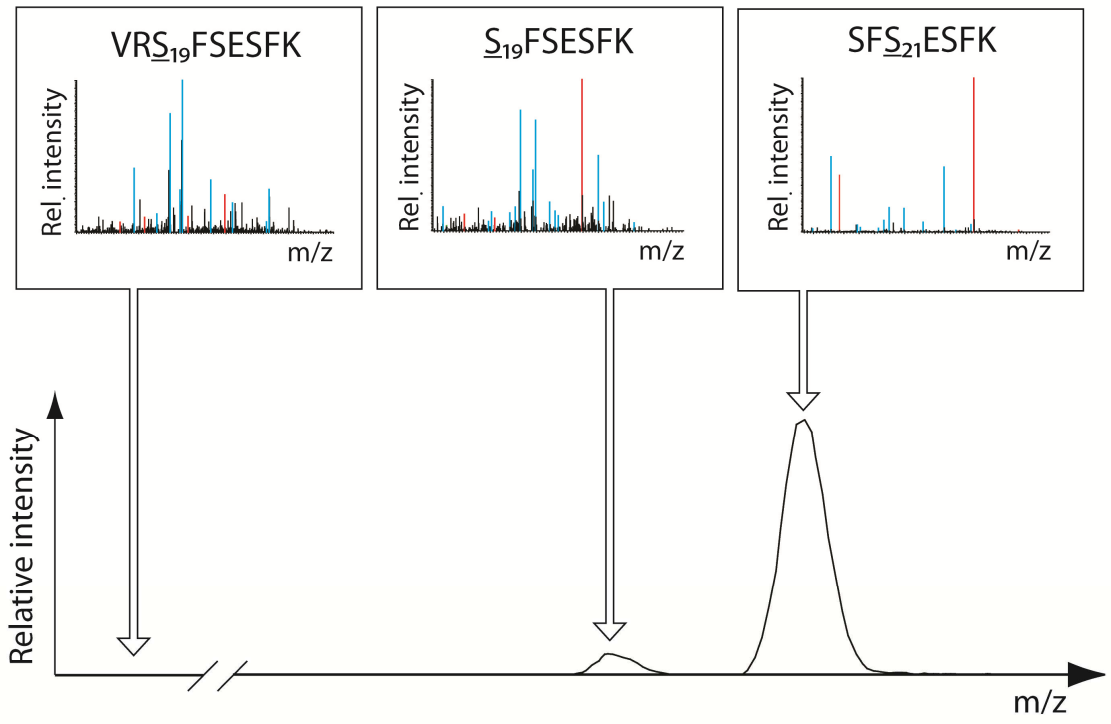

Figure 3.12: Effect of positional phospho-site isomers on phospho-site quantitation. The tryptic peptide containing the phosphorylation sites for S19 and S21 of Kkq8 occur in different forms depending on the site of phosphorylation. For site-specific quantitation the signal of phosphorylated S19 splits into two ion tracings, $\underline{S}_{19}$FSESFK (middle panel) and VR$\underline{S}_{19}$FSESFK (left panel) generated by incomplete cleavage by trypsin. Ion signals in blue could be assigned to b- or y-ions, while signals in red are those allowing the localization of the phosphorylation site.

Recently, the phosphorylation stoichiometry in *S. cerevisiae* was assessed on a system wide level [141]. A comparison of the present and the system wide study revealed striking similarities at least for the few common sites (Table 3.7). The stoichiometries for the in-depth LC-MS/MS analysis were slightly lower, suggesting that the phosphopeptides are probably ionized with a slightly lower efficiency in comparison with the non-phosphorylated peptides. However, this minor discrepancy in the two data sets could be also a consequence of the phosphopeptide dephosphorylation performed by Wu *et al.* which, in case of multiple phosphorylated peptides, leads to a sum of all stoichiometries and therefore to an overestimation of the stoichiometry of the singly phosphorylated peptide.

		Stoichiometry (%)	
Protein	**Phospho-Site**	**In-depth LC-MS/MS (no rapamycin)**	**Wu *et al.***
Isw2-HA	S831	65.3	87
Mtc1-HA	S72	0.1	7
	S75	5.4	7
Nap1-HA*	S76	0.7	1
	S82	1.0	1
Noc2-HA	S70	0.4	2

Table 3.7: Comparison of the phosphorylation stoichiometries obtained in the in-depth LC-MS/MS analysis and in the published large-scale study [141]. Note that in the large-scale analysis precise localization of the sites of phosphorylation is not possible. * For the in-depth LC-MS/MS analysis of Nap1 see section 3.3.3.

Having established that the phosphorylation stoichiometry in our study is correct in a first approximation, the lack of a shift of SDS-PAGE migration of some candidate proteins can be easily explained (Figure 3.10). For example, S831 of Isw2 is the site with the highest phosphorylation occupancy but its extent of phosphorylation does not change upon rapamycin treatment (Figure 3.11). On the other hand, the phosphorylation of T1079 of Isw2 changes dramatically by rapamycin treatment, but its site occupancy is quite low. Dephosphorylation, even though extensive, probably does not translate into an observable band shift. If this is the case, dephosphorylation of the major site of phosphorylation by λ protein phosphatase treatment of Isw2 should induce a mobility shift during SDS-PAGE. For this, Isw2-HA was immunoprecipitated from control and rapamycin-treated cells and one half of the immunoprecipitates was subjected to dephosphorylation by λ protein phosphatase while the other half was mock-incubated (Figure 3.13). After complete dephosphorylation of Isw2-HA by λ protein phosphatase a pronounced mobility shift was seen during SDS PAGE, despite its high molecular weight of 130 kDa. In contrast, both the phosphoproteomic analysis and in-depth LC-MS/MS analysis revealed the presence of a single low-stoichiometry phospho-site in Noc2-HA that was unable to induce a band shift following rapamycin treatment (Figure 3.10). This supports the hypothesis that band shifts only occur when high stoichiometry phospho-sites become altered by rapamycin treatment.

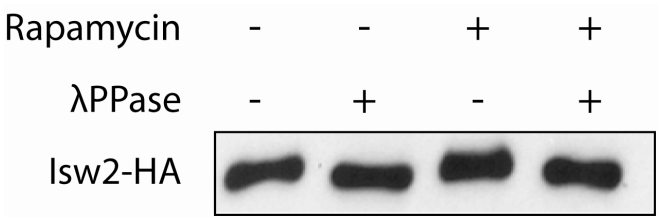

Figure 3.13: Band shift assay of Isw2-HA. Rapamycin treatment leads to a decrease of the phosphorylation of low-stoichiometry sites while phosphatase treatment removes the phosphate from all, including high stoichiometry sites. λPPase indicates phosphatase treatment.

Even though the phosphorylation stoichiometries measured in the in-depth LC-MS/MS analysis were relatively low, T1079 in Isw2 showed quite a remarkable change upon rapamycin treatment (from 9% to 29% phosphorylation occupancy). Since ISW2 deletion has been shown to confer higher sensitivity to rapamycin, it was interesting to mutate T1079 into alanine (*ISW2*^{T1079A}*-HA*), aspartic acid (*ISW2*^{T1079D}*-HA*), or glutamic acid (and *ISW2*^{T1079E}*-HA*) and check the rapamycin sensitivity of such point mutants. As shown in Figure 3.14A the strains expressing the mutant protein from a centromeric plasmid were all functional but, surprisingly, the rapamycin sensitivity of the three point mutant strains was comparable to the one of the WT strain (Figure 3.14B). It should be noted that a slightly higher sensitivity to rapamycin was observed in the ISW2^{T1079A}-HA strain. These data suggests that T1079 may not be the primary site, which TORC1 impinges on. In this context it should be noted that 37% of the Isw2 protein could not me covered in the in-depth LC-MS/MS analysis and this missing part contains 32% of the total serine and threonine residues. It is therefore possible that a dominant site regulated by TORC1 of Isw2 escaped the in-depth LC-MS/MS analysis.

Next, to gain some more information about the regulation of Isw2 activity by TORC1, the gene expression of *INO1* and *SIP4* has been investigated by quantitative real time PCR. Both genes were chosen as reporters because their expression is up-regulated in presence of rapamycin [42] as well as in *isw2Δ* mutants [142]. As expected, treatment with rapamycin of the WT strain as well as deletion of *ISW2* led to an increase in both mRNAs (Figure 3.14C). However the combined effect of *ISW2* deletion and rapamycin treatment led to an even more pronounced increase in Ino1 and Sip4 mRNAs (Figure 3.14C). Thus, it seems that the effect of TORC1 and Isw2 on INO1 and SIP4 expression occurs via two distinct pathways.

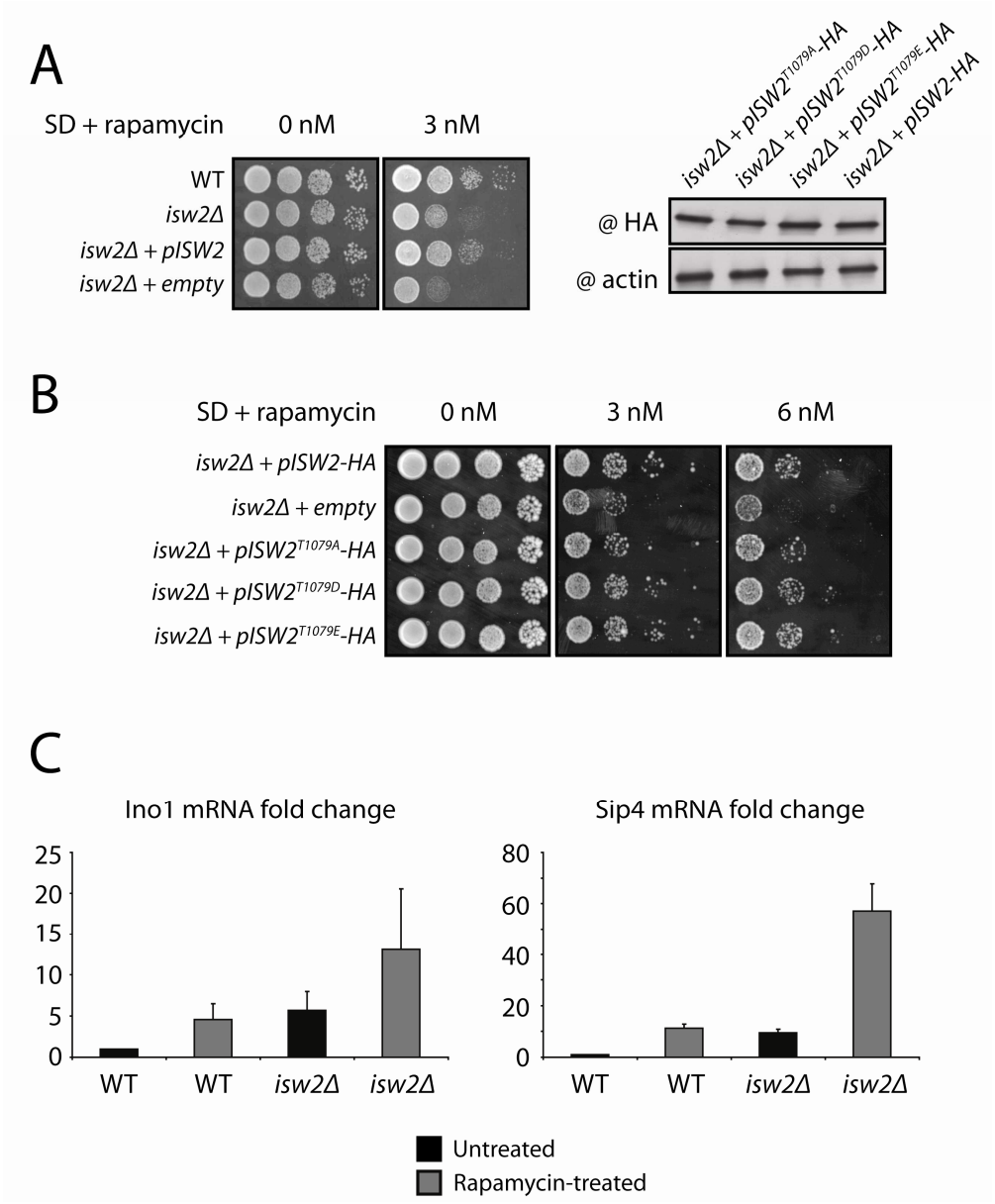

Figure 3.14: Functional analysis of Isw2. (A) Evaluation of the functionality of the *ISW2* mutant strains and (B) evaluation of their rapamycin sensitivity. (C) Gene expression of *INO1* and *SIP4* in response to rapamycin treatment and *ISW2* deletion.

3.3.3. *In Vitro* Kinase Assay of Selected Regulated Phosphoproteins

Because rapamycin acutely inhibits the activity of TORC1 [21], proteins whose extent of phosphorylation decrease following rapamycin treatment, qualify, in theory, as direct substrates for TORC1. Among the regulated phosphoproteins that were chosen for validation, four had a decreased extent of phosphorylation upon rapamycin treatment (Nap1, Reg1, Vtc2 and Vtc3, Table 3.5 and 3.8). Thus, it was important to check whether these proteins can become directly phosphorylated by TORC1. Among the candidate proteins, Nap1 qualifies particularly well as a direct TORC1 substrate since it contains two rapamycin-sensitive TP sites, a motif that has been shown to be often phosphorylated by (m)TORC1 [66, 143].

To examine whether TORC1 can directly phosphorylate the candidate proteins, they were immunoprecipitated from yeast cells and incubated *in vitro* with recombinant mTOR in presence of radioactive ATP. For an activity test, the canonical *in vivo* substrate 4E-BP was incubated with recombinant mTOR. 4E-BP was robustly phosphorylated by mTOR (Figure 3.15A, left panel) and phosphorylation of 4E-BP was abolished with the mTOR-specific inhibitor PP242 (Figure 3.15A, left panel). Similarly, the direct yeast TORC1 substrate Sch9-HA isolated from rapamycin-treated cells was also efficiently phosphorylated by mTOR (Figure 3.15A, right panel). Next, the candidate proteins Nap1-HA, Reg1-HA, Vtc2-HA and Vtc3-HA were *in vitro* phosphorylated with mTOR. Recombinant mTOR specifically phosphorylated Nap1-HA and Vtc2-HA, while Reg1-HA and Vtc3-HA became also phosphorylated when mTOR was completely inhibited with PP242 (Figure 3.15B). This is most likely due to co-precipitating PP242-resistant protein kinases. The presence of additional protein kinases in the immunoprecipitates was suspected because peptides from casein kinase II were found in the immunoprecipitates of Reg1-HA (data not shown). Since Reg1 contains several phosphorylation sites conforming to the casein kinase II motif (e.g. S490, S614 and S485) it can be assumed that the mTOR-independent phosphorylation is caused by casein kinase II. Also interesting was that Vtc2-HA was apparently stabilized by mTOR phosphorylation (Figure 3.15B). Indeed, when Vtc2-HA was incubated at 30°C in absence of mTOR for different time points, protein aggregates were observed at the boundary between the

stacking and the running gels (Figure 3.15C). The use of protease inhibitor did not have any effect on the stabilization of the protein (Figure 3.15C).

Protein	Phosphopeptide sequence	Av. Ratio ± SD
Nap1	**SSMQIDNAP<u>T</u>$_{20}$PHNTPASVLNPSYLK**	**0.42**
	SSMQIDNAPTPHN<u>T</u>$_{24}$PASVLNPSYLK	**0.59 ± 0.00**
	SSMQIDNAP<u>T</u>$_{20}$PHN<u>T</u>$_{24}$PASVLNPSYLK	**0.47 ± 0.10**
	SSMQIDNAP<u>T</u>$_{20}$PHN<u>T</u>$_{24}$PA<u>S</u>$_{27}$VLNPSYLK	**0.10**
	LG<u>S</u>$_{76}$LVGQDSGYVGGLPK	0.88 ± 0.10
	II<u>S</u>$_{140}$GQEQPKPEQIAK	1.41 ± 0.52
Reg1	<u>S</u>$_{75}$MGLLDEYIDPTK	1.02 ± 0.10
	<u>S</u>$_{570}$DSGVHSPITDNSSVASSTTSR	**0.41 ± 0.04**
	RTL<u>S</u>$_{769}$LGK	0.80
	<u>S</u>$_{773}$GSTNSLYDLAQPSLSSATPQQK	1.04 ± 0.15
	<u>S</u>$_{773}$GSTN<u>S</u>$_{778}$LYDLAQPSLSSATPQQK	0.97
	<u>S</u>$_{773}$GSTNSL<u>Y</u>$_{780}$DLAQPSLSSATPQQK	0.97
	SG<u>S</u>$_{775}$<u>T</u>$_{776}$NSLYDLAQPSLSSATPQQK	0.77 ± 0.06
	SG<u>S</u>$_{775}$TNSL<u>Y</u>$_{780}$DLAQPSLSSATPQQK	0.71
	SGS<u>T</u>$_{776}$NSLYDLAQPSLSSATPQQK	0.93
	SGS<u>T</u>$_{776}$N<u>S</u>$_{778}$LYDLAQPSLSSATPQQK	0.97
Vtc2	**SNFNTA<u>S</u>$_{182}$EPLASASK**	**0.37 ± 0.02**
	SNFNTA<u>S</u>$_{182}$EPLA<u>S</u>$_{187}$ASK	**0.07**
	FSSIV<u>S</u>$_{196}$NDIDMNFR	**0.40**
	RL<u>S</u>$_{583}$NLK	**0.24 ± 0.03**
	ITSQGDLEADG<u>S</u>$_{615}$<u>S</u>$_{616}$DEETEQEPHSK	0.91 ± 0.06
	LMGVD<u>S</u>$_{657}$EEEEIELPPGVK	0.96 ± 0.06
Vtc3	SSVD<u>S</u>$_{43}$WSER	0.82 ± 0.05
	L<u>S</u>$_{195}$HFSNLEDASFK	1.13
	LSHF<u>S</u>$_{198}$NLEDASFK	0.74 ± 0.22
	SNSL<u>S</u>$_{269}$SDGNSNQDVEIGK	0.96
	SNSLS<u>S</u>$_{270}$DGNSNQDVEIGK	0.99
	LSKI<u>S</u>$_{592}$VPDGK	**0.54 ± 0.15**
	HVIADLEDHE<u>S</u>$_{621}$<u>S</u>$_{622}$DEEGTALPK	1.00 ± 0.29

Table 3.8: List of selected candidate proteins that become significantly dephosphorylated upon rapamycin treatment. Phosphopeptides in bold are significantly less phosphorylated in presence of rapamycin. Two <u>T</u>P sites are present in Nap1 (T20 and T24) whereas the PKA consensus site is clearly evident in Vtc2 (S583). For additional information see also Table 3.5.

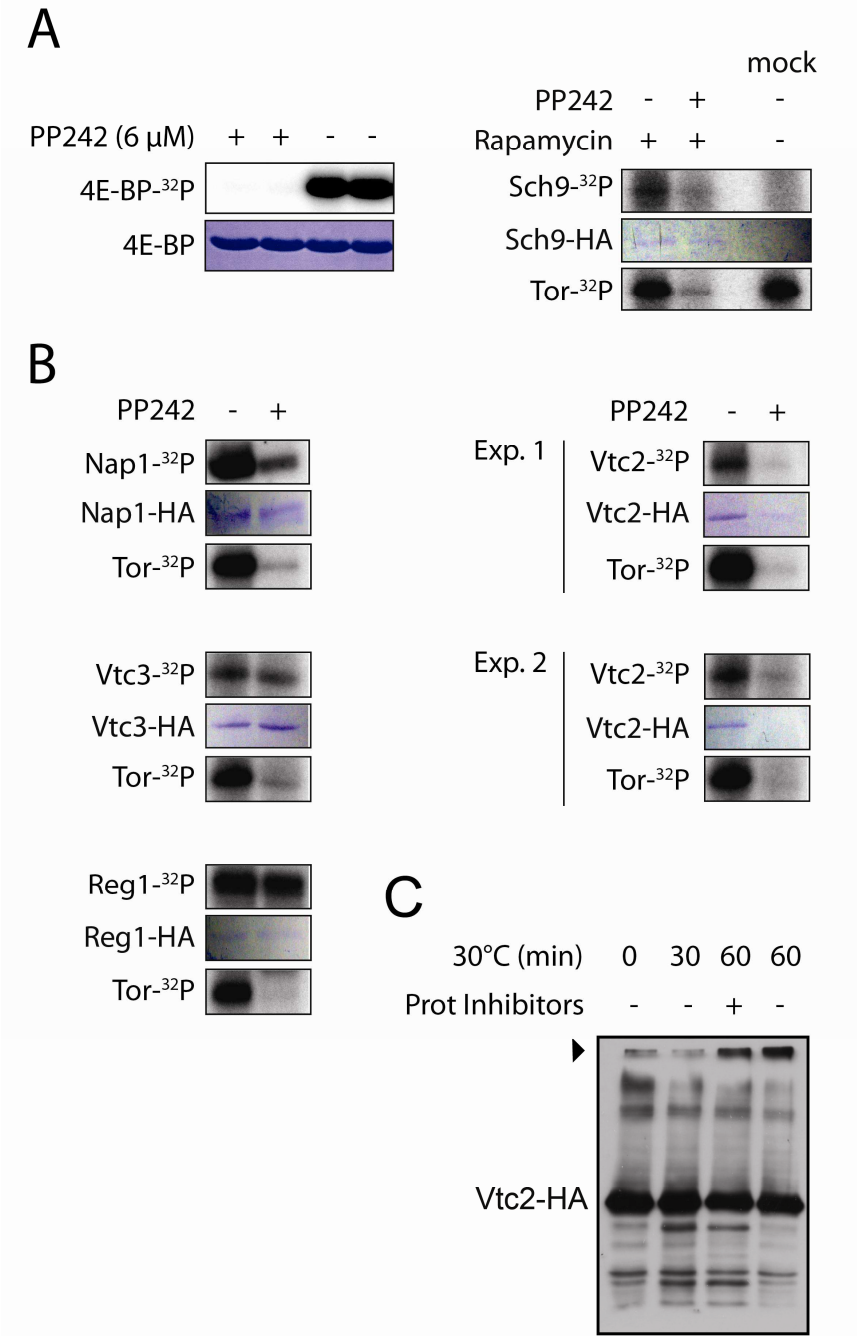

Figure 3.15: *In vitro* kinase assay of selected candidate proteins whose extent of phosphorylation decrease following rapamycin treatment. Kinase assay was with recombinant mTOR. (A) The physiological mTOR substrates 4E-BP and Sch9 are robustly phosphorylated *in vitro* by mTOR. PP242 indicates treatment with the mTOR-specific inhibitor. The panels labeled with ^{32}P indicate autoradiographies and those labeled just with the protein name designate the Coomassie-stained substrates. Tor-^{32}P indicates autophosphorylation of the mTOR kinase. (B) *In vitro* phosphorylation of HA-tagged Nap1, Vtc3, Reg1 and Vtc2. The labeling of the panels is as in (A). (C) Vtc2 is prone to aggregation at 30°C. The migration of the protein is indicated by Vtc2, while the arrow shows the appearance of protein aggregates.

Nap1-HA was robustly and specifically phosphorylated by mTOR *in vitro*. The specificity was given by the fact that no phosphorylation of Nap1 occurred when mTOR was completely inhibited with PP242 or when mTOR was omitted from the *in vitro* kinase assay (Figure 3.16A). Furthermore, higher phosphorylation by mTOR was seen when Nap1-HA was either isolated from rapamycin-treated cells or when the immunoprecipitate was dephopshorylated by λ protein phosphatase (Figure 3.16B). At this point, it was fundamental to know if *in vitro* phosphorylation of Nap1-HA by mTOR occurs at the same sites as those observed in the phosphoproteome.

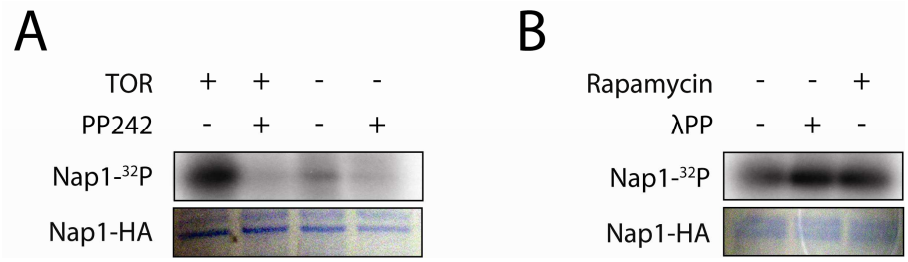

Figure 3.16: (A) *In vitro* phosphorylation of HA-Nap1 by mTOR. (B) Prior treatment of HA-Nap1 by rapamycin or λ protein phosphatase increases its *in vitro* phosphorylation by mTOR.

For this, Nap1-HA was isolated from a 4 l culture, immunoprecipitated, and dephosphorylated by λ protein phosphatase for maximal phosphorylation by mTOR. To enable the tracing of both unlabelled phosphate in the mass spectrometer and radioactively labeled phosphate during liquid chromatography, the ratio of cold ATP to ^{32}P-labelled ATP was titrated and optimal incorporation of ^{32}P into Nap1-HA was achieved with 30 µM cold ATP (data not shown). For efficient phosphorylation of Nap1-HA, BSA was required to stabilize mTOR during the kinase assay (data not shown). *In vitro* phosphorylated Nap1-HA was digested with trypsin and the digest was fractionated by RP-HPLC. The radioactively labeled phosphopeptides were located in the fractions by liquid scintillation counting and the peak of the radioactivity was analyzed by LC-MS/MS (Figure 3.17).

HPLC peptide mapping of Nap1 phosphorylated *in vitro* by mTOR revealed one major peak of radioactivity that was preceded by a broad, less intense peak (Figure 3.17B). Overall recovery of the radioactivity was approximately 80%. The two radioactive fractions (a, b in Figure 3.17B) were analysed by LC-MS/MS. In the first peak of radioactivity (peak a) the phosphopeptide II$\underline{S}_{140}$GQEQPKPEQIAK was identified, whereas the second fraction (peak b) contained the peptides LG$\underline{S}_{76}$LVGQDSGYVGGLPK and LGSLVGQD$\underline{S}_{82}$GYVGGLPK. The same results were obtained when the Nap1 digest was subjected to RP-HPLC fractionation after phosphopeptide enrichment via IMAC (data not shown). In the PP242-treated kinase assay, virtually no radioactivity was eluted from the column (Figure 3.17A/B). In accordance, the ion intensities of the individual phosphopeptides were also strongly reduced in the sample treated with PP242 (while the ion intensities of other Nap1-HA peptides did not show a comparably significant reduction) (Figure 3.17C). Figure 3.17D summarized the results from the *in vitro* phosphomapping and the phosphoproteomic analysis.

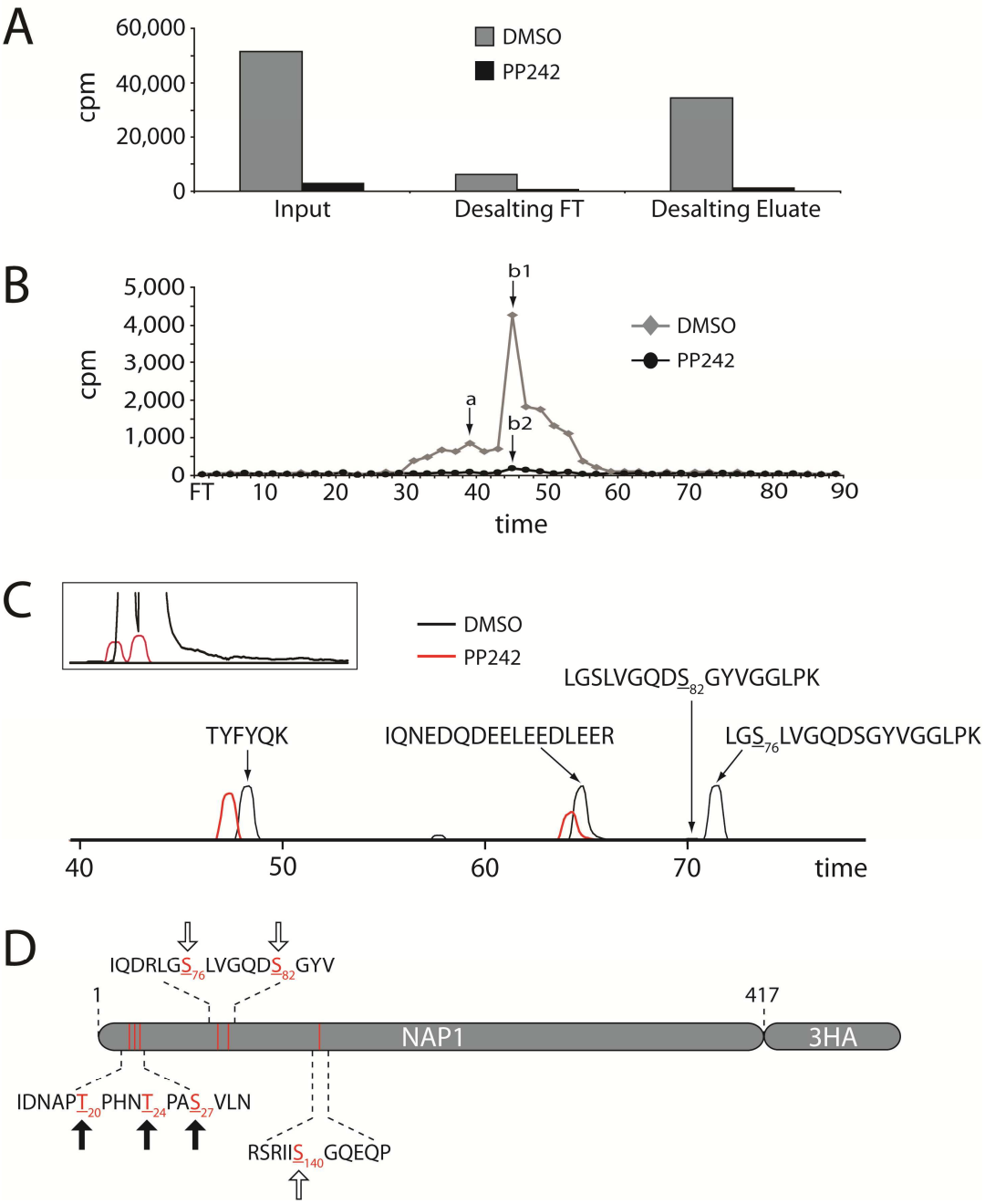

Figure 3.17: Identification of the phosphorylation sites on Nap1-HA after *in vitro* phosphorylation by mTOR. (A) Recovery of radioactivity along the purification steps used to isolate radiolabeled peptides. (B). RP-HPLC elution of radioalabeled peptides from *in vitro* phosphorylated HA-Nap1 digested with trypsin. The fractions a, b1 and b2 were subjected to LC-MS/MS analysis (C) LC-MS/MS analysis of fractions b1 and b2. The same protein amount for both untreated and PP242-treated Nap1-HA was measured as shown by two non-phosphorylated Nap1-HA peptides. The snapshot shows the elution peaks of the two *in vitro* phosphorylated Nap1-HA peptides. (D) Schematic overview of the phosphorylation sites identified in Nap1 in the phosphoproteomic analysis (full and open arrows) and after *in vitro* phosphorylation (open arrows).

These findings are surprising because in the phosphoproteome the N-terminal phospho-sites (T20, T24, and S27) were those down-regulated upon rapamycin treatment, while S76 and S140 were not affected by the treatment (Table 3.8). Consequently, it was essential to investigate the *in vivo* phosphorylation of S76, S82 and S140 to be really sure that no change was occurring at these positions. For this an in-depth LC-MS/MS analysis was performed, where Nap1-HA was first isolated by immunoprecipitation and then digested with different proteases to map in a reliable way S76, S82 and S140 (Figure 3.18A). Moreover, such experiment would have been helpful to map the N-terminal phospho-sites and confirm their regulation upon rapamycin treatment. Unfortunately the N-terminal part of Nap1-HA could be only detected in the unphosphorylated form, making impossible to confirm the regulation of T20, T24 and S27. The same result was obtained using a genomically-tagged Nap1-HA strain (data not shown), thus the absence of these phospho-sites was very likely not due to overexpression problems. The possibility that those sites were erroneously identified in the phosphoproteome could be also ruled out because, manual investigation of the full MS spectra and MS/MS spectra obtained in phosphoproteomic analysis clearly showed that these sites are phosphorylated and that they are more phosphorylated in the untreated samples. This was further supported by other phosphoproteomes where those N-terminal sites were found in Nap1. On the other hand, S76, S82 and S140 could be consistently mapped but, as shown in the phosphoproteome, their phosphorylation remained unaffected over three different rapamycin treatment times (Figure 3.18B). Furthermore, in agreement with the large-scale phosphorylation stoichiometry analysis published by Wu *et al.* [141], the phosphorylation occupancy at S76, S82 and S140 was lower than 1% (Figure 3.18C and Table 3.7), suggesting that they probably play a minor physiological role.

In conclusion, even though Nap1-HA could be phosphorylated *in vitro* by mTOR, the *in vitro* phosphorylation sites do not correspond to those found regulated in the phosphoproteomic analysis. On the other hand, the rapamycin-sensitive phospho-sites found in the phosphoproteome do not seem to be directly phosphorylated by mTOR and, for technical reason, could not be identified in the in-depth LC-MS/MS analysis. Nevertheless, the *in vitro* phosphorylation sites on Nap1 conform rather well with the known (m)TOR consensus motif. Especially S76 and S140, the two main mTOR

phosphorylation sites *in vitro*, are surrounded by hydrophobic residues (I/G/L/V), which agrees with the (m)TOR preference to phosphorylate either S/TP sites or hydrophobic motifs [66, 143].

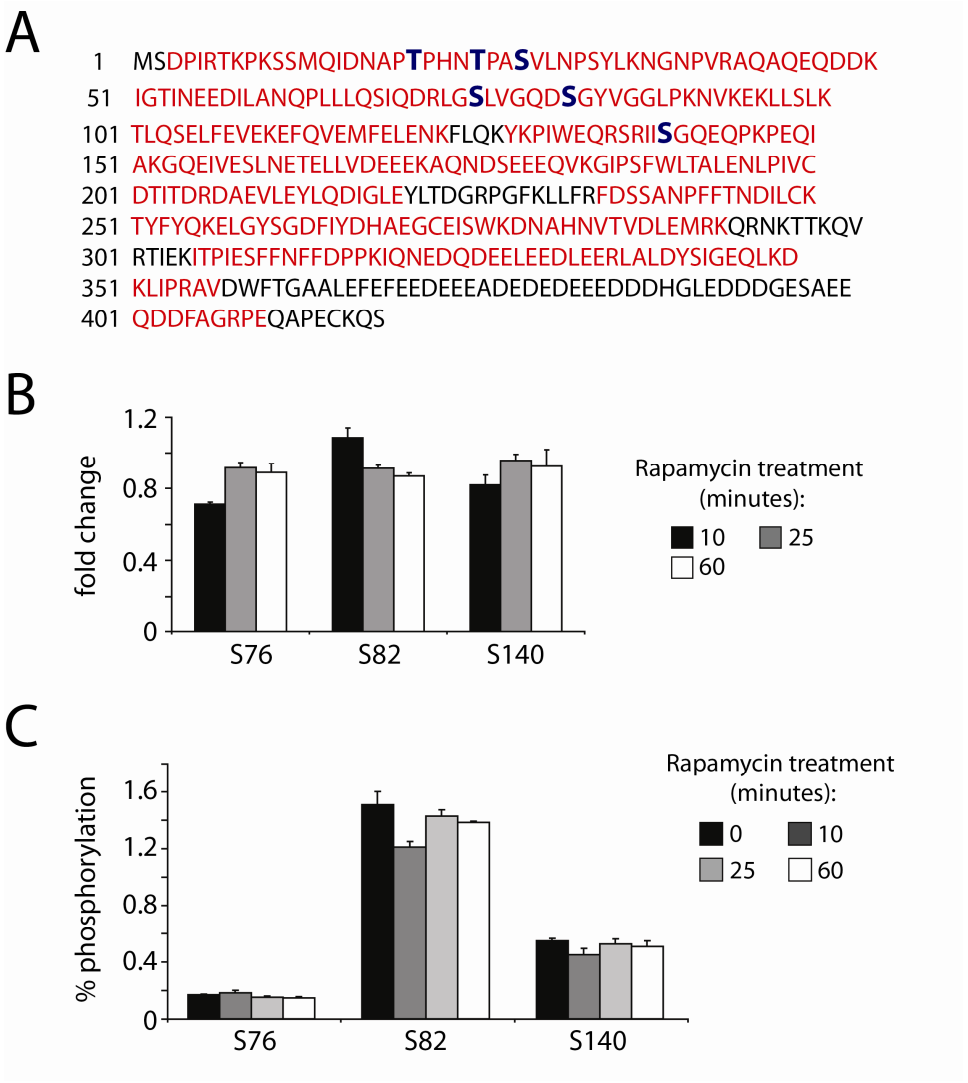

Figure 3.18: In-depth LC-MS/MS analysis of *in vivo* phosphorylated Nap1-HA. (A) By using different proteases, about 80% of Nap1 could be sequenced (residues in red). The expected phosphorylation sites are marked in blue. Time course of the phosphorylation fold change (B) and the site occupancy (C) of Nap1-HA following rapamycin treatment.

4. Discussion

Yeast cells grown under favorable conditions accumulate cellular mass, whereas cells grown under unfavorable growth conditions arrest the cell cycle and become quiescent. This means that yeasts, like other unicellular or multicellular organisms, are able to sense nutrient cues and to adapt cell growth accordingly. The highly-conserved kinase TORC1 plays a central role in nutrient sensing and in transducing these signals to downstream effectors to eventually regulate cell growth. Active TORC1 promotes anabolic processes like ribosome biogenesis, translation initiation and nutrient uptake and represses catabolic processes like autophagy and stress response. Given its central role in the regulation of cell growth and the many readouts regulated by TORC1, it is surprising that up to date only three well characterized substrates of TORC1 have been identified in the yeast *S. cerevisiae*, i.e. Tap42, Sch9 and Sfp1 [32, 65, 66]. Furthermore, the signaling pathways linking TORC1 to its known readouts are still incompletely understood. To shed some light on the signaling cascades regulated by TORC1 and to get some insights in novel TORC1 targets, a phosphoproteomic approach was established to globally analyze the phosphorylation changes induced by rapamycin, a specific inhibitor of TORC1.

4.1. Production of a Rapamycin-sensitive Yeast Phosphoproteome

The strategy used in the present study to quantify rapamycin-induced phosphorylation changes was based on stable isotope labeling with amino acid in cell culture (SILAC) [117]. To increase the statistical significance of each quantified phosphopeptide hit, four biological replicates were performed and in total 2,607 unique phosphorylation sites from 972 phosphoproteins could be quantified (Figure 3.4B and Appendix IV). In each of the four experiments, on average, 1,145 phosphopeptides could

be identified, a significantly lower number than the one obtained in the qualitative phosphoproteomic analysis (1,672 phosphopeptides per experiment) (Figure 3.2B and Appendix I-II). Since the two procedures were almost identical, the higher number of identified phosphopeptides in the qualitative phosphoproteome must be due to the SILAC labeling. This is very likely a consequence of the higher sample complexity generated by SILAC labeling, where for each peptide two signals are recorded in the survey scan. As a result, the higher complexity of the SILAC samples probably led to undersampling of the phosphoproteome.

An alternative to SILAC is the chemical labeling of peptides with the iTRAQ reagents [115]. In contrast to SILAC the derivatization of the same peptide with two different iTRAQ tags does not change the overall molecular mass of the peptide. In the present study, iTRAQ labeling was initially chosen to quantify rapamycin-induced changes in phosphorylation. Due to the disappointingly low number of phosphopeptides identified, the iTRAQ method was not pursued further (Appendix III). A possible reason for the low yield of phosphopeptides is the increase in the charge states of iTRAQ-labeled peptides in comparison to the unlabeled peptides, which severely complicates the analysis of the fragmentation spectra [116]. A second explanation relates to the unfavorable conditions used during the iTRAQ labeling procedure. For derivatization, the peptides are incubated with the iTRAQ reagent in 100% ethanol, which can reasonably lead to severe losses of the hydrophilic phosphopeptides.

An alternative technique to SILAC is label-free quantitation. This technique is based on the comparison of precursor ion intensities across multiple LC-MS/MS runs and it can be used for the simultaneous comparison of many conditions. Because label-free quantitation requires that every biological sample is measured separately, inter-experimental variation can become relatively high. Moreover, label-free quantitation works best when the same sample is measured several times by LC-MS/MS, which obviously puts a high demand on the instrument's measurement time. Another label-free quantitation can be done by spectral counting. This method uses the number of MS/MS spectra assigned to a protein/peptide as an estimation of protein/peptide abundance [144]. However, since spectral counting relies on peptide identification, it is unsuitable for

large-scale phosphoproteomic analysis because of undersampling of such complex peptide mixtures.

Recently another quantitative rapamycin-sensitive yeast phosphoproteome was published [34], which was based on the label-free technology rather than SILAC labeling of cells. In that study 2,260 phosphopeptides from 751 phosphoproteins were quantified. This compares very well to the quantitative phosphoproteome in the present study (2,382 phosphopeptides from 972 phosphoproteins). Although the two methods gave comparable phosphoproteome coverages, the overlap between the regulated phosphoproteins of the two studies was marginal (Figure 3.7). Only 12% of the down-regulated and 13% of the up-regulated phosphoproteins were common to the two studies. The poor overlap can, in part, be explained by the different growth conditions and technical approaches employed in the two studies: the duration of rapamycin treatment (30 versus 20 minutes), the protein digestion regimes (in-solution versus in-gel digestion), the different phosphopeptide enrichment techniques (TiO_2 versus IMAC), and the bioinformatics pipeline employed to analyze the quantitative mass spectrometric data (SuperHirn versus MaxQuant).

4.2. Dissection of Rapamycin-induced Changes in Expression and Rapamycin-induced Changes in Phosphorylation

Of the total 972 phosphoproteins quantified in this study, the phosphorylation states of 130 phosphoproteins were significantly altered by rapamycin treatment. Among them, 78 were more (i.e. up-regulated) and 55 less phosphorylated (i.e. down-regulated) upon rapamycin treatment (Table 3.1 and 3.2). The 78 proteins whose extent of phosphorylation was increased upon rapamycin treatment cannot be direct TORC1 substrates, since inhibition of TORC1 by rapamycin should cause a decrease in phosphorylation of direct targets. On the contrary, the 55 down-regulated phosphoproteins are potential direct TORC1 substrates.

However, before concluding that a change in phosphorylation is due to a difference in the activity of the upstream protein kinase/phosphatase, it should be noted that TORC1 not only modulates the activity of phosphatases and kinases but it also controls the activity of several transcription factors (e.g. Fhl1, Gln3, Maf1, Msn2/4, Rtg1/3, and Sfp1). Thus, rapamycin treatment also elicits changes in protein expression. The impact on transcription obviously depends on the duration of the treatment: short treatments leave distal TORC1 readouts, like gene transcription, unaffected. Early transcriptomic studies in yeast treated with rapamycin revealed that the effect of rapamycin on the mRNA levels are very fast (<20 minutes) [41, 42, 145]. As a result, one must be aware that every rapamycin-sensitive phosphoproteome is a snapshot of two effects, i.e. proteins whose expression or phosphorylation is affected by rapamycin treatment.

There are several solutions to distinguish between the two effects. The first is the measurement of a sample before and after phosphopeptide enrichment to measure both expression and phosphorylation changes (Appendix IV-V). Unfortunately the overlap between the proteome and phosphoproteome can be very small and, in the present study, only 34% of the proteins could be observed in both analyses (Table 3.1 and 3.2). The second solution relies on the identification of more than one phosphopeptide per phosphoprotein. If all phosphopeptides derived from the same protein change the same way, for example all are up-regulated, this is a good evidence for an expressional rather than phosphorylation change. This cannot be used in every instance, because there are proteins which are affected at several sites by rapamycin treatment (e.g. Atg13, Maf1, and Sch9). In addition, in the present study only 53% of the phosphoproteins were identified with multiple phosphopeptides (Appendix IV). For all the other phosphoproteins identified with only a single phosphopeptide it is impossible to know *a priori* whether the measured change is a consequence of altered expression or altered phosphorylation. Finally, the phosphoproteomic data can be compared with transcriptomic data to check whether rapamycin treatment affects the mRNA level of a specific gene. In the present study, 25% of the regulated phosphoproteins displayed similar changes at their mRNA levels upon rapamycin treatment (Table 3.1 and 3.2), suggesting that the phosphorylation changes measured for these proteins were probably

caused by changes in their gene expressions rather than in their phosphorylations. Some examples are described in more detail below.

Among the up-regulated phosphoproteins there are the permeases Can1, Dip5, Mep2, Ptr2, and Put4, which have also up-regulated mRNA levels upon rapamycin treatment [41, 42] (Table 3.1). Similarly but in the opposite direction, Gnp1 was found down-regulated both in the present phosphoproteome and in previously published transcriptomes [41, 42] (Table 3.2). These observations are probably a consequence of the transcriptional changes caused by rapamycin. Nitrogen starvation, via TORC1 inhibition, triggers the expression of several low-specificity permeases, like Put4 (Pro permease), Mep2 (NH_4^+ permease) and Ptr2 (di/tripeptide transporter), whereas high-affinity permeases like Gnp1 are internalized from the plasma membrane and degraded. Interestingly, the rapamycin effect on Can1, Dip5 and Ptr2 seen in the phosphoproteome and transcriptome could be also seen in the proteome, where their protein levels were increased after rapamycin treatment (Table 3.3). Also up-regulated in the proteome were the permeases Agp1 and Gap1, two low-affinity and broad-specificity amino acid permeases able to import almost all 20 amino acids (Table 3.3). These observations suggests that the phosphorylation changes measured for Can1, Dip5, Ptr2 and probably Mep2 and Put4, are due to altered gene expression rather than to a difference in the activity of the upstream protein kinases/phosphatases. Surprisingly, this was not the case for Gnp1, because its protein level was unaffected after 20 minutes of rapamycin treatment (Appendix V). This is clearly in contrast with the decreased Gnp1 mRNA level measured in transcriptomic studies and suggests that the decrease in Gnp1 phosphorylation is not an indirect consequence of a decrease in *GNP1* gene expression. It should be however noted that a decrease in Gnp1 mRNA will probably results, at a later time point, in a decrease in Gnp1 protein level. This hypothesis is further supported by a global analysis showing that there is a delayed correlation between mRNA and protein level changes after rapamycin treatment [146]. However, a rapamycin treatment of only 20 minutes is most likely too short to elicit a significant change in protein expression. Combining all information from transcriptome, proteome and phosphoproteome the decrease in Gnp1 phosphorylation is perhaps a signal to trigger its endocytosis. This is also evidenced by the fact that the regulated phospho-site in Gnp1 is predicted to face the

cytosol, where it could act as signal to modulate Gnp1 stability at the plasma membrane. These examples underline the importance of analyzing protein expression and phosphorylation simultaneously, to rule out that a change observed in protein phosphorylation is brought about by increased mRNA levels.

The two enzymes Tps3 and Tsl1 are up-regulated both in the phosphoproteome and in previously published transcriptomes [41, 42] (Table 3.1). However, similar to Gnp1, these changes are not caused by expression changes because the protein levels of Tps3 and Tsl1 are not affected by rapamycin treatment (Appendix V), probably because 20 minutes rapamycin treatment are not enough to cause a significant change in the proteins levels of Tps2 and Tsl1. Interestingly, an increase in the abundance of the two enzymes would make fits with their involvement in trehalose biosynthesis which, like glycogen, is a storage carbohydrate needed to endure nutrient starvation periods [147].

The proteins Gdh2 and Dcs2 were hyperphosphorylated upon rapamycin treatment (Table 3.1). This is very likely to be caused by increased mRNA levels since their expression is under the control of the transcription factors Gln3 [148-150] and Msn2/4 [151], respectively, which are both activated by rapamycin treatment. This can be partially confirmed at the protein level for the protein Dcs2, where a slight increase in expression (1.60 ± 0.04) was observed upon rapamycin treatment (Appendix V).

Finally, the proteins Esf1, Lhp1 and Zuo1 were down-regulated in the phosphoproteome and in previously published transcriptomes [41, 42] (Table 3.2). These proteins influence processes (pre-rRNA processing (Esf1), tRNA maturation (Lhp1), ribosome biogenesis (Zuo1)) that are positively regulated by TORC1. At a first glance it would be logical to conclude that the change in phosphorylation observed for these proteins is a consequence of the change in their mRNA levels. However within the time frame of the experiment (20 minutes rapamycin treatment) their protein levels remain unaffected (Appendix V). As a result the dephosphorylation of the three proteins upon rapamycin treatment could very well play a role in modulating their functions. Similarly to Gnp1, prolonging the treatment with rapamycin will almost certainly decrease Tps3 and Tsl1 protein levels as a consequence of a decrease in their mRNA levels.

Interestingly, for some proteins an inverse correlation between phosphorylation and mRNA change was observed (Table 3.1 and Table 3.2). Two prominent examples are

Kin2 and Tif5. Kin2 is a serine/threonine protein kinase involved in exocytosis. In a recent interactomic study, Kin2 was shown to physically associate with Kog1, a TORC1 subunit. Kin2 also interacts with Ksp1 and Kdx1, which themselves associate physically with Tor1, Kog1, Lst8, and Tco89 [129]. Whether Kin2 is part of TORC1 signaling is very likely but it does not seem to be a direct substrate of TORC1, since an increase rather than a decrease in phosphorylation at S888 was observed in the phosphoproteomic analysis. The second protein with an opposite change in phosphorylation and mRNA abundance is Tif5 (also know as eIF5). Tif5 is the GTP activating protein for eIF2 necessary for joining the 40S and 60S ribosomal subunits. This is a particularly interesting observation because TORC1 regulates translation initiation at multiple steps and could therefore very well signal to Tif5. The fact that altered phosphorylation was found on Tif4632 (also known as eIF4G) and Eap1, a putative yeast orthologue of mammalian 4E-BPs, supports this idea (Table 3.1 and 3.2).

4.3. Targeted Analysis of Selected Candidate Proteins Reveals their Involvement in TORC1 Signaling

At this point it was interesting to validate some of the proteins found in the present phosphoproteomic analysis. For this, seven up-regulated (Hal5, Isw2, Kkq8, Ldb19, Mtc1, Noc2, and Sec7) and four down-regulated (Nap1, Reg1, Vtc2, and Vtc3) phosphoproteins were chosen. For validation single deletions were generated and the rapamycin sensitivity and glycogen accumulation of the null mutants were checked. These two criteria were chosen because many TORC1 effectors have altered rapamycin sensitivity [6, 43, 66, 147] when deleted.

The two assays revealed that some of the proteins chosen for validation are involved in TORC1 signaling. For instance the mutants *hal5Δ, isw2Δ, kkq8Δ, ldb19Δ,* and *reg1Δ* had increased rapamycin sensitivity (Figure 3.8), while the mutants *mtc1Δ, nap1Δ, vtc2Δ,* and *vtc3Δ* were equally sensitive as the wild type. Similarly, the mutants *hal5Δ, isw2Δ, ldb19Δ,* and *reg1Δ* accumulated more glycogen than wild type cells (Figure 3.9).

Since for some deletion strains only wild type behavior was observed, a third experiment was performed to reveal the effect of rapamycin on the phosphorylation state of the candidate proteins. The change in phosphorylation of the tagged proteins was monitored by a shift in migration during SDS-PAGE (Figure 3.10). Surprisingly, the majority of the proteins did not show any alteration in electrophoretic mobility following rapamycin treatment. This can be, in part, explained by the high molecular weight of the analyzed proteins but could also be a consequence of small phosphorylation changes induced by the rapamycin treatment, which are not able to elicit a mobility shift of the intact protein (see below). Nevertheless for the proteins Ldb19, Kkq8 and to some extent Sec7, a migration shift upon rapamycin treatment was observed. Phosphatase treatment abolished their mobility shift, demonstrating that it was caused by a change in protein phosphorylation.

In summary, the three assays used show that five out of eleven phosphoproteins are probably part of TORC1 signaling, i.e. Hal5, Isw2, Kkq8, Ldb19, and Reg1. But are the phosphorylation sites identified in the phosphoproteome involved in the signaling process? Are there additional regulated phosphorylation sites in these proteins to the one found in the phosphoproteome? To answer these questions, five proteins were chosen for in-depth phosphomapping: three proteins that fulfilled all validation criteria (i.e. Isw2, Kkq8, and Ldb19) and two proteins that did not (i.e. Mtc1 and Noc2). It should be noted that the phosphoproteomic analysis already revealed that these proteins contain rapamycin-sensitive sites but an in-depth phosphomapping was required to check whether additional and maybe more relevant sites were present. This concern arises because several TORC1 effectors were found to be regulated at multiple rather than at single phosphorylation sites: six rapamycin-sensitive sites in Sch9 [66], seven in Maf1 [34] and eight sites in Atg13 [152]. Furthermore, since in the phosphoproteomic analysis very complex samples were subjected to LC-MS/MS analysis, only a few MS/MS spectra per phosphopeptide were acquired, thereby increasing the risk of mislocalization of the phosphorylation site.

In-depth LC-MS/MS analysis allowed extensive sequence coverage of all five phosphoproteins. Starting from immunoprecipitates five different proteases were used to cover from 50% to 80% of the entire protein sequences. This is a striking improvement

over the phosphoproteomic analyses, where only a few phosphopeptides per protein could be identified. This is also an important prerequisite to reduce the risk that major regulated phospho-sites escape phosphomapping. This also highlights one of the caveats of nowadays phosphoproteomics. The vast majority of all phosphoproteomic workflows are based on protein digestion with trypsin. This obviously precludes the identification of certain phospho-sites because the phosphopeptides obtained by trypsinolysis are either too short or too long to be retained by reverse-phase chromatography.

For all five phosphoproteins except Noc2, several sites could be identified in the in-depth LC-MS/MS analysis in addition to those already mapped in the phosphoproteome (Figure 3.11). With twelve phosphorylation sites, Kkq8 was particularly highly phosphorylated. Out of twelve sites, ten could be quantified. The remaining two phospho-sites could not be quantified due to the high numbers of lysine and arginine residues which, upon trypsin cleavage, generates many partially cleaved peptides that hamper label-free quantitation. The phosphorylation sites affected most by rapamycin treatment were S1079 of Isw2, T795 of Ldb19, S266 of Mtc1, S70 of Noc2 and S63/S66 of Kkq8 (Figure 3.11). In addition, some phospho-sites that were weakly regulated were identified at position S1073 of Isw2, T619 of Ldb19, S72 of Mtc1 and S37 of Kkq8 (Figure 3.11). Surprisingly, the site occupancy of the rapamycin-sensitive sites rarely exceeded 50%. Nevertheless, for both Ldb19 and Kkq8 the change in phosphorylation following rapamycin treatment was enough to elicit a gel migration shift (Figure 3.10). This observation raised two different questions. Are the phosphorylation stoichiometries measured in the in-depth LC-MS/MS analysis a good estimation of the true phospho-site occupancy? Can these phosphorylation sites play a biological role even though they have low to moderate occupancies? These two aspects will be considered in the next section.

4.3.1. Identification of Physiologically Relevant Phosphorylation Sites

It is a common belief that the functional significance of a phosphorylation site depends on its fractional stoichiometry. This is a presumption that lacks experimental evidence. There are however, some reasons in favor of this idea. For example, there is a bioenergetic argument: it is reasonable to assume that a highly phosphorylated site has a biological function because just keeping a site occupied is a mere waste of ATP. The contrary is not necessarily true, since a low stoichiometry site could well be non-functional but, since it is not very abundant, there is little to no evolutionary pressure to eliminate it.

The concept that a cell contains non-functional, low occupancy phosphorylation sites is in contrast to the observation that several phospho-sites are well conserved among different organisms, and many of them have low to moderate stoichiometries. For example, a comparison of human and mouse orthologues revealed that 88% of the phosphoserine and 85% of the phosphothreonine sites are conserved [153]. Moreover, a recent study comparing the evolutionary conservation of high, moderate and low occupancy phospho-sites in different yeast species, showed that low occupancy sites are on average more conserved than high stoichiometry sites [141].

Concerning the phosphorylation stoichiometries obtained in the present in-depth LC-MS/MS analysis, it seems that the rapamycin-regulated phospho-sites have generally low to moderate occupancies. This is particularly striking for S1073 of Isw2, S70 of Noc2, S72 of Mtc1, T619 of Ldb19 and S37 of Kkq8. At a first glance this would argue against their physiological relevance but there are at least four arguments suggesting that they may play a role in modulating protein function. (1) The yeast cells used for these experiments were not synchronized. Therefore, the measured phosphorylation state of each protein corresponds to an average of all different phosphorylation states observable throughout the cell cycle. This issue has been addressed in some phosphoproteomic analysis that showed dramatic changes in the phosphorylation throughout the cell cycle when synchronized cells were used [154]. (2) The effect of rapamycin could be restricted to a certain fraction of the total protein molecules present in the cell, which are however averaged during cell lysis. This is the case when a protein is present in different

subcellular compartments but only one of them physically interacts with the TORC1 network. This sounds plausible because many proteins are found at different locations in the cell: TORC2 itself has been reported to localize at the plasma membrane [131], in intracellular membrane compartments [24], in the cytoplasm [155] and to associate with ribosomes [156]. The Snf1 kinase localizes to the nucleus, the cytoplasm and the vacuole depending on the associating β-subunits [157]. (3) The five phosphoproteins validated were all more phosphorylated when yeast cells were treated with rapamycin for 15 minutes. It is possible (and interesting to pursue) that a prolonged rapamycin treatment could lead to increased phosphorylation at those sites. (4) The method used to calculate the phosphorylation stoichiometries in this study may underestimate the true *in vivo* occupancy because it assumes that no difference exist in the ionization and detection efficiencies of phosphorylated and unphosphorylated peptides.

The impact of a phosphate group on the ionization efficiency of a phosphopeptide has long been debated and contradictory results have been reported. There are three approaches to circumvent this problem. The first approach relies on the empirical determination of so-called response ratios of a phosphopeptide and its unphosphorylated cognate using synthetic peptide standards spiked in known quantities [158]. These ratios are subsequently used to correct the phosphorylation stoichiometries obtained by dividing the phosphopeptide intensity by the sum of the intensities of the phosphopeptide and its non-phosphorylated counterpart. This approach has the disadvantage that the response ratios vary according to the experimental set-up and need to be determined for each phosphopeptide. This limits its applicability for large-scale studies. The second strategy is based on absolute quantification (AQUA) of peptides, which are synthesized with incorporated stable isotopes and can be spiked into a sample in known quantities [159]. The spiked peptides and phosphopeptides can then be used to quantify in absolute terms the phosphorylation stoichiometry. Again, the use of AQUA peptides is limited to known phosphorylations and cannot be used for large-scale studies. The third method requires that a sample is split in two fractions, which are then differentially labeled with isotopic-coded tags. One of the two fractions is then dephosphorylated before being pooled with the untreated fraction [160-163]. This method is used to calculate the phospho-site occupancy simply by subtracting the intensity of the non-phosphorylated peptide from

the sum of the intensity of the dephosphorylated phosphopeptide and the non-phosphorylated peptide. In this way all calculations are done using the non-phosphorylated ion species so that the problem associated with different ionization efficiencies is circumvented.

In a recent study, where this last method was employed on a large-scale [141], similar results to those obtained in the present in-depth LC-MS/MS analysis were reported (Table 3.7). This suggests that the low phosphorylation stoichiometries measured for S1073 of Isw2, S70 of Noc2, S72 of Mtc1, T619 of Ldb19 and S37 of Kkq8 are not a consequence of differences in the ionization efficiencies between a peptide and its cognate phosphopeptide. In more general terms this also demonstrates that, under the LC-MS/MS conditions used in present in-depth LC-MS/MS analysis, ionization efficiency differences do not significantly affect the calculation of phosphorylation stoichiometries. As a result the direct comparison of the ion tracings of a phosphopeptide and its unphosphorylated cognate seems to be a reliable way to estimate phospho-site occupancy levels. Interestingly, even though very similar, the phosphorylation stoichiometries obtained in the present study were on average slightly lower than those obtained by Wu *et al.* This can be explained by the fact that in that study the phosphopeptides were dephosphorylated, which means that for multiply phosphorylated peptides the phosphorylation stoichiometries could be overestimated because the contribution of each phospho-isoform is summed up and cannot be distinguished in the final stoichiometry value.

4.4. Biological Relevance of the Selected Candidate Proteins

In the two previous sections four assays, namely rapamycin sensitivity and glycogen accumulation of the single deletion strains, SDS-PAGE migration shift upon rapamycin treatment, and in depth-LC-MS/MS phosphomapping were applied to establish a link between the candidate proteins Hal5, Isw2, Kkq8, Ldb19, Reg1, Sec7, Mtc1 and Noc2 and TORC1. Furthermore, it has been shown that the phosphorylation

stoichiometries obtained in the in-depth LC-MS/MS analysis are a very good approximation of the real *in vivo* phospho-site occupancies. The question that immediately arises is which roles these proteins play in the TORC1 signaling network? In the next sections, the implications of some of the validated phosphoproteins in TORC1 signaling will be presented.

4.4.1. Isw2 and Ino1 Link TORC1 Signaling to Inositol Metabolism

Among the validated candidates, Isw2 is very interesting. Isw2 is an ATP-dependent chromatin remodeling factor [164]. It is involved in repressing *INO1* [132], early meiotic genes [165] and *MAT***a**-specific genes [166] in haploid and *MAT*$\boldsymbol{\alpha}$ cells. To perform these functions, Isw2 associates with Itc1 to form the so-called ISW2 complex [167]. Several lines of evidence suggest that TORC1 indirectly controls Isw2, which in turn regulates *INO1* expression. *ISW2* deletion, as shown in this study, results in rapamycin sensitivity and glycogen accumulation (Figure 3.8 and 3.9). Deletion of *INO1* causes, in turn, a decrease in glycogen accumulation [137]. The proteomic analysis revealed that *INO1* expression is controlled by TORC1, since rapamycin treatment resulted in an elevated Ino1 protein level (Table 3.3). Elevated mRNA levels have also been reported for Ino1 upon rapamycin treatment (Figure 3.14C) [42]. At the molecular level, both the phosphoproteomic analysis and the in-depth phosphomapping showed that TORC1 inhibition stimulates Isw2 phosphorylation at S1079 (Figure 3.11). Interestingly, LC-MS/MS analysis of Isw2 showed that Itc1, the second subunit of the ISW2 complex, was exclusively present in Isw2 immunoprecipitates from untreated cells (data not shown). These data suggest that TORC1 indirectly regulates Isw2 phosphorylation and by this also the association of Isw2 and Itc1. In presence of rapamycin the Isw2/Itc1 complex dissociates and is no longer able to repress *INO1* transcription. A possible model fitting these observations is illustrated in Figure 4.1.

If TORC1 would regulate *INO1* expression exclusively through Isw2, the Ino1 mRNA levels in *isw2Δ* cells treated with rapamycin should be the same as those

measured in untreated *isw2Δ* cells. Surprisingly this was not the case and rapamycin-treated *isw2Δ* cells displayed a stronger derepression of *INO1* expression in comparison with the untreated *isw2Δ* cells (Figure 3.14C). The fact that *ISW2* deletion and rapamycin treatment are additive on *INO1* expression could be due to two independent signaling branches impinging on *INO1*, i.e. TORC1 and Isw2. Alternatively, TORC1 could signal to *INO1* both in an Isw2-dependent and independent manner.

It is interesting to note that besides Isw2 and Ino1 the phosphorylation of the inositol transporter Itr1 and the inositol pyrophosphate synthase Kcs1 were significantly affected by rapamycin treatment. The phosphorylation of Itr1 was increased, while Kcs1 phosphorylation was decreased upon rapamycin treatment (Table 3.1 and 3.2). Thus there is evidence that TORC1 regulates inositol metabolism.

To shed additional light on the regulation of *INO1* by Isw2 and TORC1, it is important to investigate whether *INO1* deletion can compensate the *ISW2* deletion in regards to glycogen accumulation. Equally important would be to determine whether *INO1* deletion causes resistance to rapamycin and whether this phenotype can compensate the increased sensitivity of *isw2Δ* cells. Finally, to get a complete picture of the link between TORC1 and the ISW2 complex, the kinase or phosphatase connecting TORC1 to Isw2 must be identified. This could be done by monitoring T1079 phosphorylation of Isw2-HA expressed in different yeast strains carrying single kinase and phosphatase deletions. Particular attractive are the null mutants of kinases and phosphatases which are active and inactive, respectively, when TORC1 is inhibited.

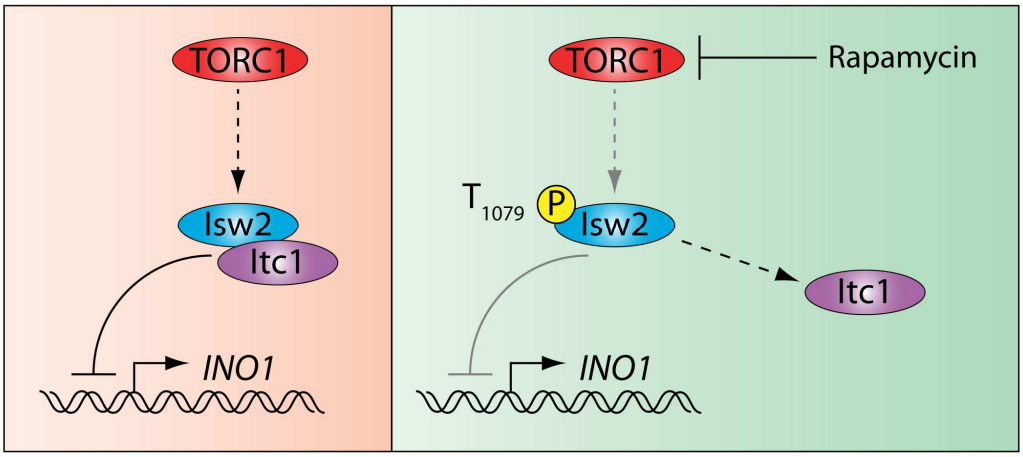

Figure 4.1: Model of TORC1-dependent INO1 expression through the control of Isw2/Itc1 association.

4.4.2. Ldb19 and Aly2 are Involved in the Regulation of Amino Acid Permeases by TORC1

Among the phosphoproteins analyzed in more details, the arrestin-related ubiquitin-ligase adaptor Ldb19 is an interesting candidate. Ldb19 (also known as Art1) has two PY domains that target the E3 ubiquitin-ligase Rsp5 to its substrates (e.g. Can1) for subsequent degradation [128]. Ldb19 is mono-ubiquitinated, as seen by the presence of two bands in SDS PAGE that are 7-8 kDa apart (Figure 3.10). Both isoforms are phosphorylated in a rapamycin-dependent fashion, suggesting that ubiquitination of Ldb19 is independent of TORC1. The link between Ldb19 and TORC1 signaling was revealed in a recent report showing that another arrestin-related ubiquitin-ligase adaptor, Aly2 (also known as Art3), is directly phosphorylated by the TORC1 target Npr1 [168]. Aly2 is necessary to mediate the recycling of Gap1 back from the endosome to the Trans Golgi Network [168]. Therefore it is conceivable that a similar mechanism exists linking TORC1 and Ldb19 to regulate the trafficking of Can1.

In the present phosphoproteomic analysis, S155 phosphorylation in Aly2 was moderately increased upon rapamycin treatment (1.68 ± 0.28). This change was however

not statistically significant based on the stringent statistical criteria chosen for this study. It would be intriguing to confirm *in vitro* phosphorylation of Aly2 by Npr1 and to check whether S155 is the regulated phospho-site. It should be noted that S155 (…RTL$\underline{S}_{155}$DNE…) is not located within the known Npr1 consensus motif (K/RSxxK/R) [169]. However, since the Npr1 consensus sequence was derived with a set of synthetic peptides, it remains possible that Npr1 is able to phosphorylate S155 *in vivo*. Similar considerations apply to Ldb19. Like Aly2, the two regulated phospho-sites in Ldb19 (…EDI$\underline{T}_{619}$PVN… and …HVL$\underline{T}_{795}$PHS…) do not conform to the known Npr1 consensus site but this should be confirmed in an *in vitro* phosphorylation assay. Figure 4.2 depicts a model explaining the TORC1-dependent regulation of Gap1 and Can1 ubiquitination via Aly2 and Ldb19, respectively.

Other observations linking Ldb19 to TORC1 came from localization studies of GFP-tagged Ldb19. The protein perfectly co-localizes with Sec7 [128], the guanine nucleotide exchange factor (GEF) for ARF proteins. This is intriguing for two reasons. Firstly, in the phosphoproteomic analysis a strikingly increase in Sec7 phosphorylation at S772 was measured after rapamycin treatment (Table 3.1). This phosphorylation site is closely located to the so-called Sec7 domain (residues 824-1010) [170], which is responsible for the ARF GEF catalytic activity of Sec7. Secondly, Sec7 contains a C-terminal domain responsible for the interaction with the E3 ubiquitin-ligase Rsp5 [171]. The fact that so many proteins involved in membrane trafficking and permease sorting (i.e. Ldb19, Aly2, Npr1, Sec7 and Bul1) were found differentially phosphorylated in the phosphoproteomic analysis upon rapamycin treatment is astonishing and should be further investigated (Table 3.1 and 3.2). In particular, the two rapamycin-sensitive sites in Ldb19 should be mutated and the rapamycin sensitivity and glycogen accumulation of such mutants should be investigated. Furthermore it is intriguing to see if these Ldb19 phospho-mutants can still co-localize with Sec7 *in vivo*.

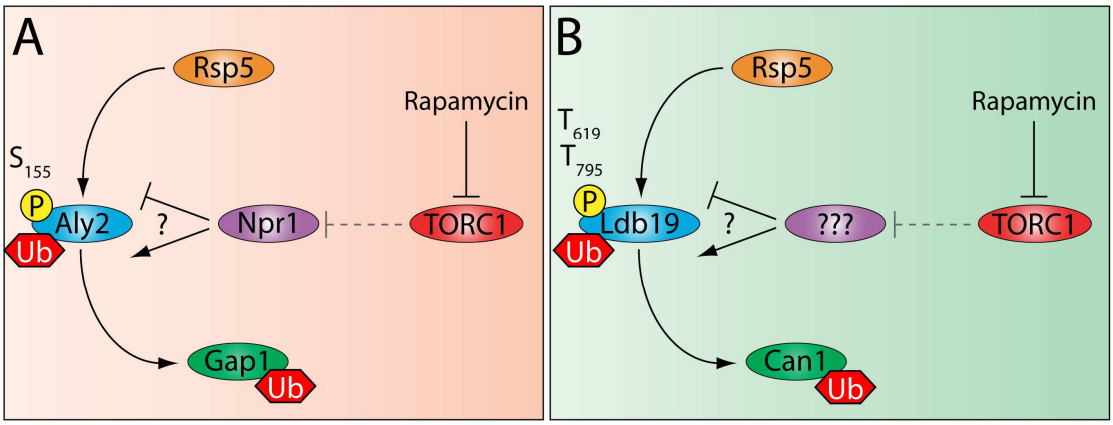

Figure 4.2: Model of TORC1-dependent Gap1 and Can1 ubiquitination via (A) Aly2 and (B) Ldb19.

4.4.3. TORC1 Indirectly Regulates Nap1 and Gin4 Phosphorylations

Among the phosphoproteins chosen for further validation there were Nap1, Reg1, Vtc2 and Vtc3. The corresponding deletion mutants, except *reg1Δ*, had normal rapamycin sensitivity and glycogen accumulation (Figure 3.8 and 3.9). Since these proteins are less phosphorylated in rapamycin-treated cells, they qualify for *in vitro* kinase assays to check whether they become directly phosphorylated by recombinant Tor.

Nap1, a pleiotropic protein involved in microtubule dynamics, bud morphogenesis and histones transport [172, 173], was specifically phosphorylated by Tor *in vitro* (Figure 3.15B and 3.16). Several lines of evidence suggest that TORC1 signals to Nap1. (1) In the phosphoproteome, Nap1 phosphorylation on T20, T24 and S27 decreased in response to rapamycin treatment (Table 3.2). (2) T20 and T24 are TP sites that are typically phosphorylated by (m)TORC1 consensus motifs [66, 143]. (3) In a recent yeast interactomic study, Nap1 was shown to physically interact with Tor1 and other Tor1-associated proteins [129]. (4) The *nap1Δ* strain is more sensitive to rapamycin [135] and it has abnormal cellular localization of the Gin4 kinase. (5) The *gin4Δ* strain in turn is more resistant to rapamycin and accumulates less glycogen than wild-type [137].

(6) In the present phosphoproteomic analysis Gin4 phosphorylation responded to rapamycin treatment: S502 became less, and S666 more phosphorylated (Table 3.1 and Table 3.2). All these data, and the fact that recombinant Tor phosphorylates Nap1 *in vitro*, suggest that TORC1 signals to Nap1 (and Gin4).

To confirm the phosphorylation sites found in the present phosphoproteome, in-depth phosphomapping of Nap1 was carried out. Unfortunately, even though the region of the protein that contains T20, T24 and/or S27 could be easily recovered by trypsinolysis, phosphorylation at these sites could never be detected in immunoprecipitates of Nap1 (Figure 3.18). Identical results were obtained when Nap1 was expressed from a multi-copy plasmid or from a genomically tagged strain (data not shown). Also, in the case of very low-level phosphorylation, phosphopeptide enrichment did not indicate any phosphorylation at these N-terminal sites (data not shown). A possible explanation of these conflicting findings is that the N-terminal phospho-sites identified in the phosphoproteome are incorrect. This is, however, very unlikely because the same phospho-sites were found in several other phosphoproteomic studies [92, 110, 174, 175]. Moreover, manual inspection of the phosphoproteomic data confirmed the presence of the three phosphorylation sites and their rapamycin regulation. Correct identification was supported by the high Mascot scores (~50-60) of the MS/MS spectra. Another possibility to explain the lack of the phosphorylated residues is inadvertent dephosphorylation during the immunoprecipitation. To alleviate the problem, Nap1-HA could be immunoprecipitated for a shorter time or, alternatively, cell lysis could be carried out in a strongly denaturing SDS buffer to stop unwanted dephosphorylation.

Nevertheless, even though the regulated phospho-sites identified in the phosphoproteome could not be identified in the subsequent in-depth LC-MS/MS analysis, the fact that Tor phosphorylates Nap1 *in vitro* left the possibility open whether Nap1 is a true TORC1 substrate. One way out of the dilemma was to identify the sites phosphorylated *in vitro* by recombinant Tor. For this, *in vitro* phosphorylated Nap1 was digested and analyzed by LC-MS/MS. Surprisingly, identification of the fractions by LC-MS/MS that contained radioactively-labeled Nap1 phosphopeptides revealed that the *in vitro* phosphorylation sites are S76, S82 and S140 (Figure 3.17). This rules the possibility out that T20, T24 and S27 become phosphorylated *in vitro*. Moreover, this data suggests

that *in vitro* phosphorylation of Nap1 by recombinant Tor is not physiologically relevant, as both the phosphoproteomic and the subsequent in-depth LC-MS/MS analysis showed that the sites S76, S82 and S140 are not affected by rapamycin treatment (Table 3.8 and Figure 3.18).

These results suggest that, even though physically interacting, Nap1 is not a direct substrate of TORC1. Nevertheless, genetic and biochemical evidences support the view that Nap1 is part of the TORC1 network and that the kinase Gin4 is also involved in this signaling branch. In addition, even though they could not be identified in the in-depth LC-MS/MS analysis, T20, T24 and S27 remain very likely rapamycin-sensitive sites, since they were consistently and significantly found regulated in the phosphoproteomic analysis (Figure 3.2). In a recent global phosphorylation stoichiometry survey [141], the occupancy of these sites has been estimated around 25%, which makes them attractive physiological sites for a regulation by TORC1. Finally the observation that Nap1 is phosphorylated *in vitro* at S76, S82 and S140, a non-physiological event, confirms the preference of Tor toward the phosphorylation of hydrophobic motifs.

4.4.4. TORC1 Impinges on Snf1 Signaling via Reg1

Similar to Nap1, Reg1 was also found hypophosphorylated upon rapamycin treatment in the phosphoproteomic analysis, which qualified Reg1 for *in vitro* kinase assays with recombinant Tor. Interestingly, Reg1 was robustly phosphorylated *in vitro* even when Tor was incubated with its specific inhibitor PP242 (Figure 3.15B). This is probably due to a kinase co-immunoprecipitating with Reg1. Since Reg1 contains in its C-terminus several residues conforming to the canonical casein kinase II (CK II) consensus site, it is likely that the *in vitro* phosphorylation of Reg1 is caused by active CK II stably associating with Reg1 during immunoprecipitation. This was further supported by the identification by LC-MS/MS of peptides from all four CK II subunits in Reg1 immunoprecipitates (data not shown).

Reg1 remains an interesting candidate despite the fact that it is not a direct TORC1 substrate. Its deletion influenced both rapamycin sensitivity and glycogen accumulation (Figure 3.8 and 3.9). Furthermore, its role in activating the Snf1 kinase makes Reg1 a likely TORC1 effector. Reg1 is necessary for Snf1 inactivation by dephosphorylation of the essential T210 [133]. Interestingly, even though TORC1 primarily senses the level of amino acids and Snf1 is necessary for growth in the absence of glucose, it was shown that TORC1 signals to Snf1 because T210 is phosphorylated in a rapamycin-dependent manner [134]. Therefore, it seems that both glucose depletion and TORC1 inhibition up-regulate Snf1 activity and, as a result, it is likely that Reg1 is inhibited under such conditions. This renders S570 phosphorylation an activating event. To demonstrate this hypothesis all rapamycin-sensitive phosphorylation sites in Reg1 should be mapped and the activity of Snf1 should be investigated in cells lacking those phosphorylation sites. This could be addressed, for example, by measuring the expression of Snf1-sensitive genes (like Adr1, Mig1, and Sip4) in a Reg1 S/T-to-A mutant.

4.4.5. The VTC Proteins Link TORC1 and Microautophagy

Similar to Nap1, the vacuolar protein Vtc2 was also specifically phosphorylated by Tor *in vitro* (Figure 3.15B). Vtc2 is unusual because its protein level was dependent on its phosphorylation state. Phosphorylation of Vtc2 stabilizes the protein. This is a common feature among protein kinases that have been found to be thermally unstable when certain residues are not phosphorylated [176, 177]. This also agrees with the observation that Vtc2 is prone to aggregation when it is alone incubated at 30°C (Figure 3.15C). The effect of TORC1 on Vtc2 is intriguing when considering the sub-cellular localization and physiological function of Vtc2. Vtc2 together with Vtc1, Vtc3 and Vtc4 forms the so-called vacuolar transporter chaperone (VTC) complex [178]. The VTC complex is involved in microautophagy, a process of direct invagination of the vacuolar membrane into the vacuolar lumen. This process compensates for the massive influx of membranes caused by macroautophagy. In the phosphoproteome, both Vtc2 and Vtc3

were less phosphorylated upon rapamycin treatment (Table 3.2), while Vtc1 and Vtc4 could not be detected. This agrees with their membrane topology, since Vtc1 and Vtc4 are integral membrane proteins, whereas the majority of Vtc2 and Vtc3 proteins do not span the vacuolar membrane [179]. As a result, it is likely that Vtc1 and Vtc4, but not Vtc2 and Vtc3, are lost by aggregation when the cell extract is heated to 95°C prior to gel electrophoresis. In the phosphoproteome, Vtc2 was found to be differentially phosphorylated at S182, S187, S196 and S583 (Table 3.2). These residues are located within the cytosolic part of Vtc2 (residues 1-693) and are therefore physically accessible to TORC1 all the more that TORC1 was found to be localized to the outer vacuolar membrane [131, 155, 180]. Furthermore, the involvement of the VTC proteins in TORC1 signaling is also highlighted by the finding that their sub-cellular localization is affected by rapamycin treatment or nitrogen starvation [181]. To shed more light into the regulation of the VTC proteins, and more specifically Vtc2, by TORC1, exhaustive phosphomapping of all *in vivo* phosphorylation sites should be done. In parallel the *in vitro* phosphorylated sites on Vtc2 should be mapped. Next it would be intriguing to check whether the mutation of those regulated phospho-sites is impairing microautophagy and affecting the subcellular localization change induced by rapamycin treatment.

4.5. Novel Less Characterized TORC1 Targets Identified in the Quantitative Phosphoproteomic Analysis

Recently a global protein kinase and phosphatase interaction network in yeast has been published [129]. In this study it was found that TORC1 physically interacts with Cdc14, Fmp48, Kdx1, Ksp1, Mks1, Nap1, Nnk1, Npr1, Rck1, Rtg3, Sky1, and Tax4. Interestingly six of these proteins (Ksp1, Mks1, Nap1, Npr1, Rtg3, and Sky1) were also found in the present phosphoproteome to be affected at the phosphorylation level by rapamycin treatment (Table 3.1 and Table 3.2). All of them except Rtg3 were less

phosphorylated in presence of rapamycin, suggesting that they may be direct TORC1 substrates.

Ksp1 is a serine/threonine protein kinase required for haploid filamentous growth (Bharuca 2008). In the present study Ksp1 was found to be phosphorylated by PKA in a TORC1-specific manner (Figure 3.6), which was in agreement with the phosphoproteomic experiments that revealed a down-regulation in phosphorylation at S827 and S884 (RRL$\underline{S}_{827}$MEQ and RRS$\underline{S}_{884}$ANE) upon rapamycin treatment (Table 3.2) [122]. However, Ksp1 was found regulated at two additional sites in the phosphoproteomic analysis, for instance T525 and/or S529 (DFF$\underline{T}_{525}$PP$\underline{S}_{529}$VQH) (Table 3.2). The first of them is surrounded by hydrophobic residues and is a TP site, which would agree with the hypothetical (m)TORC1 consensus motif [66, 143]. To verify this hypothesis, an *in vitro* kinase assay using recombinant Tor should be performed and, in case of a positive outcome, the *in vitro* phosphorylated sites should be mapped to confirm that phosphorylation is really occurring at these specific residues. Interestingly, if Ksp1 will be eventually shown to be a direct TORC1 substrate, it will be one of the many proteins targeted by both TORC1 and PKA. Furthermore, since yeast filamentation requires Snf1 phosphorylation, Ksp1 could be involved in its regulation.

Mks1 was already shown to be involved in TORC1 signaling as a negative regulator of RTG gene expression [49, 182] and it was found less phosphorylated at S518 in the phosphoproteomic analysis (Table 3.2). This site (RRQ$\underline{S}_{518}$MDI) conforms very well to the know PKA consensus motif [122], which has been however never shown to be directly targeted by TORC1 [66, 143].

Sky1 is a mRNA splicing factor and, considering that 90% of mRNA splicing is devoted to process RP mRNAs [26], it would be reasonable that TORC1 directly impinges on this protein as an alternative way to regulate ribosome biogenesis. However the regulated phospho-sites identified in the phosphoproteome (S445/S449) do not conform to the known TORC1 consensus motif (Table 3.2) [66, 143]. Interestingly, a second protein involved in mRNA processing, Ccr4, was found less phosphorylated upon rapamycin treatment (Table 3.2). Ccr4 is a component of the CCR4-NOT transcriptional complex, responsible for deadenylation-dependent mRNA decay, which may explain how TORC1 regulates mRNA stability.

References

1. Perler, F.B., Xu, M.Q., and Paulus, H. (1997). Protein splicing and autoproteolysis mechanisms. Curr Opin Chem Biol *1*, 292-299.
2. Manning, G., Whyte, D.B., Martinez, R., Hunter, T., and Sudarsanam, S. (2002). The protein kinase complement of the human genome. Science *298*, 1912-1934.
3. Stock, A.M., Robinson, V.L., and Goudreau, P.N. (2000). Two-component signal transduction. Annu Rev Biochem *69*, 183-215.
4. Cohen, P. (2000). The regulation of protein function by multisite phosphorylation--a 25 year update. Trends in biochemical sciences *25*, 596-601.
5. Yaffe, M.B., and Elia, A.E. (2001). Phosphoserine/threonine-binding domains. Curr Opin Cell Biol *13*, 131-138.
6. Beck, T., and Hall, M.N. (1999). The TOR signalling pathway controls nuclear localization of nutrient-regulated transcription factors. Nature *402*, 689-692.
7. Carvalho, J., and Zheng, X.F. (2003). Domains of Gln3p interacting with karyopherins, Ure2p, and the target of rapamycin protein. The Journal of biological chemistry *278*, 16878-16886.
8. Willems, A.R., Goh, T., Taylor, L., Chernushevich, I., Shevchenko, A., and Tyers, M. (1999). SCF ubiquitin protein ligases and phosphorylation-dependent proteolysis. Philos Trans R Soc Lond B Biol Sci *354*, 1533-1550.
9. Ishikawa, S., Yano, Y., Arihara, K., and Itoh, M. (2004). Egg yolk phosvitin inhibits hydroxyl radical formation from the fenton reaction. Biosci Biotechnol Biochem *68*, 1324-1331.
10. Pinna, L.A. (2003). The raison d'etre of constitutively active protein kinases: the lesson of CK2. Acc Chem Res *36*, 378-384.
11. Taylor, S.S., Buechler, J.A., and Yonemoto, W. (1990). cAMP-dependent protein kinase: framework for a diverse family of regulatory enzymes. Annu Rev Biochem *59*, 971-1005.
12. Harper, J.W., and Adams, P.D. (2001). Cyclin-dependent kinases. Chem Rev *101*, 2511-2526.
13. Komander, D., Kular, G., Deak, M., Alessi, D.R., and van Aalten, D.M. (2005). Role of T-loop phosphorylation in PDK1 activation, stability, and substrate binding. The Journal of biological chemistry *280*, 18797-18802.
14. Yang, J., Cron, P., Thompson, V., Good, V.M., Hess, D., Hemmings, B.A., and Barford, D. (2002). Molecular mechanism for the regulation of protein kinase B/Akt by hydrophobic motif phosphorylation. Molecular cell *9*, 1227-1240.
15. Yang, J., Cron, P., Good, V.M., Thompson, V., Hemmings, B.A., and Barford, D. (2002). Crystal structure of an activated Akt/protein kinase B ternary complex with GSK3-peptide and AMP-PNP. Nat Struct Biol *9*, 940-944.
16. Pearce, L.R., Komander, D., and Alessi, D.R. (2010). The nuts and bolts of AGC protein kinases. Nat Rev Mol Cell Biol *11*, 9-22.
17. Newton, A.C. (2003). Regulation of the ABC kinases by phosphorylation: protein kinase C as a paradigm. Biochem J *370*, 361-371.

18. Lucas, K.A., Pitari, G.M., Kazerounian, S., Ruiz-Stewart, I., Park, J., Schulz, S., Chepenik, K.P., and Waldman, S.A. (2000). Guanylyl cyclases and signaling by cyclic GMP. Pharmacol Rev *52*, 375-414.
19. Currie, R.A., Walker, K.S., Gray, A., Deak, M., Casamayor, A., Downes, C.P., Cohen, P., Alessi, D.R., and Lucocq, J. (1999). Role of phosphatidylinositol 3,4,5-trisphosphate in regulating the activity and localization of 3-phosphoinositide-dependent protein kinase-1. Biochem J *337 (Pt 3)*, 575-583.
20. Malumbres, M., and Barbacid, M. (2007). Cell cycle kinases in cancer. Curr Opin Genet Dev *17*, 60-65.
21. Heitman, J., Movva, N.R., and Hall, M.N. (1991). Targets for cell cycle arrest by the immunosuppressant rapamycin in yeast. Science *253*, 905-909.
22. Loewith, R., Jacinto, E., Wullschleger, S., Lorberg, A., Crespo, J.L., Bonenfant, D., Oppliger, W., Jenoe, P., and Hall, M.N. (2002). Two TOR complexes, only one of which is rapamycin sensitive, have distinct roles in cell growth control. Mol Cell *10*, 457-468.
23. Reinke, A., Anderson, S., McCaffery, J.M., Yates, J., 3rd, Aronova, S., Chu, S., Fairclough, S., Iverson, C., Wedaman, K.P., and Powers, T. (2004). TOR complex 1 includes a novel component, Tco89p (YPL180w), and cooperates with Ssd1p to maintain cellular integrity in Saccharomyces cerevisiae. J Biol Chem *279*, 14752-14762.
24. Wedaman, K.P., Reinke, A., Anderson, S., Yates, J., 3rd, McCaffery, J.M., and Powers, T. (2003). Tor kinases are in distinct membrane-associated protein complexes in Saccharomyces cerevisiae. Mol Biol Cell *14*, 1204-1220.
25. Barbet, N.C., Schneider, U., Helliwell, S.B., Stansfield, I., Tuite, M.F., and Hall, M.N. (1996). TOR controls translation initiation and early G1 progression in yeast. Mol Biol Cell *7*, 25-42.
26. Warner, J.R. (1999). The economics of ribosome biosynthesis in yeast. Trends Biochem Sci *24*, 437-440.
27. Claypool, J.A., French, S.L., Johzuka, K., Eliason, K., Vu, L., Dodd, J.A., Beyer, A.L., and Nomura, M. (2004). Tor pathway regulates Rrn3p-dependent recruitment of yeast RNA polymerase I to the promoter but does not participate in alteration of the number of active genes. Mol Biol Cell *15*, 946-956.
28. Martin, D.E., Soulard, A., and Hall, M.N. (2004). TOR regulates ribosomal protein gene expression via PKA and the Forkhead transcription factor FHL1. Cell *119*, 969-979.
29. Schawalder, S.B., Kabani, M., Howald, I., Choudhury, U., Werner, M., and Shore, D. (2004). Growth-regulated recruitment of the essential yeast ribosomal protein gene activator Ifh1. Nature *432*, 1058-1061.
30. Wade, J.T., Hall, D.B., and Struhl, K. (2004). The transcription factor Ifh1 is a key regulator of yeast ribosomal protein genes. Nature *432*, 1054-1058.
31. Marion, R.M., Regev, A., Segal, E., Barash, Y., Koller, D., Friedman, N., and O'Shea, E.K. (2004). Sfp1 is a stress- and nutrient-sensitive regulator of ribosomal protein gene expression. Proc Natl Acad Sci U S A *101*, 14315-14322.
32. Lempiainen, H., Uotila, A., Urban, J., Dohnal, I., Ammerer, G., Loewith, R., and Shore, D. (2009). Sfp1 interaction with TORC1 and Mrs6 reveals feedback regulation on TOR signaling. Molecular cell *33*, 704-716.

33. Huber, A., French, S.L., Tekotte, H., Yerlikaya, S., Stahl, M., Perepelkina, M.P., Tyers, M., Rougemont, J., Beyer, A.L., and Loewith, R. (2011). Sch9 regulates ribosome biogenesis via Stb3, Dot6 and Tod6 and the histone deacetylase complex RPD3L. EMBO J.
34. Huber, A., Bodenmiller, B., Uotila, A., Stahl, M., Wanka, S., Gerrits, B., Aebersold, R., and Loewith, R. (2009). Characterization of the rapamycin-sensitive phosphoproteome reveals that Sch9 is a central coordinator of protein synthesis. Genes Dev *23*, 1929-1943.
35. Lee, J., Moir, R.D., and Willis, I.M. (2009). Regulation of RNA polymerase III transcription involves SCH9-dependent and SCH9-independent branches of the target of rapamycin (TOR) pathway. J Biol Chem *284*, 12604-12608.
36. Cherkasova, V.A., and Hinnebusch, A.G. (2003). Translational control by TOR and TAP42 through dephosphorylation of eIF2alpha kinase GCN2. Genes Dev *17*, 859-872.
37. Garcia-Barrio, M., Dong, J., Cherkasova, V.A., Zhang, X., Zhang, F., Ufano, S., Lai, R., Qin, J., and Hinnebusch, A.G. (2002). Serine 577 is phosphorylated and negatively affects the tRNA binding and eIF2alpha kinase activities of GCN2. J Biol Chem *277*, 30675-30683.
38. Cosentino, G.P., Schmelzle, T., Haghighat, A., Helliwell, S.B., Hall, M.N., and Sonenberg, N. (2000). Eap1p, a novel eukaryotic translation initiation factor 4E-associated protein in Saccharomyces cerevisiae. Molecular and cellular biology *20*, 4604-4613.
39. Reiter, A., Steinbauer, R., Philippi, A., Gerber, J., Tschochner, H., Milkereit, P., and Griesenbeck, J. (2011). Reduction in ribosomal protein synthesis is sufficient to explain major effects on ribosome production after short-term TOR inactivation in Saccharomyces cerevisiae. Molecular and cellular biology *31*, 803-817.
40. Van Belle, D., and Andre, B. (2001). A genomic view of yeast membrane transporters. Curr Opin Cell Biol *13*, 389-398.
41. Hardwick, J.S., Kuruvilla, F.G., Tong, J.K., Shamji, A.F., and Schreiber, S.L. (1999). Rapamycin-modulated transcription defines the subset of nutrient-sensitive signaling pathways directly controlled by the Tor proteins. Proceedings of the National Academy of Sciences of the United States of America *96*, 14866-14870.
42. Huang, J., Zhu, H., Haggarty, S.J., Spring, D.R., Hwang, H., Jin, F., Snyder, M., and Schreiber, S.L. (2004). Finding new components of the target of rapamycin (TOR) signaling network through chemical genetics and proteome chips. Proceedings of the National Academy of Sciences of the United States of America *101*, 16594-16599.
43. Cardenas, M.E., Cutler, N.S., Lorenz, M.C., Di Como, C.J., and Heitman, J. (1999). The TOR signaling cascade regulates gene expression in response to nutrients. Genes & development *13*, 3271-3279.
44. Tate, J.J., Georis, I., Dubois, E., and Cooper, T.G. (2010). Distinct phosphatase requirements and GATA factor responses to nitrogen catabolite repression and rapamycin treatment in Saccharomyces cerevisiae. J Biol Chem *285*, 17880-17895.

45. Tate, J.J., Georis, I., Feller, A., Dubois, E., and Cooper, T.G. (2009). Rapamycin-induced Gln3 dephosphorylation is insufficient for nuclear localization: Sit4 and PP2A phosphatases are regulated and function differently. The Journal of biological chemistry *284*, 2522-2534.
46. De Craene, J.O., Soetens, O., and Andre, B. (2001). The Npr1 kinase controls biosynthetic and endocytic sorting of the yeast Gap1 permease. J Biol Chem *276*, 43939-43948.
47. Schmidt, A., Beck, T., Koller, A., Kunz, J., and Hall, M.N. (1998). The TOR nutrient signalling pathway phosphorylates NPR1 and inhibits turnover of the tryptophan permease. The EMBO journal *17*, 6924-6931.
48. Dilova, I., Aronova, S., Chen, J.C., and Powers, T. (2004). Tor signaling and nutrient-based signals converge on Mks1p phosphorylation to regulate expression of Rtg1.Rtg3p-dependent target genes. The Journal of biological chemistry *279*, 46527-46535.
49. Dilova, I., Chen, C.Y., and Powers, T. (2002). Mks1 in concert with TOR signaling negatively regulates RTG target gene expression in S. cerevisiae. Curr Biol *12*, 389-395.
50. Tate, J.J., Cox, K.H., Rai, R., and Cooper, T.G. (2002). Mks1p is required for negative regulation of retrograde gene expression in Saccharomyces cerevisiae but does not affect nitrogen catabolite repression-sensitive gene expression. J Biol Chem *277*, 20477-20482.
51. Kamada, Y., Funakoshi, T., Shintani, T., Nagano, K., Ohsumi, M., and Ohsumi, Y. (2000). Tor-mediated induction of autophagy via an Apg1 protein kinase complex. J Cell Biol *150*, 1507-1513.
52. Scott, S.V., Nice, D.C., 3rd, Nau, J.J., Weisman, L.S., Kamada, Y., Keizer-Gunnink, I., Funakoshi, T., Veenhuis, M., Ohsumi, Y., and Klionsky, D.J. (2000). Apg13p and Vac8p are part of a complex of phosphoproteins that are required for cytoplasm to vacuole targeting. J Biol Chem *275*, 25840-25849.
53. Gasch, A.P., and Werner-Washburne, M. (2002). The genomics of yeast responses to environmental stress and starvation. Funct Integr Genomics *2*, 181-192.
54. Wanke, V., Cameroni, E., Uotila, A., Piccolis, M., Urban, J., Loewith, R., and De Virgilio, C. (2008). Caffeine extends yeast lifespan by targeting TORC1. Mol Microbiol *69*, 277-285.
55. Wanke, V., Pedruzzi, I., Cameroni, E., Dubouloz, F., and De Virgilio, C. (2005). Regulation of G0 entry by the Pho80-Pho85 cyclin-CDK complex. The EMBO journal *24*, 4271-4278.
56. Toda, T., Cameron, S., Sass, P., and Wigler, M. (1988). SCH9, a gene of Saccharomyces cerevisiae that encodes a protein distinct from, but functionally and structurally related to, cAMP-dependent protein kinase catalytic subunits. Genes Dev *2*, 517-527.
57. Zurita-Martinez, S.A., and Cardenas, M.E. (2005). Tor and cyclic AMP-protein kinase A: two parallel pathways regulating expression of genes required for cell growth. Eukaryot Cell *4*, 63-71.

58. Smith, A., Ward, M.P., and Garrett, S. (1998). Yeast PKA represses Msn2p/Msn4p-dependent gene expression to regulate growth, stress response and glycogen accumulation. EMBO J *17*, 3556-3564.
59. Reinders, A., Burckert, N., Boller, T., Wiemken, A., and De Virgilio, C. (1998). Saccharomyces cerevisiae cAMP-dependent protein kinase controls entry into stationary phase through the Rim15p protein kinase. Genes Dev *12*, 2943-2955.
60. Santhanam, A., Hartley, A., Duvel, K., Broach, J.R., and Garrett, S. (2004). PP2A phosphatase activity is required for stress and Tor kinase regulation of yeast stress response factor Msn2p. Eukaryot Cell *3*, 1261-1271.
61. Schmelzle, T., Beck, T., Martin, D.E., and Hall, M.N. (2004). Activation of the RAS/cyclic AMP pathway suppresses a TOR deficiency in yeast. Mol Cell Biol *24*, 338-351.
62. Stephan, J.S., Yeh, Y.Y., Ramachandran, V., Deminoff, S.J., and Herman, P.K. (2009). The Tor and PKA signaling pathways independently target the Atg1/Atg13 protein kinase complex to control autophagy. Proc Natl Acad Sci U S A *106*, 17049-17054.
63. Pedruzzi, I., Dubouloz, F., Cameroni, E., Wanke, V., Roosen, J., Winderickx, J., and De Virgilio, C. (2003). TOR and PKA signaling pathways converge on the protein kinase Rim15 to control entry into G0. Mol Cell *12*, 1607-1613.
64. Di Como, C.J., and Arndt, K.T. (1996). Nutrients, via the Tor proteins, stimulate the association of Tap42 with type 2A phosphatases. Genes & development *10*, 1904-1916.
65. Jiang, Y., and Broach, J.R. (1999). Tor proteins and protein phosphatase 2A reciprocally regulate Tap42 in controlling cell growth in yeast. The EMBO journal *18*, 2782-2792.
66. Urban, J., Soulard, A., Huber, A., Lippman, S., Mukhopadhyay, D., Deloche, O., Wanke, V., Anrather, D., Ammerer, G., Riezman, H., et al. (2007). Sch9 is a major target of TORC1 in Saccharomyces cerevisiae. Molecular cell *26*, 663-674.
67. Zheng, Y., and Jiang, Y. (2005). The yeast phosphotyrosyl phosphatase activator is part of the Tap42-phosphatase complexes. Mol Biol Cell *16*, 2119-2127.
68. Duvel, K., and Broach, J.R. (2004). The role of phosphatases in TOR signaling in yeast. Curr Top Microbiol Immunol *279*, 19-38.
69. Beck, T., Schmidt, A., and Hall, M.N. (1999). Starvation induces vacuolar targeting and degradation of the tryptophan permease in yeast. The Journal of cell biology *146*, 1227-1238.
70. Yan, G., Shen, X., and Jiang, Y. (2006). Rapamycin activates Tap42-associated phosphatases by abrogating their association with Tor complex 1. The EMBO journal *25*, 3546-3555.
71. Jacinto, E., Guo, B., Arndt, K.T., Schmelzle, T., and Hall, M.N. (2001). TIP41 interacts with TAP42 and negatively regulates the TOR signaling pathway. Molecular cell *8*, 1017-1026.
72. Ptacek, J., Devgan, G., Michaud, G., Zhu, H., Zhu, X., Fasolo, J., Guo, H., Jona, G., Breitkreutz, A., Sopko, R., et al. (2005). Global analysis of protein phosphorylation in yeast. Nature *438*, 679-684.

73. Knebel, A., Morrice, N., and Cohen, P. (2001). A novel method to identify protein kinase substrates: eEF2 kinase is phosphorylated and inhibited by SAPK4/p38delta. The EMBO journal *20*, 4360-4369.
74. Shah, K., and Shokat, K.M. (2003). A chemical genetic approach for the identification of direct substrates of protein kinases. Methods Mol Biol *233*, 253-271.
75. Blethrow, J.D., Glavy, J.S., Morgan, D.O., and Shokat, K.M. (2008). Covalent capture of kinase-specific phosphopeptides reveals Cdk1-cyclin B substrates. Proceedings of the National Academy of Sciences of the United States of America *105*, 1442-1447.
76. Matsuoka, S., Ballif, B.A., Smogorzewska, A., McDonald, E.R., 3rd, Hurov, K.E., Luo, J., Bakalarski, C.E., Zhao, Z., Solimini, N., Lerenthal, Y., et al. (2007). ATM and ATR substrate analysis reveals extensive protein networks responsive to DNA damage. Science *316*, 1160-1166.
77. Oda, Y., Nagasu, T., and Chait, B.T. (2001). Enrichment analysis of phosphorylated proteins as a tool for probing the phosphoproteome. Nature biotechnology *19*, 379-382.
78. Tao, W.A., Wollscheid, B., O'Brien, R., Eng, J.K., Li, X.J., Bodenmiller, B., Watts, J.D., Hood, L., and Aebersold, R. (2005). Quantitative phosphoproteome analysis using a dendrimer conjugation chemistry and tandem mass spectrometry. Nat Methods *2*, 591-598.
79. Zhou, H., Watts, J.D., and Aebersold, R. (2001). A systematic approach to the analysis of protein phosphorylation. Nat Biotechnol *19*, 375-378.
80. Scanff, P., Yvon, M., and Pelissier, J.P. (1991). Immobilized Fe3+ affinity chromatographic isolation of phosphopeptides. J Chromatogr *539*, 425-432.
81. Ficarro, S.B., McCleland, M.L., Stukenberg, P.T., Burke, D.J., Ross, M.M., Shabanowitz, J., Hunt, D.F., and White, F.M. (2002). Phosphoproteome analysis by mass spectrometry and its application to Saccharomyces cerevisiae. Nature biotechnology *20*, 301-305.
82. Sugiyama, N., Masuda, T., Shinoda, K., Nakamura, A., Tomita, M., and Ishihama, Y. (2007). Phosphopeptide enrichment by aliphatic hydroxy acid-modified metal oxide chromatography for nano-LC-MS/MS in proteomics applications. Mol Cell Proteomics *6*, 1103-1109.
83. Bodenmiller, B., Mueller, L.N., Mueller, M., Domon, B., and Aebersold, R. (2007). Reproducible isolation of distinct, overlapping segments of the phosphoproteome. Nat Methods *4*, 231-237.
84. Thingholm, T.E., Jensen, O.N., Robinson, P.J., and Larsen, M.R. (2008). SIMAC (sequential elution from IMAC), a phosphoproteomics strategy for the rapid separation of monophosphorylated from multiply phosphorylated peptides. Mol Cell Proteomics *7*, 661-671.
85. Villen, J., and Gygi, S.P. (2008). The SCX/IMAC enrichment approach for global phosphorylation analysis by mass spectrometry. Nat Protoc *3*, 1630-1638.
86. Lemeer, S., Pinkse, M.W., Mohammed, S., van Breukelen, B., den Hertog, J., Slijper, M., and Heck, A.J. (2008). Online automated in vivo zebrafish phosphoproteomics: from large-scale analysis down to a single embryo. J Proteome Res *7*, 1555-1564.

87. McNulty, D.E., and Annan, R.S. (2008). Hydrophilic interaction chromatography reduces the complexity of the phosphoproteome and improves global phosphopeptide isolation and detection. Mol Cell Proteomics *7*, 971-980.
88. Roepstorff, P., and Fohlman, J. (1984). Proposal for a common nomenclature for sequence ions in mass spectra of peptides. Biomed Mass Spectrom *11*, 601.
89. Huang, Y., Triscari, J.M., Tseng, G.C., Pasa-Tolic, L., Lipton, M.S., Smith, R.D., and Wysocki, V.H. (2005). Statistical characterization of the charge state and residue dependence of low-energy CID peptide dissociation patterns. Anal Chem *77*, 5800-5813.
90. Wysocki, V.H., Tsaprailis, G., Smith, L.L., and Breci, L.A. (2000). Mobile and localized protons: a framework for understanding peptide dissociation. J Mass Spectrom *35*, 1399-1406.
91. Beausoleil, S.A., Jedrychowski, M., Schwartz, D., Elias, J.E., Villen, J., Li, J., Cohn, M.A., Cantley, L.C., and Gygi, S.P. (2004). Large-scale characterization of HeLa cell nuclear phosphoproteins. Proceedings of the National Academy of Sciences of the United States of America *101*, 12130-12135.
92. Gruhler, A., Olsen, J.V., Mohammed, S., Mortensen, P., Faergeman, N.J., Mann, M., and Jensen, O.N. (2005). Quantitative phosphoproteomics applied to the yeast pheromone signaling pathway. Mol Cell Proteomics *4*, 310-327.
93. Schroeder, M.J., Shabanowitz, J., Schwartz, J.C., Hunt, D.F., and Coon, J.J. (2004). A neutral loss activation method for improved phosphopeptide sequence analysis by quadrupole ion trap mass spectrometry. Anal Chem *76*, 3590-3598.
94. Zubarev, R.A. (2004). Electron-capture dissociation tandem mass spectrometry. Current opinion in biotechnology *15*, 12-16.
95. Syka, J.E., Coon, J.J., Schroeder, M.J., Shabanowitz, J., and Hunt, D.F. (2004). Peptide and protein sequence analysis by electron transfer dissociation mass spectrometry. Proceedings of the National Academy of Sciences of the United States of America *101*, 9528-9533.
96. Ulintz, P.J., Yocum, A.K., Bodenmiller, B., Aebersold, R., Andrews, P.C., and Nesvizhskii, A.I. (2009). Comparison of MS(2)-only, MSA, and MS(2)/MS(3) methodologies for phosphopeptide identification. J Proteome Res *8*, 887-899.
97. Sweet, S.M., Bailey, C.M., Cunningham, D.L., Heath, J.K., and Cooper, H.J. (2009). Large scale localization of protein phosphorylation by use of electron capture dissociation mass spectrometry. Mol Cell Proteomics *8*, 904-912.
98. Zubarev, R.A., Horn, D.M., Fridriksson, E.K., Kelleher, N.L., Kruger, N.A., Lewis, M.A., Carpenter, B.K., and McLafferty, F.W. (2000). Electron capture dissociation for structural characterization of multiply charged protein cations. Anal Chem *72*, 563-573.
99. Swaney, D.L., McAlister, G.C., and Coon, J.J. (2008). Decision tree-driven tandem mass spectrometry for shotgun proteomics. Nat Methods *5*, 959-964.
100. Chi, A., Huttenhower, C., Geer, L.Y., Coon, J.J., Syka, J.E., Bai, D.L., Shabanowitz, J., Burke, D.J., Troyanskaya, O.G., and Hunt, D.F. (2007). Analysis of phosphorylation sites on proteins from Saccharomyces cerevisiae by electron transfer dissociation (ETD) mass spectrometry. Proceedings of the National Academy of Sciences of the United States of America *104*, 2193-2198.

101. Molina, H., Horn, D.M., Tang, N., Mathivanan, S., and Pandey, A. (2007). Global proteomic profiling of phosphopeptides using electron transfer dissociation tandem mass spectrometry. Proceedings of the National Academy of Sciences of the United States of America *104*, 2199-2204.
102. Guthrie, C., and Fink, G.R. (1991). Guide to yeast genetics and molecular biology.
103. Gietz, R.D., Schiestl, R.H., Willems, A.R., and Woods, R.A. (1995). Studies on the transformation of intact yeast cells by the LiAc/SS-DNA/PEG procedure. Yeast *11*, 355-360.
104. Wach, A., Brachat, A., Pohlmann, R., and Philippsen, P. (1994). New heterologous modules for classical or PCR-based gene disruptions in Saccharomyces cerevisiae. Yeast *10*, 1793-1808.
105. Zheng, L., Baumann, U., and Reymond, J.L. (2004). An efficient one-step site-directed and site-saturation mutagenesis protocol. Nucleic Acids Res *32*, e115.
106. Steen, H., Stensballe, A., and Jensen, O.N. (2007). Preparation and Use of Microcolumns for Sample Desalting or Nanoscale IMAC. CSH Protoc *2007*, pdb prot4608.
107. Cox, J., and Mann, M. (2008). MaxQuant enables high peptide identification rates, individualized p.p.b.-range mass accuracies and proteome-wide protein quantification. Nature biotechnology *26*, 1367-1372.
108. Perkins, D.N., Pappin, D.J., Creasy, D.M., and Cottrell, J.S. (1999). Probability-based protein identification by searching sequence databases using mass spectrometry data. Electrophoresis *20*, 3551-3567.
109. Hilger, M., Bonaldi, T., Gnad, F., and Mann, M. (2009). Systems-wide analysis of a phosphatase knock-down by quantitative proteomics and phosphoproteomics. Mol Cell Proteomics *8*, 1908-1920.
110. Li, X., Gerber, S.A., Rudner, A.D., Beausoleil, S.A., Haas, W., Villen, J., Elias, J.E., and Gygi, S.P. (2007). Large-scale phosphorylation analysis of alpha-factor-arrested Saccharomyces cerevisiae. J Proteome Res *6*, 1190-1197.
111. Haas, W., Faherty, B.K., Gerber, S.A., Elias, J.E., Beausoleil, S.A., Bakalarski, C.E., Li, X., Villen, J., and Gygi, S.P. (2006). Optimization and use of peptide mass measurement accuracy in shotgun proteomics. Mol Cell Proteomics *5*, 1326-1337.
112. Ubersax, J.A., and Ferrell, J.E., Jr. (2007). Mechanisms of specificity in protein phosphorylation. Nat Rev Mol Cell Biol *8*, 530-541.
113. Lindberg, R.A., Quinn, A.M., and Hunter, T. (1992). Dual-specificity protein kinases: will any hydroxyl do? Trends in biochemical sciences *17*, 114-119.
114. Gander, S., Bonenfant, D., Altermatt, P., Martin, D.E., Hauri, S., Moes, S., Hall, M.N., and Jenoe, P. (2008). Identification of the rapamycin-sensitive phosphorylation sites within the Ser/Thr-rich domain of the yeast Npr1 protein kinase. Rapid Commun Mass Spectrom *22*, 3743-3753.
115. Ross, P.L., Huang, Y.N., Marchese, J.N., Williamson, B., Parker, K., Hattan, S., Khainovski, N., Pillai, S., Dey, S., Daniels, S., et al. (2004). Multiplexed protein quantitation in Saccharomyces cerevisiae using amine-reactive isobaric tagging reagents. Mol Cell Proteomics *3*, 1154-1169.

116. Thingholm, T.E., Palmisano, G., Kjeldsen, F., and Larsen, M.R. (2010). Undesirable charge-enhancement of isobaric tagged phosphopeptides leads to reduced identification efficiency. J Proteome Res *9*, 4045-4052.
117. Ong, S.E., Blagoev, B., Kratchmarova, I., Kristensen, D.B., Steen, H., Pandey, A., and Mann, M. (2002). Stable isotope labeling by amino acids in cell culture, SILAC, as a simple and accurate approach to expression proteomics. Mol Cell Proteomics *1*, 376-386.
118. Wilson-Grady, J.T., Villen, J., and Gygi, S.P. (2008). Phosphoproteome analysis of fission yeast. J Proteome Res *7*, 1088-1097.
119. Ghaemmaghami, S., Huh, W.K., Bower, K., Howson, R.W., Belle, A., Dephoure, N., O'Shea, E.K., and Weissman, J.S. (2003). Global analysis of protein expression in yeast. Nature *425*, 737-741.
120. Schwartz, D., and Gygi, S.P. (2005). An iterative statistical approach to the identification of protein phosphorylation motifs from large-scale data sets. Nature biotechnology *23*, 1391-1398.
121. Budovskaya, Y.V., Stephan, J.S., Deminoff, S.J., and Herman, P.K. (2005). An evolutionary proteomics approach identifies substrates of the cAMP-dependent protein kinase. Proceedings of the National Academy of Sciences of the United States of America *102*, 13933-13938.
122. Shabb, J.B. (2001). Physiological substrates of cAMP-dependent protein kinase. Chem Rev *101*, 2381-2411.
123. Moir, R.D., Lee, J., Haeusler, R.A., Desai, N., Engelke, D.R., and Willis, I.M. (2006). Protein kinase A regulates RNA polymerase III transcription through the nuclear localization of Maf1. Proc Natl Acad Sci U S A *103*, 15044-15049.
124. Wei, Y., Tsang, C.K., and Zheng, X.F. (2009). Mechanisms of regulation of RNA polymerase III-dependent transcription by TORC1. The EMBO journal *28*, 2220-2230.
125. Bharucha, N., Ma, J., Dobry, C.J., Lawson, S.K., Yang, Z., and Kumar, A. (2008). Analysis of the yeast kinome reveals a network of regulated protein localization during filamentous growth. Mol Biol Cell *19*, 2708-2717.
126. Verma, R., Iida, H., and Pardee, A.B. (1988). Modulation of expression of the stress-inducible p118 of Saccharomyces cerevisiae by cAMP. II. A study of p118 expression in mutants of the cAMP cascade. The Journal of biological chemistry *263*, 8576-8582.
127. Milkereit, P., Gadal, O., Podtelejnikov, A., Trumtel, S., Gas, N., Petfalski, E., Tollervey, D., Mann, M., Hurt, E., and Tschochner, H. (2001). Maturation and intranuclear transport of pre-ribosomes requires Noc proteins. Cell *105*, 499-509.
128. Lin, C.H., MacGurn, J.A., Chu, T., Stefan, C.J., and Emr, S.D. (2008). Arrestin-related ubiquitin-ligase adaptors regulate endocytosis and protein turnover at the cell surface. Cell *135*, 714-725.
129. Breitkreutz, A., Choi, H., Sharom, J.R., Boucher, L., Neduva, V., Larsen, B., Lin, Z.Y., Breitkreutz, B.J., Stark, C., Liu, G., et al. (2010). A global protein kinase and phosphatase interaction network in yeast. Science *328*, 1043-1046.
130. Longtine, M.S., Theesfeld, C.L., McMillan, J.N., Weaver, E., Pringle, J.R., and Lew, D.J. (2000). Septin-dependent assembly of a cell cycle-regulatory module in Saccharomyces cerevisiae. Molecular and cellular biology *20*, 4049-4061.

131. Berchtold, D., and Walther, T.C. (2009). TORC2 plasma membrane localization is essential for cell viability and restricted to a distinct domain. Mol Biol Cell *20*, 1565-1575.
132. Sugiyama, M., and Nikawa, J. (2001). The Saccharomyces cerevisiae Isw2p-Itc1p complex represses INO1 expression and maintains cell morphology. Journal of bacteriology *183*, 4985-4993.
133. Hong, S.P., Leiper, F.C., Woods, A., Carling, D., and Carlson, M. (2003). Activation of yeast Snf1 and mammalian AMP-activated protein kinase by upstream kinases. Proceedings of the National Academy of Sciences of the United States of America *100*, 8839-8843.
134. Orlova, M., Kanter, E., Krakovich, D., and Kuchin, S. (2006). Nitrogen availability and TOR regulate the Snf1 protein kinase in Saccharomyces cerevisiae. Eukaryotic cell *5*, 1831-1837.
135. Parsons, A.B., Brost, R.L., Ding, H., Li, Z., Zhang, C., Sheikh, B., Brown, G.W., Kane, P.M., Hughes, T.R., and Boone, C. (2004). Integration of chemical-genetic and genetic interaction data links bioactive compounds to cellular target pathways. Nature biotechnology *22*, 62-69.
136. Lillie, S.H., and Pringle, J.R. (1980). Reserve carbohydrate metabolism in Saccharomyces cerevisiae: responses to nutrient limitation. Journal of bacteriology *143*, 1384-1394.
137. Wilson, W.A., Wang, Z., and Roach, P.J. (2002). Systematic identification of the genes affecting glycogen storage in the yeast Saccharomyces cerevisiae: implication of the vacuole as a determinant of glycogen level. Mol Cell Proteomics *1*, 232-242.
138. Hardy, T.A., Huang, D., and Roach, P.J. (1994). Interactions between cAMP-dependent and SNF1 protein kinases in the control of glycogen accumulation in Saccharomyces cerevisiae. The Journal of biological chemistry *269*, 27907-27913.
139. Huang, D., Farkas, I., and Roach, P.J. (1996). Pho85p, a cyclin-dependent protein kinase, and the Snf1p protein kinase act antagonistically to control glycogen accumulation in Saccharomyces cerevisiae. Molecular and cellular biology *16*, 4357-4365.
140. Suter, B., Graham, C., and Stagljar, I. (2008). Exploring protein phosphorylation in response to DNA damage using differentially tagged yeast arrays. Biotechniques *45*, 581-584.
141. Wu, R., Haas, W., Dephoure, N., Huttlin, E.L., Zhai, B., Sowa, M.E., and Gygi, S.P. (2011). A large-scale method to measure absolute protein phosphorylation stoichiometries. Nat Methods *8*, 677-683.
142. Hughes, T.R., Marton, M.J., Jones, A.R., Roberts, C.J., Stoughton, R., Armour, C.D., Bennett, H.A., Coffey, E., Dai, H., He, Y.D., et al. (2000). Functional discovery via a compendium of expression profiles. Cell *102*, 109-126.
143. Hsu, P.P., Kang, S.A., Rameseder, J., Zhang, Y., Ottina, K.A., Lim, D., Peterson, T.R., Choi, Y., Gray, N.S., Yaffe, M.B., et al. (2011). The mTOR-regulated phosphoproteome reveals a mechanism of mTORC1-mediated inhibition of growth factor signaling. Science *332*, 1317-1322.

144. Liu, H., Sadygov, R.G., and Yates, J.R., 3rd (2004). A model for random sampling and estimation of relative protein abundance in shotgun proteomics. Anal Chem *76*, 4193-4201.
145. Powers, T., and Walter, P. (1999). Regulation of ribosome biogenesis by the rapamycin-sensitive TOR-signaling pathway in Saccharomyces cerevisiae. Mol Biol Cell *10*, 987-1000.
146. Fournier, M.L., Paulson, A., Pavelka, N., Mosley, A.L., Gaudenz, K., Bradford, W.D., Glynn, E., Li, H., Sardiu, M.E., Fleharty, B., et al. (2010). Delayed correlation of mRNA and protein expression in rapamycin-treated cells and a role for Ggc1 in cellular sensitivity to rapamycin. Mol Cell Proteomics *9*, 271-284.
147. Pedruzzi, I., Dubouloz, F., Cameroni, E., Wanke, V., Roosen, J., Winderickx, J., and De Virgilio, C. (2003). TOR and PKA signaling pathways converge on the protein kinase Rim15 to control entry into G0. Molecular cell *12*, 1607-1613.
148. Coschigano, P.W., and Magasanik, B. (1991). The URE2 gene product of Saccharomyces cerevisiae plays an important role in the cellular response to the nitrogen source and has homology to glutathione s-transferases. Molecular and cellular biology *11*, 822-832.
149. Daugherty, J.R., Rai, R., el Berry, H.M., and Cooper, T.G. (1993). Regulatory circuit for responses of nitrogen catabolic gene expression to the GLN3 and DAL80 proteins and nitrogen catabolite repression in Saccharomyces cerevisiae. Journal of bacteriology *175*, 64-73.
150. Soussi-Boudekou, S., and Andre, B. (1999). A co-activator of nitrogen-regulated transcription in Saccharomyces cerevisiae. Mol Microbiol *31*, 753-762.
151. Malys, N., Carroll, K., Miyan, J., Tollervey, D., and McCarthy, J.E. (2004). The 'scavenger' m7GpppX pyrophosphatase activity of Dcs1 modulates nutrient-induced responses in yeast. Nucleic Acids Res *32*, 3590-3600.
152. Kamada, Y., Yoshino, K., Kondo, C., Kawamata, T., Oshiro, N., Yonezawa, K., and Ohsumi, Y. (2010). Tor directly controls the Atg1 kinase complex to regulate autophagy. Molecular and cellular biology *30*, 1049-1058.
153. Gnad, F., Ren, S., Cox, J., Olsen, J.V., Macek, B., Oroshi, M., and Mann, M. (2007). PHOSIDA (phosphorylation site database): management, structural and evolutionary investigation, and prediction of phosphosites. Genome Biol *8*, R250.
154. Olsen, J.V., Vermeulen, M., Santamaria, A., Kumar, C., Miller, M.L., Jensen, L.J., Gnad, F., Cox, J., Jensen, T.S., Nigg, E.A., et al. (2010). Quantitative phosphoproteomics reveals widespread full phosphorylation site occupancy during mitosis. Sci Signal *3*, ra3.
155. Sturgill, T.W., Cohen, A., Diefenbacher, M., Trautwein, M., Martin, D.E., and Hall, M.N. (2008). TOR1 and TOR2 have distinct locations in live cells. Eukaryotic cell *7*, 1819-1830.
156. Zinzalla, V., Stracka, D., Oppliger, W., and Hall, M.N. (2011). Activation of mTORC2 by association with the ribosome. Cell *144*, 757-768.
157. Vincent, O., Townley, R., Kuchin, S., and Carlson, M. (2001). Subcellular localization of the Snf1 kinase is regulated by specific beta subunits and a novel glucose signaling mechanism. Genes & development *15*, 1104-1114.
158. Jin, L.L., Tong, J., Prakash, A., Peterman, S.M., St-Germain, J.R., Taylor, P., Trudel, S., and Moran, M.F. (2010). Measurement of protein phosphorylation

stoichiometry by selected reaction monitoring mass spectrometry. J Proteome Res *9*, 2752-2761.

159. Gerber, S.A., Rush, J., Stemman, O., Kirschner, M.W., and Gygi, S.P. (2003). Absolute quantification of proteins and phosphoproteins from cell lysates by tandem MS. Proceedings of the National Academy of Sciences of the United States of America *100*, 6940-6945.
160. Domanski, D., Murphy, L.C., and Borchers, C.H. (2010). Assay development for the determination of phosphorylation stoichiometry using multiple reaction monitoring methods with and without phosphatase treatment: application to breast cancer signaling pathways. Anal Chem *82*, 5610-5620.
161. Zhang, X., Jin, Q.K., Carr, S.A., and Annan, R.S. (2002). N-Terminal peptide labeling strategy for incorporation of isotopic tags: a method for the determination of site-specific absolute phosphorylation stoichiometry. Rapid Commun Mass Spectrom *16*, 2325-2332.
162. Hegeman, A.D., Harms, A.C., Sussman, M.R., Bunner, A.E., and Harper, J.F. (2004). An isotope labeling strategy for quantifying the degree of phosphorylation at multiple sites in proteins. J Am Soc Mass Spectrom *15*, 647-653.
163. Kanshin, E., Wang, S., Ashmarina, L., Fedjaev, M., Nifant'ev, I., Mitchell, G.A., and Pshezhetsky, A.V. (2009). The stoichiometry of protein phosphorylation in adipocyte lipid droplets: analysis by N-terminal isotope tagging and enzymatic dephosphorylation. Proteomics *9*, 5067-5077.
164. Tsukiyama, T., Palmer, J., Landel, C.C., Shiloach, J., and Wu, C. (1999). Characterization of the imitation switch subfamily of ATP-dependent chromatin-remodeling factors in Saccharomyces cerevisiae. Genes & development *13*, 686-697.
165. Goldmark, J.P., Fazzio, T.G., Estep, P.W., Church, G.M., and Tsukiyama, T. (2000). The Isw2 chromatin remodeling complex represses early meiotic genes upon recruitment by Ume6p. Cell *103*, 423-433.
166. Ruiz, C., Escribano, V., Morgado, E., Molina, M., and Mazon, M.J. (2003). Cell-type-dependent repression of yeast a-specific genes requires Itc1p, a subunit of the Isw2p-Itc1p chromatin remodelling complex. Microbiology *149*, 341-351.
167. Gelbart, M.E., Rechsteiner, T., Richmond, T.J., and Tsukiyama, T. (2001). Interactions of Isw2 chromatin remodeling complex with nucleosomal arrays: analyses using recombinant yeast histones and immobilized templates. Molecular and cellular biology *21*, 2098-2106.
168. O'Donnell, A.F., Apffel, A., Gardner, R.G., and Cyert, M.S. (2010). Alpha-arrestins Aly1 and Aly2 regulate intracellular trafficking in response to nutrient signaling. Mol Biol Cell *21*, 3552-3566.
169. Gander, S., Martin, D., Hauri, S., Moes, S., Poletto, G., Pagano, M.A., Marin, O., Meggio, F., and Jenoe, P. (2009). A modified KESTREL search reveals a basophilic substrate consensus for the Saccharomyces cerevisiae Npr1 protein kinase. J Proteome Res *8*, 5305-5316.
170. Morinaga, N., Moss, J., and Vaughan, M. (1997). Cloning and expression of a cDNA encoding a bovine brain brefeldin A-sensitive guanine nucleotide-exchange protein for ADP-ribosylation factor. Proceedings of the National Academy of Sciences of the United States of America *94*, 12926-12931.

171. Dehring, D.A., Adler, A.S., Hosseini, A., and Hicke, L. (2008). A C-terminal sequence in the guanine nucleotide exchange factor Sec7 mediates Golgi association and interaction with the Rsp5 ubiquitin ligase. The Journal of biological chemistry *283*, 34188-34196.
172. Mosammaparast, N., Ewart, C.S., and Pemberton, L.F. (2002). A role for nucleosome assembly protein 1 in the nuclear transport of histones H2A and H2B. The EMBO journal *21*, 6527-6538.
173. Calvert, M.E., Keck, K.M., Ptak, C., Shabanowitz, J., Hunt, D.F., and Pemberton, L.F. (2008). Phosphorylation by casein kinase 2 regulates Nap1 localization and function. Molecular and cellular biology *28*, 1313-1325.
174. Albuquerque, C.P., Smolka, M.B., Payne, S.H., Bafna, V., Eng, J., and Zhou, H. (2008). A multidimensional chromatography technology for in-depth phosphoproteome analysis. Mol Cell Proteomics *7*, 1389-1396.
175. Smolka, M.B., Albuquerque, C.P., Chen, S.H., and Zhou, H. (2007). Proteome-wide identification of in vivo targets of DNA damage checkpoint kinases. Proceedings of the National Academy of Sciences of the United States of America *104*, 10364-10369.
176. Bornancin, F., and Parker, P.J. (1996). Phosphorylation of threonine 638 critically controls the dephosphorylation and inactivation of protein kinase Calpha. Current biology : CB *6*, 1114-1123.
177. Yonemoto, W., McGlone, M.L., Grant, B., and Taylor, S.S. (1997). Autophosphorylation of the catalytic subunit of cAMP-dependent protein kinase in Escherichia coli. Protein Eng *10*, 915-925.
178. Cohen, A., Perzov, N., Nelson, H., and Nelson, N. (1999). A novel family of yeast chaperons involved in the distribution of V-ATPase and other membrane proteins. The Journal of biological chemistry *274*, 26885-26893.
179. Muller, O., Neumann, H., Bayer, M.J., and Mayer, A. (2003). Role of the Vtc proteins in V-ATPase stability and membrane trafficking. J Cell Sci *116*, 1107-1115.
180. Binda, M., Peli-Gulli, M.P., Bonfils, G., Panchaud, N., Urban, J., Sturgill, T.W., Loewith, R., and De Virgilio, C. (2009). The Vam6 GEF controls TORC1 by activating the EGO complex. Molecular cell *35*, 563-573.
181. Uttenweiler, A., Schwarz, H., Neumann, H., and Mayer, A. (2007). The vacuolar transporter chaperone (VTC) complex is required for microautophagy. Mol Biol Cell *18*, 166-175.
182. Liu, Z., Sekito, T., Spirek, M., Thornton, J., and Butow, R.A. (2003). Retrograde signaling is regulated by the dynamic interaction between Rtg2p and Mks1p. Molecular cell *12*, 401-411.

Acknowledgements

I would like to thank Dr. Paul Jenö for giving me the opportunity to work in his lab. He supported me during my entire PhD study, providing me constant advices. He patiently taught me the basics of mass spectrometry, introducing me to this very exciting research field. Many thanks to Prof. Michael N. Hall for supporting my project, both scientifically and financially. I also would like to thank Prof. Jan Hofsteenge for being in my thesis committee and Prof. Christoph Moroni, who supported me during my master and PhD studies.

Special thanks to Suzette Moes and Markus Beer for providing me constant help in the lab work and for sharing with me their technical skills. I also would like to thank Dr. Alexandre Soulard and Dr. Vittoria Zinzalla for critical discussions about my experiments and for teaching me the fundamentals of molecular and yeast biology. They were always present when I had questions to ask!

Likewise, I am very grateful to all past and present members of the Hall lab for scientific and moral support: Daniele Stracka (who formed with me and Vittoria the [Swiss]Italian lab team), Dr. Marion Cornu, Aaron Robitaille, Simon Hauri, Asami Hagiwara, Dr. Raul Duran Diaz, Dr. Eva Dazert, Charles Betz, Dr. Mitsugu Shimobayashi, Verena Albert, Wolfgang Oppliger, Andrea Löschmann, Dr. Nadine Cybulski, Dr. Adiel Cohen, Dr. Pazit Polak and the two master students Steve Kunnakatt and Vincent Pillonel. I also would like to thank all the members of the 5th floor of the Biozentrum who helped me during my thesis.

Special thanks belong to Dr. Sjouke Hoving, Dr. Bertran Gerrits and Dr. Débora Bonenfant, who gave me helpful scientific suggestions. Furthermore, I would like to thank Sjouke and my other friends Ilario, Angelo, Valentina and Stefano for their moral support during my thesis.

Last but not least, I would like to mention my family, who has supported me during all my studies.